

MICROSCOPIC COMPUTATIONS IN
THE FRACTIONAL QUANTUM
HALL EFFECT

Stephanie Jane Huntington



A thesis submitted for the degree of Doctor of
Philosophy at Lancaster University, Department
of Physics.

November 2014

Abstract

The microscopic picture for fractional quantum Hall effect (FQHE) is difficult to work with analytically for a large number of electrons. Therefore to make predictions and attempt to describe experimental measurements on quantum Hall systems, effective theories are usually employed such as the chiral Luttinger liquid system. In this thesis the Monte Carlo method is used for Laughlin-type quantum Hall systems to compute microscopic observables. In particular such computations are carried out for the large system size expansion of the free energy. This work was motivated by some disagreement in the literature about the form of the free energy expansion and is still an ongoing project. Tunnelling in the FQHE is an interesting problem since the tunnelling operators are derived from an effective theory which has not yet been checked microscopically. To perform a test for the effective tunnelling Hamiltonian, microscopic calculations were performed numerically for charges tunnelling across the bulk states of a FQH device. To compute these matrix elements, two methods were found to overcome a phase problem encountered in the Monte Carlo simulations. The Monte Carlo results were compared to the matrix elements predicted by the effective tunnelling Hamiltonian and there was a good match between the data. Performing this comparison enabled the operator ordering in the effective tunnelling Hamiltonian to be deduced and the data also showed that the quasiparticle tunnelling processes were more relevant than the electron tunnelling processes for all system sizes, supporting the idea that when tunnelling is considered at a weak barrier, the electron tunnelling process can be neglected.

Declaration

The work contained in this thesis is my original research work unless stated otherwise. The original research presented has not been submitted towards the award of higher degree elsewhere.

Dedication

This thesis is affectionately dedicated to my Grandad, Kenneth Bridgwater.
I am grateful for all your inspiration and encouragement, you are missed every
day and I hope you are proud.

Acknowledgements

First and foremost, I would like to thank my supervisor, Dr. Vadim Cheianov, who has shown an abundance of enthusiasm, insight, and patience throughout my time in Lancaster. For his encouragement throughout my undergraduate degree and to join the condensed matter theory group at Lancaster University, I thank Prof. Vladimir Falko. I would also like to acknowledge Dr. Kyrylo Snizhko for many interesting and helpful discussions related to the fractional quantum Hall effect. Dr. Evgeni Burovski and Dr. Neil Drummond have also been extremely helpful with answering any questions related to numerical, computational methods.

It has been a pleasure to be a part of the condensed matter theory group at Lancaster, and for this I would like to thank other group members that I have not already mentioned above; Elaheh Mostaani, Dr. Yury Shurkenov, Dr. Diana Cosma, Dr. Charles Poli, Dr. John Wallbank, Simon Malzard, Dr. Edward McCann and Prof. Henning Schomerus.

I would also like to thank Phil Furneaux, who has not only been a great Outreach officer for the Physics Department at Lancaster University, but who has also been very encouraging throughout the last couple of years; participating in the Outreach program has been an exciting and fulfilling experience. I am very grateful to the people who took the time to read chapters of this thesis, Dr. Edward Guise, Bogdan Ganchev and Dr. Chris Poole.

All of my family and friends have shown a huge amount of support over the past

four years including my Grandparents and brothers, in particular I would like to thank my Mum, Dad, Kevin and Wendy. I owe you all a great deal.

List of Figures

1.1	Quantum Hall bar with four-terminal geometry	4
1.2	Plot for resistivity measurements for the QHE	4
1.3	Landau level spectrum for an electron in a magnetic field	11
1.4	Boundary effects on the Landau levels	13
1.5	Disk geometry for a FQH device	29
4.1	Disk geometry of a FQH device include impurity	67
4.2	Plot of data for zero mode electron tunnelling for $\nu = 1$	84
4.3	Plot of data for zero mode quasiparticle and electron tunnelling for $\nu = 1/3$	86
5.1	Sketch of density profile, $\rho_0^{(1)}$	102
5.2	Sketch of density profile, $\rho_0^{(2)}$	105

List of Tables

3.1	Data for the overlap of states containing edge excitations.	64
5.1	Comparison of numerical data and the model for the free energy expansion $\tau^{(1)}(\kappa)$	109
5.2	Comparison of numerical data and the model for the free energy expansion $\tau^{(2)}(\kappa)$	110
5.3	Comparison of numerical data and the model for the coefficient of the linear N term, $\Delta(m)$ for the free energy expansion	111

List of Abbreviations

A list of commonly used abbreviations throughout this thesis is given below.

QH	Quantum Hall
IQHE	Integer quantum Hall effect
FQHE	Fractional quantum Hall effect
FQH	Fractional quantum Hall
LL	Landau level
LLL	Lowest Landau level
2DEG	Two-dimensional electron gas
QPC	Quantum point contact
OCP	One-component plasma
RG	Renormalization group
MC	Monte Carlo
CoE	Condition of ergodicity
CoDB	Condition of detailed balance

Contents

1	Introduction	1
1.1	Classical Hall Conductance	5
1.2	Quantum Treatment of an Electron Subject to a Magnetic Field . .	7
1.3	The Integer Quantum Hall Effect	11
1.4	The Fractional Quantum Hall Effect and Laughlin States	14
1.4.1	Analogy Between the Laughlin State and the One-Component Plasma	16
1.4.2	Laughlin Excitations	19
1.5	Review of Literature Probing Transport Properties in the FQHE . .	23
1.6	Disk Geometry Fractional Quantum Hall Device	28
2	The Monte Carlo Method	32
3	Edge Excitations in Laughlin-Type States	42
3.1	Microscopic Representation of Edge Excitations	43

3.2	Phenomenological Theory Representation of Edge Excitations . . .	49
3.2.1	Chiral Luttinger Liquid Formalism	50
3.3	Numerical Verification of Analytic Formulas for Overlap Integrals .	60
4	Zero-Mode Tunnelling Matrix Elements	65
4.1	Microscopic Computation of the Zero Mode Tunnelling Matrix El- ements	66
4.1.1	Phase Problem Solution: Method 1 for $\chi \leq 1$	70
4.1.2	Phase Problem Solution: Method 2 for $\chi = m$	72
4.2	Zero Mode Tunnelling Matrix Elements Using the Effective Hamil- tonian	76
4.3	Results for Zero Mode Tunnelling Matrix Elements	82
4.3.1	Simulation Details	82
4.3.2	Tunnelling Results for $\nu = 1$	83
4.3.3	Tunnelling Results for $\nu = 1/3$	85
4.4	Summary and Conclusions	87
5	Numerical Testing for the Free Energy Expansion in the Semi- classical Limit	92
5.1	Introduction to the Formalism Used in the Free Energy Expansion .	94
5.2	Analytic Expressions for the Free Energy Expansions for Particular Choices of $W(z)$	99

5.2.1	Free Energy Expansion with Potential $W_0(z)$	100
5.2.2	Free Energy Expansion with Potential $W_1(z)$	101
5.2.3	Free Energy Expansion with Potential $W_2(z)$	104
5.3	Numerical Calculation of the Free Energy	106
5.4	Simulation Details	108
5.5	Results for MC Computations for the Free Energy Expansion	109
5.6	Summary and Conclusion	111
6	Summary, Conclusions, and Future Work	114
Appendix A Theory of Symmetric Functions and the Free Fermion		
	QHE	123
A.1	Introduction to the Theory of Symmetric Polynomials	123
A.2	Analytical Calculations for Overlap Integrals in the Free Fermion QHE	132
Appendix B Calculating the Norm of Laughlin States		143
B.1	Boson Field Theory Reformulation for a Laughlin-Type System . . .	144
B.2	Laughlin States Including Edge Excitations	149

Overview

This thesis investigates how Monte Carlo computations can be performed in the microscopic picture of the fractional quantum Hall effect in the large system size limit. Using this tool, numerous tests have been performed to check the validity of effective theories commonly used to calculate observable quantities in the fractional quantum Hall effect (FQHE).

Chapter 1 is the introductory chapter to this thesis. Many important concepts and behaviours of quantum Hall (QH) systems are discussed which are useful for understanding work presented in later chapters. In particular the Laughlin wavefunction is introduced as a microscopic representation of fractional quantum Hall (FQH) states occupying the lowest possible energy level. A disk-type geometry FQH device is also introduced at the end of this chapter; this system is used for future calculations presented in later chapters.

Many of the original computations carried out in this thesis use the Monte Carlo (MC) method. Chapter 2 gives a description of how this method works, and in particular why it is a good numerical method to use for computations involving the FQHE. It turns out that the Laughlin states can be thought of as a two-dimensional one-component plasma which provides an effective partition function such that statistical averages of observables in the FQHE can be computed.

In Chapter 3 the formalism for the low-energy excitations of Laughlin's wavefunction is reviewed in some detail. Initially the edge excitations are introduced from

a microscopic perspective where it will be shown there exists a bosonic representation to describe the edge modes as collective sound waves on the boundary of the FQH system. The microscopic picture however, is hard to work with for large system sizes and so in the second part of Chapter 3 a phenomenological theory of the edge states is introduced, referred to as the chiral Luttinger liquid. In this theory bosonized fermion operators are derived to describe the low-energy excitations and the theory is able to make many predictions about transport properties of the FQHE that can be experimentally tested and verified. The last section of Chapter 3 presents original work for the computation of overlap integrals for Laughlin states using the MC method.

One of the main results of the work carried out for this thesis is presented in Chapter 4. The question asked is, can the effective theory of tunnelling across bulk states in the FQHE be verified microscopically? To answer this question zero mode tunnelling matrix elements are calculated according to the effective tunnelling Hamiltonian using the bosonized operators derived in Chapter 3. This calculation is then compared to a microscopic picture where the zero mode tunnelling matrix elements are computed using the MC method. In the microscopic picture, tunnelling between edge states is initiated by inserting an impurity into the bulk. The results show that the effective tunnelling Hamiltonian does accurately describe tunnelling processes across bulk states in the FQHE.

In Chapter 5 another numerical test is carried out, but this time for the free energy expansion in the large N -limit. This is an interesting study since there are conflicting proposals for a Liouville-type equation for the equilibrium density distribution in some external potential. These Liouville-type equations are derived from the same field theory that gives the free energy expansion in the large N limit. Thus testing the free energy expansion indirectly provides information about the accuracy of the Liouville-type equations. This investigation is still ongoing.

Finally in Chapter 6 the summary and conclusion of this thesis are presented

as well as discussing further avenues of possible study that relate to the original computations presented in this thesis.

CHAPTER 1

Introduction

The discovery of the quantum Hall effect (QHE) came about when research began on magnetotransport properties of two-dimensional electron systems. The existence of such a two-dimensional electronic system was first shown by Fowler *et al.* [1]. The authors demonstrated that at a semiconductor interface there existed an electron gas which when placed inside a magnetic field exhibited behaviour that could only be attributed to electrons constrained to two dimensions. It will be shown in Section 1.2 that for a two-dimensional electron gas (2DEG) subject to a perpendicular magnetic field, the dispersion energies of electrons become quantised. These discrete, equally spaced energy levels are referred to as Landau levels. This physics played a major role in the explanation of the first quantum Hall effect to be discovered experimentally, known as the integer quantum Hall effect (IQHE).

The IQHE was first discovered by Klaus von Klitzing [2] when a 2DEG formed in a metal oxide semiconductor field-effect transistor (MOSFET) was placed in a strong, perpendicular magnetic field at low temperatures. The signature observations of this phenomenon are plateaus in measurements of the Hall resistivity, ρ_H , whilst the longitudinal resistivity, ρ_L , tends to zero as the magnetic field, or electron density is varied. The Hall and longitudinal resistivities can be extracted by measuring the Hall and longitudinal resistance respectively of a Hall bar, depicted

in Figure 1.1. Due to the longitudinal resistance being zero, at the plateaus the current flow through the system is dissipationless. Figure 1.2 is an example of the results from such an experiment. These plateaus occur at certain values of $h/(\nu e^2)$ in the Hall resistivity, where ν is some integer. As emphasised in Klitzing's paper, the fact that the Hall resistivity is proportional to a ratio of two fundamental constants means that it can be experimentally measured to a high accuracy. The reason for the universal nature of ρ_H is related to the two-dimensional nature of the system. It can be shown that for a rectangular geometry (see Figure 1.1) at a plateau such that the longitudinal resistivity $\rho_L = 0$, the Hall resistivity is exactly equal to the Hall resistance $\rho_H \equiv R_H$. Since resistivity is a local quantity, the results for R_H are therefore insensitive to the fine details of the sample. Not only does the QHE allow a definition of an accurate resistance standard but the system can also be used to increase the accuracy of fundamental constants such as the fine structure constant [2].

A description of the IQHE can be formulated completely in a free electron picture where all electron-electron interactions are disregarded. Then the observed behaviour of the IQHE is a consequence of the gaps between the adjacent Landau levels. In particular, when impurities are present in the 2DEG, the Landau levels become a spectrum of smoothed out, delta-like functions. It is the space of localised states between the Landau levels that allows the plateaus in the Hall resistivity to occur. Using this explanation, it is the number of filled Landau levels ν which gives the value of the integer in the expression for the Hall resistivity $h/(\nu e^2)$. This argument is discussed in more detail in Section 1.3.

Just as a clear explanation of the IQHE was formulated, a completely unexpected observation was made in an experiment performed on a quantum Hall (QH) device by Tsui, Stormer and Gossard [3]. Due to technological advances in semiconductor physics, Tsui *et al.* were able to use a much cleaner sample than used by Klitzing with higher carrier mobility, stronger magnetic fields and lower temperatures. The

group not only observed plateaus in Hall resistivity measurements corresponding to integer values of ν , but also the fractional value of $\nu = 1/3$. Other fractional values of ν with an odd denominator have since been observed [4–9], as well as even denominator fractions such as $\nu = 5/2$ [10–12], which are only briefly mentioned in this thesis. The observation of plateaus for which ν is a fractional value in Hall resistivity measurements is referred to as the fractional quantum Hall effect (FQHE). Some such plateaus can be seen in Figure 1.2.

A fractional value of ν corresponds to a partially filled Landau level. In the free electron picture used to describe the IQHE, there exists no gap within a given Landau level which is needed to observe the fractional plateaus. Therefore the free electron picture is insufficient to provide an explanation for the FQHE and one must consider the more complicated picture of the 2DEG being made up of strongly correlated electrons. Impurities usually destroy electron correlations which is one of the reasons why the FQHE is only observed in cleaner samples with higher mobility.

In the next section of this chapter the behaviour of electrons subject to a magnetic field is discussed which will lead onto a brief description of the observed behaviour in the Hall measurements of the IQHE. The remainder of this chapter will then focus on the FQHE; in particular Laughlin states [13] are introduced as well as a review of some literature concerned with the edges states of the FQHE and measurements on their transport properties. Throughout this thesis a specific type of quantum Hall geometry is considered and this device is introduced at the end of this chapter.

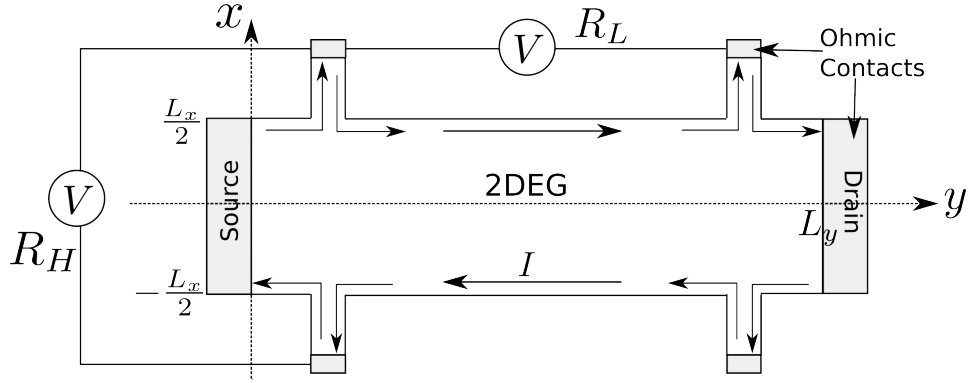


Figure 1.1: Schematic diagram of the set-up for a quantum Hall experiment with four-terminal geometry.

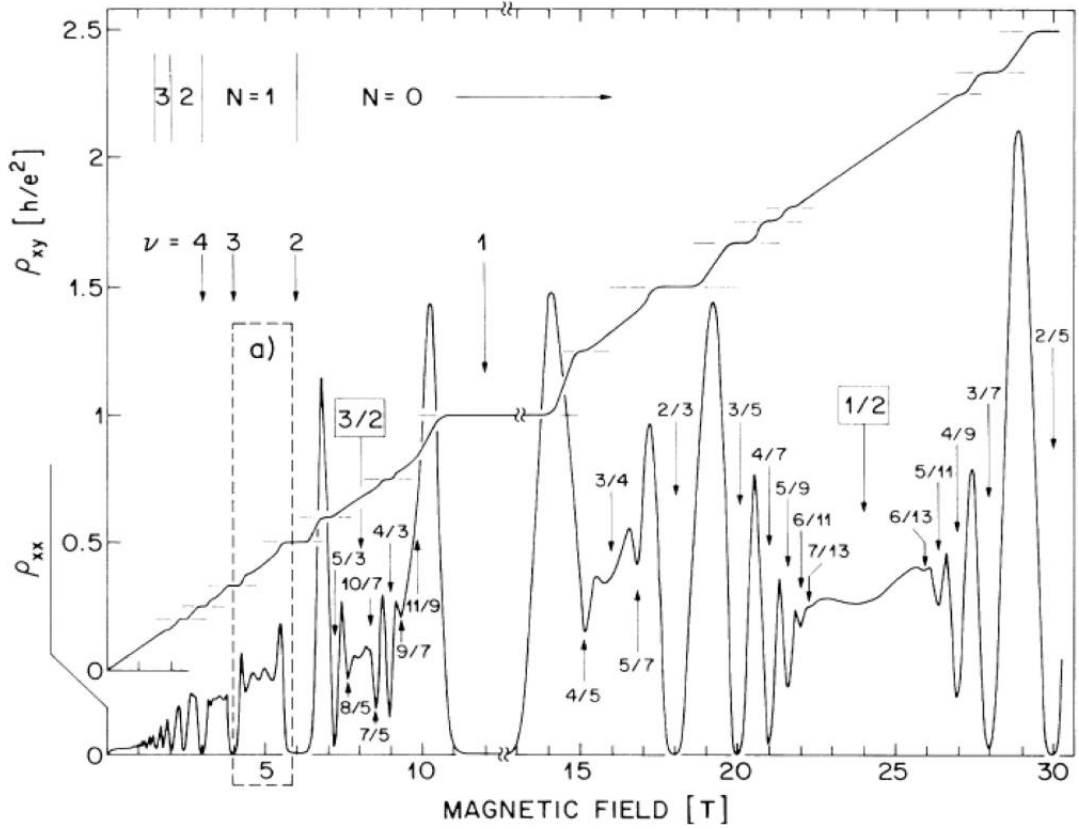


Figure 1.2: Plot of the Hall and longitudinal resistivity for a Hall bar (Figure 1.1) as a function of the out-of-plane magnetic field. Plateaus in the Hall resistivity, $\rho_{xy} \equiv \rho_H$ and minima in the longitudinal resistivity, $\rho_{xx} \equiv \rho_L$ are clearly seen and indicate FQHE behaviour. Source: [10].

1.1 Classical Hall Conductance

The effect of a voltage drop created across an electrical conductor when placed in a magnetic field perpendicular to the direction of current flow has been known since Hall's discovery in 1879 [14]. Classical considerations alone are adequate to describe this behaviour, which is attributed to the Lorentz force experienced by the electrons inside the conductor. It will be shown in this section however that classical considerations are not enough to predict the existence of Hall plateaus for a two-dimensional conductor [15–17].

From the Drude theory of electrical conductivity [18], the average drift velocity of an electron in an electric field \mathbf{E} is

$$\mathbf{v} = -\frac{e\mathbf{E}\tau_0}{m},$$

where τ_0 is the mean free path time and $-e$, m are the charge and mass of the electron respectively. The current density is

$$\mathbf{j} = -ne\mathbf{v} = \sigma_0\mathbf{E}, \tag{1.1}$$

where n is the electron density, $\sigma_0 = ne^2\tau_0/m$ is the constant electrical conductivity in the absence of a magnetic field. Including a magnetic field in the system in a perpendicular direction to the electric field e.g., $\mathbf{B} = B\hat{\mathbf{k}}$, causes the motion of the electron to be on the $x - y$ plane and thus the conductivity and resistivity become tensors σ and $\sigma^{-1} = \rho$ respectively. Adding the Lorentz force to the force created by the electric field (where it has been assumed that $d\mathbf{v}/dt = 0$) gives

$$\mathbf{v} = -e(\mathbf{E} + \mathbf{v} \times \mathbf{B})\frac{\tau_0}{m}. \tag{1.2}$$

The above equation gives the x and y components of the drift velocity in terms of the electric field components which can be substituted into (1.1) and rearranged to give,

$$\begin{aligned} E_x &= \sigma_0^{-1} j_x + \omega_c \sigma_0^{-1} \tau_0 j_y \\ E_y &= -\omega_c \sigma_0^{-1} \tau_0 j_x + \sigma_0^{-1} j_y, \end{aligned}$$

where $\omega_c = eB/m$ is the cyclotron frequency. Since $\mathbf{E} = \rho \mathbf{j}$, the components for the electric field above define the resistivity tensor to be,

$$\rho = \begin{pmatrix} \rho_L & \rho_H \\ -\rho_H & \rho_L \end{pmatrix} = \begin{pmatrix} \sigma_0^{-1} & \omega_c \sigma_0^{-1} \tau_0 \\ -\omega_c \sigma_0^{-1} \tau_0 & \sigma_0^{-1} \end{pmatrix}. \quad (1.3)$$

Components ρ_L and ρ_H are referred to the longitudinal and Hall resistivity respectively. The conductivity is then easily extracted from (1.3) using $\sigma = \rho^{-1}$.

$$\begin{aligned} \sigma_L &= \frac{\rho_L}{\rho_L^2 + \rho_H^2} = \frac{\sigma_0}{1 + \omega_c^2 \tau_0^2} \\ \sigma_H &= -\frac{\rho_H}{\rho_L^2 + \rho_H^2} = -\frac{\omega_c \tau_0 \sigma_0}{1 + \omega_c^2 \tau_0^2} = -\frac{ne}{B} + \frac{\sigma_L}{\omega_c \tau_0} \end{aligned} \quad (1.4)$$

From (1.4) it is noted that for a non-zero Hall resistivity, $\rho_H \neq 0$, the longitudinal conductivity vanishes as the longitudinal resistivity vanishes. Thus in regions where ρ_L vanishes, just as it is known to do in the QHE, the Hall conductance tends to $\sigma_H = -ne/B$. In this regime where $\rho_H \neq 0$ but $\rho_L \rightarrow 0$, the conductivity and resistivity tensors become

$$\sigma = \frac{\nu e^2}{h} \begin{pmatrix} 0 & -1 \\ 1 & 0 \end{pmatrix}, \quad \rho = \frac{h}{\nu e^2} \begin{pmatrix} 0 & 1 \\ -1 & 0 \end{pmatrix}. \quad (1.5)$$

where $\nu = nh/(eB)$; this quantity is discussed in more detail in Section 1.2. To make closer connections to the QH measurements in Figure 1.2, it would be convenient to transform resistivity values to resistances. For this a specific geometry must be chosen and here a rectangular 2DEG is considered with length L_y in the y -direction and L_x in the x -direction as shown in Figure 1.1. Resistivity is defined as $\rho = RA/W$ where A is the cross-sectional area perpendicular to the current flow and W is the length over the voltage drop. Thus for this 2D, rectangular system the result $R_H \equiv \rho_H$ is obtained and so the resistivity tensor in (1.5) is equivalently the resistance tensor. In the QHE, $\rho_L \rightarrow 0$ so then of course $R_L \rightarrow 0$ but for completeness, the relationship between the longitudinal resistance and the longitudinal resistivity is $\rho_L = R_L L_x / L_y$.

According to this classical analysis, the Hall resistance should depend linearly on the magnetic field and thus cannot predict the plateaus observed for the 2DEG when it is placed in strong magnetic fields at low temperatures. To understand how plateaus in the Hall resistance arise, a quantum treatment of an electron in a magnetic field must be discussed.

1.2 Quantum Treatment of an Electron Subject to a Magnetic Field

As already hinted in the introduction to this chapter, the IQHE lends itself to a description of a two-dimensional (2D) system of electrons free from interactions. This section will begin with an analysis of the behaviour of a single charged particle in a uniform magnetic field in the z -direction, from which the Landau level spectrum can be derived. For simplicity a spin-less system is considered for which, the Hamiltonian is given by

$$H = \frac{1}{2m} \left(-i\hbar\nabla - \frac{e}{c}\mathbf{A} \right)^2, \quad (1.6)$$

where $-e$ and m are the charge and mass of the particle respectively and \mathbf{A} is the vector potential, related to the magnetic field via $\mathbf{B} = \nabla \times \mathbf{A}$. This Hamiltonian can be solved using the Landau gauge, $\mathbf{A} = (0, -Bx, 0)$ where B is the magnitude of the magnetic field [19]. With this particular choice of gauge there is no explicit y -dependence in the Hamiltonian and thus the momentum in the y direction is conserved $[\hat{P}_y, H] = 0$. This gives a plane wave solution for the y -dependence of the wavefunction.

$$\Psi(x, y) = X(x) \frac{e^{ik_y y}}{\sqrt{L_y}}, \quad (1.7)$$

where periodic boundary conditions have been assumed such that $k_y = 2\pi n/L_y$ for some integer n and for L_y being the length of the system in the y -direction. Substituting the solution $\Psi(x, y)$ in the time independent Schrodinger equation with Hamiltonian (1.6) gives the following eigenvalue equation for the x -coordinate dependent part $X(x)$, of the wavefunction

$$\left(-\frac{\hbar^2}{2m} \frac{\partial^2}{\partial x^2} + \frac{m}{2} \omega_c^2 (x + l_B^2 k_y)^2 \right) X(x) = EX(x). \quad (1.8)$$

The magnetic length l_B is the natural length scale of the problem and ω_c is the cyclotron frequency which, corresponds to the minimum radius for the electrons circular motion in the magnetic field. Their definitions are given below.

$$\begin{aligned} l_B &= \sqrt{\frac{\hbar}{eB}} \\ \omega_c &= \frac{eB}{m} \end{aligned} \quad (1.9)$$

From inspection it can be seen that the eigenvalue equation (1.8) is equivalent to that of a one dimensional harmonic oscillator where $l_B^2 k_y$ is the shifted position of the center of the harmonic potential in the x -direction. Thus the energy spectrum of the charged particle in a uniform magnetic field is given by

$$E = \left(n + \frac{1}{2} \right) \hbar \omega_c \quad (1.10)$$

where n is some integer. Different values of n correspond to different Landau levels, with the lowest Landau level (LLL) given by $n = 0$. Note that in the LLL, the electron state is determined by a single quantum number, namely, the wave vector k_y . Solutions to (1.8) are given by

$$X_n(x) = H_n \left(\frac{x + l_B^2 k_y}{l_B} \right) \exp \left(-\frac{(x + l_B^2 k_y)^2}{2l_B^2} \right). \quad (1.11)$$

It is straightforward to show that l_B is the natural length scale of the system by considering the correspondence between the x -coordinate at which the harmonic oscillators in (1.8) are centered and the k_y momentum values; i.e. $x = -l_B^2 k_y = -l_B^2 p_y / \hbar$. By naively quantising this theory via $p_y = -i\hbar \partial_y$, then the commutator between the x and y coordinate is no longer zero, instead,

$$[x, y] = i l_B^2.$$

Thus positions x and y cannot be simultaneously localised to an area smaller than $\sim l_B^2$ near the centre of the one-dimensional harmonic oscillator. The area corresponding to a single flux quantum and therefore to an electron is $2\pi l_B^2$. The Landau levels are highly degenerate and in fact for an infinitely long system, the Landau levels would be infinitely degenerate. This degeneracy is caused by the continuous set of states for a free particle being compressed into a discrete

spectrum. To calculate this degeneracy, consider a system of length L_y in the y -direction and L_x in the x -direction. The y -axis passes through the centre of the system such that the y -directed edges intercept the x -axis at either $\pm L_x/2$ (see Figure 1.1). The largest possible momenta that an electron can occupy in the ground-state is obviously the Fermi momenta $\pm k_F$. Thus the number of states per Landau level (LL) N_D is a sum of k_y between the extremal values, since different values of k_y correspond to different states in a single Landau level.

$$N_D = \sum_{k=-k_F}^{k_F} 1 \rightarrow \frac{L_y}{2\pi} \int_{-k_F}^{k_F} dk_y = \frac{L_y k_F}{\pi}, \quad (1.12)$$

where the sum has been transformed into an integral over k_y assuming L_y is large. The extremal x -values are at the y -edges where $x = \pm L_x/2$. From the harmonic oscillator analysis, the relationship between x -space and momentum space k_y is $x = -l_B^2 k_y$ and thus $k_F = L_x/(2l_B^2)$. This value for the Fermi momenta can be substituted into (1.12). Using the form for the magnetic length given in (1.9) and recognising that $L_x L_y B$ is the total flux through the sample Φ and h/e is the magnetic flux quantum Φ_0 then

$$N_D = \frac{\Phi}{\Phi_0}. \quad (1.13)$$

Thus for each magnetic flux quantum penetrating the bar there is one state. Equation (1.13) allows the definition of another important quantity; the filling factor ν . It corresponds to the ratio of the number of electrons N to the number of available states N_D .

$$\nu = \frac{N}{N_D} \quad (1.14)$$

This is the same number that appears in the equation for the Hall resistivity at a

given plateau and it corresponds to the number of states that are occupied. $\nu \in \mathbb{Z}$ corresponds to some integer number of completely filled Landau levels, whereas $\nu = 1/3$ means that only a third of all states in the LLL are occupied.

By solving the eigenvalue equation for the Hamiltonian (1.6) the energy spectrum of the Landau levels have been derived for a single electron. These Landau levels are highly degenerate and for an integer number of filled Landau levels there is a gap of size $\hbar\omega_c$ to the next available state. In the next section it will be discussed how a slight modification to this LL spectrum can lead to the observed plateaus in the Hall resistivity measurements for the IQHE.

1.3 The Integer Quantum Hall Effect

The focus of this section is to discuss the causes for the observed plateaus in the Hall resistivity. The precise nature of how the Landau levels contribute to the transport of current through the system is also reviewed. The arguments presented here are not rigorous but the mathematical details can be found in the references given in this section.

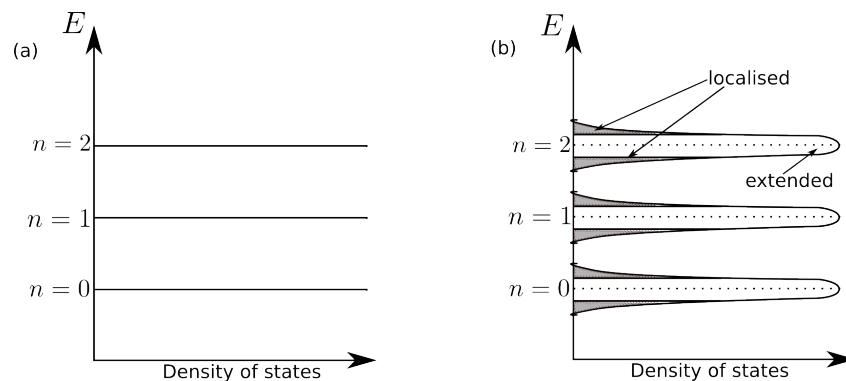


Figure 1.3: Density of states for the first three Landau levels for; (a) a clean system and (b) a dirty system containing impurities.

The 2DEG systems used in experiments are never completely free of impurities and

it turns out that it is these impurities that are essential to the observation of the QHE. The impurities cause the LLs to broaden and lifts some of the degeneracy. In turn the energy spectrum now consists of regions of extended states, in the centre of the LL and localised states at the tails of the broadened energy spectrum, see Figure 1.3. In QH experiments the Hall resistivity is measured as either the magnetic field is varied or the carrier density is varied. In both cases, this effectively means that the Fermi energy will change its position with respect to the Landau level spectrum.

The plateaus in the Hall resistivity and/or Hall conductivity appear when the Fermi energy is in a region of localised states, i.e. when some integer number of Landau levels are completely full. In this region increasing the Fermi energy only adds electrons to localised states and thus they make no difference to the total Hall conductivity. Since the longitudinal conductivity is entirely dependent on states at the Fermi energy [15], at a plateau the Fermi energy must lie in the region of localised states for $\sigma_L \rightarrow 0$. The Hall conductivity at a plateau, however could be determined by considering only the extended states below the Fermi energy. Laughlin [20] used the idea of this mobility gap between extended states along with gauge invariance arguments to calculate the Hall conductance which matched the experimental results.

Another important result used throughout this thesis which is applicable to both the IQHE and the FQHE is that the current in the system is only transported around the edges of the system and not through the bulk. This result was derived by Halperin [21] who showed that when the electron density tends to zero, there exists low-energy excited states which can transport current. Niu and Thouless [22] calculated the electron propagator of the edge states of the QHE and showed it was extended only in the direction along the edge and localized in all other directions. At the edges or near an impurity LLs bend upwards due to a confining potential that prevents electrons entering a forbidden region of space. Thus for

some cross-section of the 2DEG one would expect the energy profile to be similar to that shown in Figure 1.4.

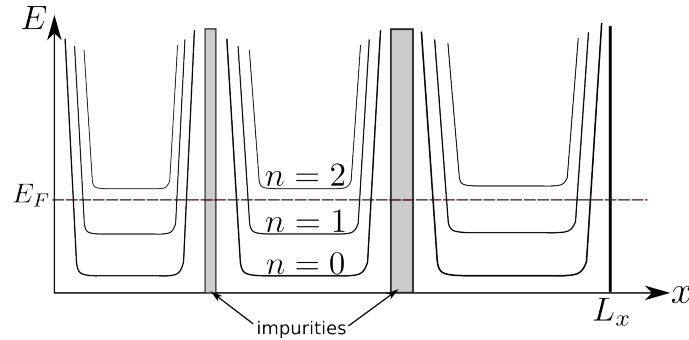


Figure 1.4: Energy levels of a 2DEG showing the first three LLs. The edges of the 2DEG are at $x = 0$ and $x = L_x$. Two impurities are also shown in the 2DEG depicted by the shaded regions.

The LLs are full up to the Fermi energy and therefore there always exist at the edges or around impurities extended states that support low energy excitations. In the bulk, however, at a plateau, the Fermi energy lies only in the region of localised states. Thus current is supported around the edges of a 2DEG or is confined to some impurity and thus will not contribute to measurements of the transport properties. This completes the brief review of the IQHE.

So far it has been shown to observe the QHE there must exist some mobility gap which arises naturally in the 2DEG as a consequence of the applied magnetic field. The mobility gap in the IQHE is the gap between extended states of the impurity-broadened LLs. So far from this analysis there is no reason why plateaus should exist at fractional values of filling factors. The remainder of this thesis is now focused on the FQHE with the next section introducing the Laughlin wavefunction.

1.4 The Fractional Quantum Hall Effect and Laughlin States

From experimental measurements of the Hall resistivity, the FQHE looks very similar to the IQHE, the only difference being that the filling factor ν is a fraction. However, the free fermion formalism that successfully predicts behaviours observed for the IQHE fails for the FQHE. The reason for this is there is no energy gap predicted within a given LL and so the FQHE is fundamentally very different to the IQHE. The fact that the FQHE is observed only in cleaner samples, lower temperatures and stronger magnetic fields [23] as compared to the IQHE suggests that a mobility gap Δ could be created by electron-electron interactions. The gap Δ within a LL then plays a similar role to the cyclotron energy gap for the IQHE.

For the remainder of this section and for the majority of this thesis, only plateaus in the Hall resistivity that correspond to the partially filled lowest Landau level (LLL) are considered. In particular we are interested in filling factors of the form $\nu = 1/m$ where m is an odd integer in this extreme quantum limit. When all electrons occupy the LLL, the kinetic energy is fixed and only the Coulomb energy and the effect of impurities need to be considered. So far there does not exist any analytic wavefunction to solve the Hamiltonian with the 2D Coulomb interaction, although it is possible to numerically compute the exact ground-state for a limited number of particles using the method of diagonalisation [13].

Pioneering work for states with $\nu = 1/m$ was carried out by Laughlin and much of the information reviewed here is from Laughlin's work [13] and his discussion in Ref. [23]. Laughlin postulated the idea of the formation of an incompressible fluid which acts to stabilise the system at particular particle densities corresponding to $\nu = 1/m$. To produce an approximate ground-state wavefunction for this system Laughlin used the reasoning; it must be anti-symmetric, reduce the amplitude of finding two electrons close together which, consequently reduces the Coulomb

repulsion and also that the wavefunction must be an eigenstate of the total angular momentum. The form of Laughlin's wavefunction is;

$$\Psi_N = \prod_{i < j}^N (z_i - z_j)^m \exp \left(- \sum_k \frac{|z_k|^2}{4l_B^2} \right), \quad (1.15)$$

where the set $\{z_i\}$ are electron coordinates on the complex plane and N is the total number of electrons in the system. The polynomial term (written above as a product) is holomorphic and reduces the probability amplitude for finding two electrons close together. Its power m must be an odd integer to keep the total wavefunction anti-symmetric. The value of m appearing in the wavefunction will be shown in the next section to be equivalent to the inverse filling factor, i.e., $\nu = 1/m$. The wavefunction (1.15) describes a circular droplet of a 2DEG and will be referred to as Laughlin's wave function. The total angular momentum of the state is $mN(N-1)\hbar/2$ and this value is proportional to the degree of the polynomial in Eq. (1.15). The maximum angular momentum, $\hbar l_{\max}$ of a given electron in the Laughlin droplet is given by the maximum power of a variable in the polynomial, so for state (1.15), $l_{\max} = m(N-1)$. Different values of l correspond to different orbitals in the LLL, from observing the various powers of the variables $\{z_i\}$, only orbitals $l = mk$, where k is an integer from 0 to $N-1$ are occupied by electrons, the remaining orbitals are vacant.

It will be shown later in Section 1.6, that the radius of the quantum droplet fluid described by (1.15) is dependent on the number of particles N and the number of any quasiparticles or quasiholes inserted into the system. Thus the area of the droplet cannot be altered without the injection or removal of particles from the system. Systems behaving in this way are incompressible and there is a cost in energy to add particles into the system. The fact that the Laughlin wavefunction predicts the existence of some energy gap Δ within the LLL, which is required to observe plateaus in the Hall resistivity, lends support for Eq. (1.15) being a valid

microscopic representation of the FQHE.

Although Laughlin's variational wavefunction is not an eigenstate of the exact Hamiltonian, it has been shown to have a large overlap with the exact eigenstate for a limited number of particles where the Coulomb Hamiltonian can be diagonalised numerically. Laughlin states are however an exact ground state for a similar two-particle interaction Hamiltonian known as Haldane pseudo-potentials [24] which will be discussed in more detail in Chapter 3. A powerful observation that Laughlin made about the wavefunction (1.15) was that it showed strong similarities to the system for a one component plasma. This analogy is responsible for many interesting predictions about the FQH system and this idea will be developed in the next section.

1.4.1 Analogy Between the Laughlin State and the One-Component Plasma

From statistical mechanics, the local density at a given position \mathbf{r} is

$$\langle \rho(\mathbf{r}) \rangle = \frac{N \int d\mathbf{r}_2 \dots d\mathbf{r}_N Z(\mathbf{r}, \mathbf{r}_2, \dots, \mathbf{r}_N)}{\int d\mathbf{r}_1 \dots d\mathbf{r}_N Z(\mathbf{r}_1, \mathbf{r}_2, \dots, \mathbf{r}_N)}, \quad (1.16)$$

where $Z(\mathbf{r}_1, \mathbf{r}_2, \dots, \mathbf{r}_N)$ is the partition function and the density operator is given by $\rho(\mathbf{r}) = \sum \delta(\mathbf{r} - \mathbf{r}_i)$. The partition function may be written in terms of the potential ε as

$$Z(\mathbf{r}_1, \mathbf{r}_2, \dots, \mathbf{r}_N) = e^{\beta \varepsilon}. \quad (1.17)$$

Using the Laughlin wavefunction one can calculate the local density at a given point z for the lowest Landau Level.

$$\langle \hat{\rho}(z) \rangle = \frac{N e^{-\frac{|z|^2}{2l_B^2}} \int \prod_{i=2}^N \left(d^2 z_i e^{-\frac{|z_i|^2}{2l_B^2}} |z - z_i|^{2m} \right) \prod_{i=2 \leq j}^N |z_i - z_j|^{2m}}{\int \prod_{i=1}^N \left(d^2 z_i e^{-\frac{|z_i|^2}{2l_B^2}} \right) \prod_{i \leq j}^N |z_i - z_j|^{2m}} \quad (1.18)$$

Requiring the quantum mechanical result be equivalent to the statistical result, we must have

$$\beta \varepsilon = m \left(\sum_{i < j}^N \ln |z_i - z_j|^2 + \sum_{n=1}^N W(z_n) \right), \quad (1.19)$$

where

$$W(z) = -\frac{|z|^2}{2ml_B^2}. \quad (1.20)$$

Here ε has the form of a potential that describes a one component, two dimensional plasma [25]. The first term in the above expression is the interaction potential between the charged particles whilst the second term is the background potential. Defining $\beta = -m$, m is therefore inversely proportional to the temperature. From the theory of plasmas, at small temperatures (corresponding to large m) plasmas are known to crystallize and there is evidence of a phase change for the Laughlin quantum fluid to a Wigner crystal at filling factors $\nu \leq 1/7$ [26]. Knowledge of the behaviour of plasmas can be exploited to help describe the FQHE phenomenon for $\nu > 1/7$.

If ρ_0 denotes the equilibrium configuration of charges then the maximum energy can be found from

$$\frac{\partial \varepsilon}{\partial z_i} = \sum_{j=1, \neq i}^N \frac{1}{z_i - z_j} + \frac{\partial}{\partial z_i} W(z_i) = 0. \quad (1.21)$$

In the continuum limit for large N values, this reads as

$$\frac{\partial}{\partial z} (\Phi_0(z) - W(z)), \quad (1.22)$$

where Φ_0 is the Coulomb potential for the equilibrium charge distribution which, is given in the large N limit by

$$\Phi_0(z) = - \int d^2 \zeta \ln |z - \zeta|^2 \rho_0(\zeta). \quad (1.23)$$

Applying partial differentiation with respect to \bar{z} to Eq. (1.22) gives a simple equation for calculating the equilibrium density using the background potential $W(z)$.

$$\Delta W(z) = \Delta \Phi_0(z) = -4\pi \rho(z), \quad (1.24)$$

where in the final expression of Eq. (1.24) Poisson's equation has been used. Therefore by calculating the Laplacian ($\Delta = 4\partial_z \partial_{\bar{z}}$) of the background potential, the equilibrium density of charges can be calculated in the large N limit.

$$\rho(z) = -\frac{1}{4\pi} \Delta W(z) = \frac{1}{2\pi m l_B^2} \quad (1.25)$$

Using the above expression for density one can show that Laughlin states actually correspond to filling factors $\nu = 1/m$. It was shown previously in the chapter that the degeneracy per Landau level is $N_D = \Phi/\Phi_0$; thus for each magnetic flux

quantum penetrating the sample there is a single state. Since $N_D/A = 1/(2\pi l_B^2)$, where A is area of the sample, the filling factor from Eq. (1.14) is $\nu = N/N_D = 2\pi l_B^2 \rho = 1/m$.

Laughlin's plasma analogy has also been used to make interesting predictions about the nature of the quasiparticles that arise from the system described by Eq. (1.15), which are the subject of the next section.

1.4.2 Laughlin Excitations

The one-component plasma (OCP) analogy introduced in the previous section provides an ideal setting for an investigation into the type of excitations that are supported by the Laughlin state. The arguments presented here can be found in Ref. [13]. Imagine that our FQH system is disk-shaped with a hole in the centre through which an infinitely long solenoid is inserted such that the flux in the conductor can be varied without altering the magnetic field. Through this solenoid a single flux quantum is passed adiabatically. The result of this process is that the Hamiltonian describing the system with the extra flux quantum added \hat{H}' differs from the original Hamiltonian \hat{H} via a gauge transformation. Therefore using a suitable gauge transformation, one can obtain an exact excited state of the original \hat{H} after the quantum flux was added to the system. Thus the excited state corresponds to the creation of a quasiparticle or quasihole depending on the sign of the quantum flux. Adding the quantum flux to the system (first consider the quantum flux to be positive) must increase the outermost Landau orbital, l by 1. Therefore the maximum l -value of the system is now $(N - 1)m + 1$ rather than $(N - 1)m$. This new state satisfying the above properties can be written as,

$$\Psi_m^{+z_0} = \prod_{i=1}^N (z_i - z_0) \Psi_m(z_1, z_2, \dots, z_N). \quad (1.26)$$

I.e., The new state is the Laughlin state multiplied by the product of the difference between the original particle coordinates z_i and the position of the solenoid z_0 (the position where the solenoid pierces the quantum liquid has been generalised to any position z_0 rather than just at the origin). Since $\langle \Psi_m^{+z_0} | \sum_i \delta(z_i - z_0) | \Psi_m^{+z_0} \rangle = 0$, there is a zero probability of finding a particle at z_0 and thus it is concluded that we have created a quasihole at this position. Equation (1.26) can be generalised for the creation of M quasiholes at positions w_1, \dots, w_M via the above reasoning as,

$$\Psi_m^{+w_1, \dots, +w_M} = \prod_{i=1}^N \prod_j^M (z_i - w_j) \Psi_m(z_1, z_2, \dots, z_N). \quad (1.27)$$

Using the analogy between the FQH system and the OCP, the charge of the quasi-hole can be calculated as follows [15]. Writing the magnitude squared of the wavefunction in (1.26) as an exponential of the potential, i.e.,

$$|\Psi_m^{+z_0}|^2 = e^{\beta \tilde{\varepsilon}}. \quad (1.28)$$

The corresponding potential $\tilde{\varepsilon}$ can be written in terms of the potential from the Laughlin wavefunction ε (1.19) with an extra logarithmic term;

$$\beta \tilde{\varepsilon} = 2m \sum_{i < j}^N \ln |z_i - z_j| + 2 \sum_k^N \ln |z_k - z_0| - \sum_n^N \frac{|z_n|^2}{2}. \quad (1.29)$$

Again the above potential is that of a classical one component plasma; however there is an extra charge positioned at z_0 whose potential is weaker by a factor of $1/m$ compared to the potential of the existing charges in the plasma. Plasmas behave as to keep the system electrically neutral wherever possible, and therefore the system will attempt to neutralise the quasi-hole with an accumulation of $1/m$ charge near z_0 . Elsewhere the charge density will remain unchanged and constant.

Since it is the electrons in the system which carry the real electric charge, the accumulation at z_0 has a net charge of $-e/m$ once the electron charge density cancels with the uniform background density. Thus it is concluded that the quasihole at z_0 must have a charge $-e/m$ where $-e$ is the electron charge.

Changing the sign of the quantum flux added to the system via the solenoid will thus create a quasiparticle and according to the reasoning above, the maximum powers of the z_j in the Laughlin wavefunction will decrease by a unit value. One way in which this can be done is to apply $\partial/\partial z_i$ to the polynomial part of the wavefunction. To generalise to the creation of such a quasiparticle at the arbitrary point z_0 , the resulting state is given by

$$\Psi_m^{-z_0} = \prod_{i=1}^N \left(\frac{\partial}{\partial z_i} - \frac{z_0}{l_M^2} \right) \Psi_m(z_1, z_2, \dots, z_N). \quad (1.30)$$

Since the quasihole created by the extra quantum flux added to the system has a charge of $-e/m$, it can be concluded that the quasiparticle must have charge $+e/m$, created when removing a quantum flux. Not only do Laughlin quasiparticles have a fractional charge, but they also obey fractional statistics. This can be seen from calculating the Berry phase when a single quasiparticle adiabatically encircles a second quasiparticle in the system [27]. The statistical phase gain from this transformation is given by $2\pi\nu$, where ν is the filling factor. The Berry phase is equivalent to a double exchange of the two quasiparticles; thus for a single exchange the wavefunction gains the phase $\pi\nu$. The fact that this result does not give a resulting Berry phase of simply 2π is intriguing since the result shows that even though the original and the final systems of quasiparticles are identical, the wavefunction has undergone a transformation. The reason for this is the two-dimensional nature of the system, where the operation of exchanging two particles twice over is not equivalent to an identity transformation as it is in three or more dimensions. Imagine adiabatically transporting a quasiparticle around a

stationary, second quasiparticle. In three or more dimensions this path can be continuously deformed into a point, thus the total phase gain by this operation must be equal to 2π . In two dimensions, however, the path of the quasiparticle around the stationary, second quasiparticle cannot be deformed to a point because of the singularity of the stationary quasiparticle position in the plane. Thus the phase gain does not necessarily have to be equal to 2π .

Particles obeying fractional statistics are referred to as anyons since the interchange of two such particles can result in any change of phase. There has been success in observing the fractional statistical behaviour of Laughlin-type quasiparticles in QH bars using interference experiments [28, 29]. The fractional statistics of Laughlin state quasiparticles is referred to as Abelian statistics and there is a proposal that some quasiparticles in FQH states may actually obey the less-trivial non-Abelian statistics.

Non-Abelian statistics is a consequence of states containing multiple quasiparticles being topologically degenerate [30]. In such cases exchanging identical particles can result in the wavefunction undergoing a unitary transformation between degenerate ground-states. FQH bars with quasiparticles obeying non-Abelian statistics have been proposed as a potential qubit for a topological quantum computer [31–35] though actually observing the non-Abelian statistics in FQH systems has proved more difficult than for the Abelian case. One possible non-Abelian QH state is the Moore-Read Pfaffian state to describe e.g., $\nu = 5/2$ [36, 37] which is a particular example of a more general class of non-Abelian states, the Read-Rezayi states [38]. However, the Moore-Read Pfaffian state is not the only proposed ground-state for the $\nu = 5/2$ FQHE [39] and it has been proposed that interference experiments (similar to those carried out for Abelian quasiparticle FQH states) should help resolve the issue of its microscopic description [40]. So far there have been no clear results from interference experiments with regards to this matter [41–44].

This section completes all the introductory material needed for a basic understand-

ing of Laughlin's wavefunction and the one component plasma analogy. It will be used continuously in this thesis as a microscopic representation of the FQH states with filling factors $\nu = 1/m$, where m is odd. In particular the Laughlin state will be used as a base for computing transport properties microscopically for a FQH device and in the next section key ideas involving transport properties of the FQHE will be discussed.

1.5 Review of Literature Probing Transport Properties in the FQHE

The primary focus of this thesis is on the transport properties of the FQHE which, since the bulk states are incompressible, are determined by the 1D edge states of the system. In this section a short overview will be given on the current theoretical understanding of the edge states in the FQHE as well as the compatibility of the theory with experiments. The discussion here will provide a motivation for the work completed in later chapters and is based on the introduction of the work by this author and V. Cheianov [45].

The 1D edge states in the FQHE consist of interacting electrons for which the Fermi liquid theory breaks down and it was first proposed by Wen [46] that they should instead, be described by a chiral Luttinger liquid. A chiral Luttinger liquid has the key feature of low-energy excitations being collective sound modes and it can be shown that the system has a four-terminal Hall conductance given by $\nu(e^2/h)$ [46]. In chapter 3 the formalism for the chiral Luttinger liquid will be introduced. It is a phenomenological theory useful for describing transport properties of the FQHE which are readily accessible to experimental measurements.

More recently, a great amount of theoretical and experimental effort has focused on the transport properties of FQH edge states when the charge carriers are faced with

a single, or multiple potential barriers and tunnelling is observed. There are two equivalent methods to initiate tunnelling in a QH device. The most common from an experimentalist's point of view is by physically moving the edges closer together at some point along a Hall bar, known as a quantum point contact (QPC). Such a constriction can be achieved by placing metallic plates above the 2D electron gas and applying a negative bias causing a local depletion of electrons. As a result edge states are brought closer together causing a finite probability of inter edge back scattering. The strength of this pinching effect on the edge states is determined by the magnitude of the bias applied to the magnetic plates. For ideal systems, the same tunnelling behaviour can be obtained from placing an impurity into the bulk which also couples the edges and allows back scattering to occur. Realistically using an impurity is a much cleaner method to observe backscattering since a QPC can have adverse effects on the surrounding quantum Hall fluid due to electrostatic reconstruction [47].

One of the first pieces of work concerned with tunnelling at a QPC was carried out by Kane and Fisher [48–50] who investigated tunnelling at both a weak link and a weak barrier in a conventional Luttinger liquid. Similar work was also carried out by Furusaki and Nagaosa [51] and Moon *et al.* [52]. At a weak link tunnelling will be dominated by electrons in the Luttinger liquid since, effectively the liquid is split into two separate islands. For a weak barrier however it is the excitations of the Luttinger liquid that tunnel. For the work carried out by Kane and Fisher a perturbative approach for the tunnelling Hamiltonian was used in conjunction with the renormalization group (RG) to discover which of the tunnelling processes were relevant in both the strong and weak back scattering limit and predictions were made about the tunnelling conductance and the zero-bias peaks in I-V characteristics. The predictions about the Luttinger liquid behaviour is in stark contrast to that of the non-interacting system, the Fermi liquid. Here, unlike the non-interacting case, the width of the zero-bias peaks are temperature dependent, and in particular the conductance away from the peak has a power law

temperature dependence where the exponent of the power law is the interaction parameter (determining the strength of the interactions between electrons) of the Luttinger liquid. The reason for the differences is of course down to the interactions between the Fermions in 1D and thus observing such behaviour in a 1D channel will be key in discovering systems that are strongly correlated, non-Fermi liquids. The form of the tunnelling Hamiltonian used in all of the referenced works in this section can be mapped onto the boundary sine-Gordon model [53] and consists of operators that annihilate a charge carrier in one direction and create another carrier traveling in the opposite direction at some barrier.

So far there is experimental agreement of non-Fermi liquid behaviour in the Laughlin type edge states of a FQH device [54, 55] though the specific value of the power of the temperature dependence of the tunnelling conductance is slightly off the expected theoretical value [56]. Experiments measuring shot noise and interference experiments (all making use of one or multiple point contacts) are predicted to prove the existence of fractionally charged carriers in the edge states as well as display their (Abelian or non-Abelian) fractional statistics. In particular it has been predicted that for Laughlin type QH states, the back scattered current in shot noise experiments should be proportional to the charge of the carriers [57] given by $e^* = \nu e$ in the weak back scattering limit at zero temperature, where ν is the filling fraction of the lowest Landau level. Experimental work has claimed to have observed Laughlin type quasiparticles in such experiments [58, 59] though not all of the work agrees that the shot noise measurement is dependent only on the charge of the quasiparticles. It has been claimed that the specifics of the tunnelling barrier as well as the energy regimes used in the experiment can effect the value of the back scattered current. This would account for a deviance in the predicted value of the quasiparticle charge in the very weak back scattering limit obtained in some experiments [60]. In particular, the boundary sine-Gordon model for various test states has not been able to resolve which ground state provides a good description for even denominator filling fractions such as $\nu = 5/2$. Experiments

at quantum point contacts for the $\nu = 5/2$ states which measure tunnelling noise and tunnelling conductance give predictions for quasiparticle charge e^* and the tunnelling particles interaction parameter, g [61]. There is still no obvious match to the theoretical predictions of the various candidate states for the edges in the $\nu = 5/2$ system [43] and even distinguishing whether the state should display Abelian or non-Abelian statistics is not obvious [39]. This problem was briefly mentioned in the previous section.

The RG approach by Kane and Fisher is based on a 1D lattice model and it is assumed that the edge states of the FQHE will display similar behaviour so this approach is frequently used as a base model for theoretical predictions on transport properties of the FQHE. There are important differences between the Luttinger liquid model used for the perturbative RG analysis by Kane and Fisher and the FQH edge states. The electron field operators in the Luttinger liquid model can be derived microscopically from the 1D Hamiltonian describing a system of interacting electrons. It is not the same for the FQH edge states since in this case, the edge states result from a two-dimensional system of electrons in a strong magnetic field, thus the low-energy effective theory is obtained by projecting the FQH states onto the space of low energy edge states. The perturbative RG approach that works so well for the lattice model Luttinger liquid cannot be extended straightforwardly to the FQH edge states since it relies on the fact that interactions between electrons can be treated perturbatively. Switching off the electron-electron interactions in the FQHE will result in a completely different system altogether. So how do these differences affect the formulation of a chiral Luttinger liquid as compared to that of a conventional Luttinger liquid?

It is already understood that the low energy projection of the edge states in the FQHE do not display exactly the same behaviour as the Luttinger liquid. One example is the low energy projection of the electron field operator. In the Luttinger liquid the anti-commutation relation for two spatially separated electron fields is

given by a delta function, the same behaviour of similar fields in the edge states of a FQH system is not observed. There is another issue with the locality of the effective tunnelling Hamiltonian for a quasiparticle being transferred between two disconnected edges in the system. In the FQHE the tunnelling Hamiltonian takes a similar form to that of the tunnelling Hamiltonian in the conventional Luttinger liquid, i.e., the operator consists of creating a particle in one of the QH edge states and annihilating a particle in the opposing edge [52, 62]. Without the perturbative RG analysis at our disposal for FQH states there is no guarantee that the effective theory tunnelling operators will be local. For the Luttinger liquid model however, local operators in the microscopic theory are guaranteed to remain local in the effective theory using the Kadanoff coarse graining procedure.

The problem of the locality of the tunnelling Hamiltonian has been investigated for a FQH system containing multiple quantum point contacts. It was observed that the tunnelling operators at one of the QPC's did not commute with the tunnelling operator at a different QPC, independent on the magnitude of their spatial separation [63]. To impose the expected locality to which the quasiparticle tunnelling operators should adhere, the effective quasiparticle operators had additional Klein factors included in their representation [63–69]. The addition of the Klein factors adds an extra phase to the quasiparticle fields and it is reasoned that this is a statistical phase which is gained during a tunnelling event between two disconnected edges. This statistical phase is a result of the fractional statistics obeyed by the quasiparticles. Including Klein factors results in the effective quasiparticle tunnelling operators at two different QPC to commute with one another. Results on observables such as tunnelling currents are greatly dependent on the inclusion of these Klein factors (for example compare work by Law *et al.* [66] with Jonckheere *et al.* [70]).

To conclude, the model used to describe tunnelling in the FQHE has not been tested microscopically so far. The model is based on the work carried out on a

conventional Luttinger liquid system and there is no obvious reason that applying this work to a chiral Luttinger liquid should provide a true representation of the behaviour observed in the FQHE. Tunnelling between edge states in the FQHE is therefore an interesting property to be studied, in particular, predictions made by the tunnelling Hamiltonian should be tested microscopically. Original work concerning this issue is presented in Chapter 4 of this thesis. The geometry of the FQH device that will be used in both Chapter 3 and Chapter 4 is introduced in the next section of this introduction.

1.6 Disk Geometry Fractional Quantum Hall Device

The first few chapters of this thesis concentrate on a FQH system with a particular type of geometry that is introduced in this section for later reference. The FQH device of interest consists of a ring of Laughlin-type FQH fluid with filling factor given by $\nu = 1/m$ where m is an odd integer. This FQH device is shown in Figure 1.5. This geometry has been chosen due to its convenient ground state wavefunction, which has axial symmetry. Experiments are typically performed using a Hall bar geometry such as that shown in Figure 1.1, however the properties of interest, discussed later in this thesis, are not affected by the choice between the ring, or Hall bar geometry. The inner radius of the ring is labelled as R_I and the outer radius is given by R_O . For convenience in later works, the domain corresponding to the inside the ring ($|z| < R_I$) is denoted by D^I and the domain which confines the charges ($R_I \leq |z| \leq R_O$) is denoted by D^M .

To create the macroscopic hole occupying the domain D^I , an integer number of M quasiholes are inserted at the center of the droplet at the coordinate $z = 0$. Including the M quasiholes means that the wavefunction describing this system,

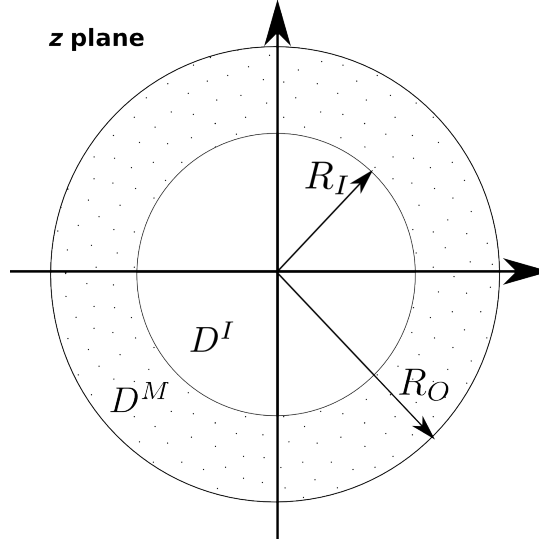


Figure 1.5: Schematic diagram for the FQH device with disk geometry. Electrons are confined to the domain D^M on the complex plane and at the edges of this domain there is a sharp decrease to zero in particle density. The radii of the inner and outer edge of D^M are given by R_I and R_O respectively. Inside the domain D^I a number M of quasiholes have been inserted at the coordinate $z = 0$ to create the inside edge of the disk. Regions excluding the domains D^M and D^I contain a vacuum.

from (1.26) is given by

$$\Psi_N^M = \prod_{i < j}^N (z_i - z_j)^m \prod_k^N z_k^M e^{-\frac{|z_k|^2}{4l_B^2}}. \quad (1.31)$$

For a ring of sufficiently large width, i.e. $R_O - R_I \gg l_B$, transport in the system will be confined to the edges due to the bulk being incompressible. At the interfaces of the domain D^M with the vacuum domains, there will be a sharp decrease to zero in particle density. The larger the number of electrons N inside domain D^M , then the sharper the decrease to zero in particle density. For the work carried out in this thesis, we will mainly be interested in the large N -limit where the density can be considered as a constant throughout the bulk of the system. In the region of the magnetic length of the radius of the FQH droplet there is an overshoot in the magnitude of the particle density before it drops to zero. This is a consequence

of the electron-electron correlations in the FQH fluid [71, 72].

The size of the macroscopic hole in the center of the droplet will depend on the number of quasiholes M inserted at the center of the complex plane. To obtain an expression for R_I in terms of M it is noted that if the area of the domain D^I was filled with electrons (rather than quasiholes), then one could fit $\pi R_I^2 \rho$ electrons into this space. Since a quasihole has charge $e^* = e/m$, then a single quasihole is $(1/m)$ 'th of a missing electron and so the domain D^I actually consists of M/m missing electrons. Therefore $\pi R_I^2 \rho \equiv M/m$ which when using the value for the electron density $\rho = 1/(2\pi m l_B^2)$ gives

$$R_I = l_B \sqrt{2M}. \quad (1.32)$$

A similar method can be used to find an expression for R_O in terms of the parameters appearing in wavefunction of the system. Inside the area πR_O^2 there are effectively $N + (M/m)$ electron-type particles and so $\pi R_O^2 \rho \equiv N + (M/m)$ which gives the magnitude of the outer radius of the ring to be

$$R_O = l_B \sqrt{2mN + 2M}. \quad (1.33)$$

These equations for the radius R_I and R_O show explicitly that system described by Laughlin is indeed incompressible since altering the area of the droplet will subsequently inject or remove electrons from the system. Altering the value of M however still preserves the area of the quantum fluid since the quasiholes correspond to low-energy excitations of the inner boundary. A detailed discussion of the low-energy edge excitations is given in Chapter 3. Since we have used $\rho = 1/(2\pi m l_B^2)$, the values for R_I and R_O are exact for the large N limit.

In this introduction both the IQHE and the FQHE have been described and in

particular the reasons for the observed plateaus in the resistivity measurements have been explained. For the IQHE, a free electron system can be considered where interactions between charges are completely disregarded. In this picture, the energy spectrum is the gaped Landau level dispersion, which with the presence of impurities in the 2DEG provide an explanation for the resistivity plateaus. One can only explain the plateaus in the FQHE however by using strongly correlated electrons. These interactions between the charges result in an energy gap opening up within the LL's. These gaps caused by electron correlations then play a similar role to the LL gaps in the IQHE.

The Laughlin wave function has also been introduced. This state provides a microscopic wavefunction for FQH states occupying the LLL. The bulk of the quantum fluid described by this state is incompressible; however low-energy excitations can be created at the edge of the fluid. Such properties, and many others, can be shown using the Laughlin plasma analogy. In Section 1.5 the importance of these low-energy excitations was discussed with respect to measurements on the transport properties of the FQHE. The concept of tunnelling across the bulk states was also discussed and how there is a lack of a solvable, microscopic description of this process in the FQHE. Original work completed with regards to the effective theory description of tunnelling will be presented in Chapter 4, after operators in the chiral Luttinger liquid theory have been derived in Chapter 3. A large part of the original work presented in this thesis uses the Monte Carlo (MC) method. This will be the subject of the next chapter.

CHAPTER 2

The Monte Carlo Method

A large amount of original work presented in this thesis uses the Monte Carlo (MC) method. In this section the main ideas and processes of MC simulations are introduced. Particular attention is paid as to how the method can be applied for computing observables in the microscopic representation of FQH systems. The MC technique has proved to be a powerful tool for studies concerning the one-component plasma (OCP) [73–76]. Since the Laughlin states for the FQHE can be represented in terms of the partition function of this plasma, naturally the MC computations have been extended to calculate many observables such as particle densities and excitation energies of the Laughlin wavefunction [71, 77, 78].

The main problem for analytically calculating observables for Laughlin states is that we are interested in the thermodynamic limit of the FQH system which holds for a large number of particles ($N \rightarrow \infty$). This means that to calculate expectation values of a general operator, \hat{A} for a Laughlin system, for example given by;

$$\langle A \rangle = \frac{\langle N, M | \hat{A} | N, M \rangle}{\langle N, M | N, M \rangle} = \frac{\int \prod_{k=1}^N d^2 z_k \bar{\Psi}_N^M \hat{A} \Psi_N^M}{\int \prod_{k=1}^N d^2 z_k |\Psi_N^M|^2}, \quad (2.1)$$

one must calculate a large number ($2N$) of integrals. In Eq. (2.1), Ψ_N^M is the wavefunction for the LLL with disk geometry originally stated in Eq. (1.31) and $\bar{\Psi}_N^M$ is its complex conjugate. For $\nu \neq 1$, where ν is the filling factor, there is no simplification one can make to calculate these integrals analytically and thus one must look to numerical methods such as the Monte Carlo procedure [79].

Looking at the averages in Eq. (2.1), the computation process that is commonly used to calculate averages with respect to some trial wavefunction is the variational Monte Carlo method, first used in calculations by W. L. McMillan [80]. The most straightforward description to discuss how the variational MC algorithm can be implemented for FQH correlators is by substituting the plasma analogy $|\Psi_N^M|^2 = e^{-\beta E}$ into Eq. (2.1) to give the following expression for the expectation value of \hat{A} .

$$\langle A \rangle = \frac{\int \prod_{k=1}^N d^2 z_k e^{-\beta E} \hat{A}}{\int \prod_{k=1}^N d^2 z_k e^{-\beta E}}. \quad (2.2)$$

The expression (2.2) is now in a form reminiscent of the familiar statistical averages with the denominator being thought of as the partition function of the system. Monte Carlo computations can provide an estimate for the expectation value of \hat{A} by sampling possible states at random from a probability distribution $p(z_1, z_2, \dots, z_N)$ to perform the average. From (2.2) one can see that the partition function is a continuous function and thus there are an infinite number of states to be averaged over. Averaging over an infinite number of states is numerically impossible and one must provide a cutoff Λ to the number of states used in the average. Introducing the cutoff will introduce some statistical errors, though for now there is no better method to perform the calculation exactly. So suppose Λ states $\{\lambda_1, \lambda_2, \dots, \lambda_\Lambda\}$ are chosen with probabilities $\{p_{\lambda_1}, p_{\lambda_2}, \dots, p_{\lambda_\Lambda}\}$ respectively, then the best estimate for $\langle A \rangle$ is now a discrete sum of the states λ_i rather than

an integral over the continuum of states,

$$A_\Lambda = \frac{\sum_{i=1}^{\Lambda} A_{\lambda_i} p_{\lambda_i}^{-1} e^{-\beta E_{\lambda_i}}}{\sum_{j=1}^{\Lambda} p_{\lambda_j}^{-1} e^{-\beta E_{\lambda_j}}}. \quad (2.3)$$

The quantity A_Λ is known as the estimator. For an accurate value for the estimator A_Λ one needs to include the states λ_i that give the largest contributions to the sum in (2.3). This process is known as importance sampling. Physical systems choose states to occupy according to the Boltzmann probability distribution, which states that the probability of the system occupying state λ_i is given by $p_{\lambda_i} = Z^{-1} e^{-\beta E_{\lambda_i}}$. It therefore makes sense to use this probability distribution for finding states which have the largest contribution to the estimator. Substituting the Boltzmann probability distribution into (2.3) gives;

$$A_\Lambda = \Lambda^{-1} \sum_{i=1}^{\Lambda} A_{\lambda_i}. \quad (2.4)$$

The next step is to form an algorithm that generates states according to the Boltzmann probabilities. This is done using the Markov process such that if the system starts in some initial state, then after a long enough running time the Markov process generates a succession of states for the system with probabilities given by the Boltzmann distribution. The states generated in this process are called the Markov chain of states.

To show how the Markov process works, one needs to define transition probabilities $P(\lambda_i \rightarrow \lambda_j)$ that give the probability that the state λ_j will be the next state in the Markov chain when the system is currently occupying state λ_i . Transition probabilities have the following conditions imposed: (i) they do not vary over time and (ii) they do not depend on the history of the Markov chain (i.e., the states

that the system has already passed through), they only depend of the current state λ_i and the next possible state in the Markov chain, λ_j . (iii) The transition probabilities must of course satisfy

$$\sum_j P(\lambda_i \rightarrow \lambda_j) = 1 \quad (2.5)$$

such that they have the correct normalisation. This constraint guarantees that at each step in the Markov chain the system will definitely be in some final state, even if it is the same as the initial state. With the transition probabilities now defined, the conditions placed on the Markov chain can now be discussed. These are the condition of ergodicity (CoE) and the condition of detailed balance (CoDB). When both of these conditions, described below, are imposed on the Markov chain then it is guaranteed that once the process has been run for a sufficiently long time, the equilibrium distribution of states being generated will match the Boltzmann distribution.

1. Condition of ergodicity (CoE): It should always be possible to reach any other state in the system from some initial state in a finite number of steps.
2. Condition of detailed balance (CoDB):

$$p_{\lambda_i} P(\lambda_i \rightarrow \lambda_j) = p_{\lambda_j} P(\lambda_j \rightarrow \lambda_i). \quad (2.6)$$

By following the CoE, one makes sure that every state has a non-zero probability of being accessed at some point in the Markov chain, just like the Boltzmann probability is non-zero for all possible states for the system. The CoDB on the other hand makes sure that the equilibrium distribution is in fact the Boltzmann distribution as opposed to some other probability distribution. The equation (2.6) comes from the fact that by the definition of a system in equilibrium, the proba-

bility for a transition into a state and out of that state must be equal. It is once the system reaches equilibrium and the probability distribution matches that of the Boltzmann distribution that measurements for the observable (for example, A_Λ in (2.3)) can be taken.

Using (2.6) and the fact that one wishes for a probability distribution equivalent to Boltzmann distribution when the system reaches equilibrium, the transition probabilities must satisfy

$$\frac{P(\lambda_i \rightarrow \lambda_j)}{P(\lambda_j \rightarrow \lambda_i)} = \frac{p_{\lambda_j}}{p_{\lambda_i}} = e^{-\beta(E_{\lambda_j} - E_{\lambda_i})}. \quad (2.7)$$

The next question is how are the transition probabilities chosen? So far there only exists a condition on the ratios of the transition probabilities and so they are not uniquely determined. This question can be avoided altogether by introducing acceptance ratios. Imagine that the transition probabilities are split into two parts such that,

$$P(\lambda_i \rightarrow \lambda_j) = g(\lambda_i \rightarrow \lambda_j)A(\lambda_i \rightarrow \lambda_j) \quad (2.8)$$

and therefore Eq. (2.7) becomes

$$\frac{P(\lambda_i \rightarrow \lambda_j)}{P(\lambda_j \rightarrow \lambda_i)} = \frac{g(\lambda_i \rightarrow \lambda_j)A(\lambda_i \rightarrow \lambda_j)}{g(\lambda_j \rightarrow \lambda_i)A(\lambda_j \rightarrow \lambda_i)} = e^{-\beta(E_{\lambda_j} - E_{\lambda_i})}. \quad (2.9)$$

The probabilities $g(a \rightarrow b)$ are called selection probabilities and $A(a \rightarrow b)$ are called acceptance ratios. To see the benefits of this notation it is noted that (2.9) is always satisfied for the same final and initial state (say, state λ_i), no matter what the value is for $P(\lambda_i \rightarrow \lambda_i)$. Therefore there is freedom in choosing and manipulating other transition probabilities $P(\lambda_i \rightarrow \lambda_j)$ if the value of $P(\lambda_i \rightarrow \lambda_i)$

can be adjusted accordingly such that (2.5) still remains satisfied. Thus the idea behind splitting the transition probability into the selection probability and the acceptance ratio is that the selection probabilities are the probabilities that a transition will happen from an initial state into a final state and the acceptance ratios give the probability that the next generated state is accepted/rejected and are chosen such that (2.9) is satisfied.

Ideally, the larger the values of the acceptance ratios the quicker the Markov process will reach equilibrium since there will be more states sampled in a shorter amount of time. Therefore the larger of the two acceptance ratios in (2.9) is always set to unity, whilst the other is adjusted accordingly so that the equation still remains satisfied.

So far the discussion has been quite general for an equilibrium Monte Carlo calculation. At this point however there are a selection of choices one could use to calculate the acceptance ratios; in this work all computations were carried out in accordance with the Metropolis algorithm [81]. The algorithm is simply defined by the choice of the selection probabilities and is one of the most simple and most common algorithms used. For the Metropolis algorithm implemented in the work in this thesis, the selection probabilities are all equal to one another, and for a system of N electrons, like for our FQH system, they are given by

$$g(\lambda_i \rightarrow \lambda_j) = N^{-1}, \quad \forall i, j. \quad (2.10)$$

The selection probabilities in the equation for detailed balance (2.9) now cancel each other and all that is left is the ratio of the acceptance ratios,

$$\frac{A(\lambda_i \rightarrow \lambda_j)}{A(\lambda_j \rightarrow \lambda_i)} = e^{-\beta(E_{\lambda_j} - E_{\lambda_i})}. \quad (2.11)$$

Recall that the optimal way to choose the acceptance ratios is to make the largest of the two in (2.11) equal to unity, therefore in the Metropolis algorithm acceptance ratios have the form,

$$A(\lambda_i \rightarrow \lambda_j) = \begin{cases} e^{-\beta(E_{\lambda_j} - E_{\lambda_i})} & \text{for } E_{\lambda_j} - E_{\lambda_i} > 0 \\ 1 & \text{otherwise.} \end{cases} \quad (2.12)$$

Other choices of acceptance ratios in the Metropolis algorithm are discussed in Ref. [82]. The acceptance ratios (2.12) are such that if the energy of the new state λ_j is less than or equal to the energy of our initial state λ_i then the new state will be accepted, otherwise the new state is accepted with the probability equal to $e^{-\beta(E_{\lambda_j} - E_{\lambda_i})}$. To decide if a new state should be accepted with a non-unity acceptance ratio, a random number r is generated such that $0 \leq r < 1$, then the new state λ_j is accepted if and only if

$$r < A(\lambda_i \rightarrow \lambda_j) = e^{-\beta(E_{\lambda_j} - E_{\lambda_i})}.$$

To be more specific about the algorithm used in this work in accordance with the FQHE, the different states of the system correspond to different positions of electrons on the complex plane. It has already been shown that the outer radius of a Laughlin FQH system with N electrons and M quasiholes at position $z = 0$ is given by $R_O = \sqrt{2mN + 2M}$, where $m = 1/\nu$ is the inverse filling factor, and the inner radius is $R_I = \sqrt{2M}$. Therefore before the Metropolis algorithm is initiated, the initial state of the system is chosen by randomly placing the electrons inside the disk on the complex plane with inner and outer radius R_I and R_O . Since in this implementation of the Metropolis algorithm the selection probabilities are all equal, to choose a new state an electron is chosen at random and its position is shifted. Whether this new state is accepted or rejected then depends on the acceptance ratios and thus the differences in energies of the initial and final state

as described in Eq. (2.12).

The exact Boltzmann energies that are chosen for a system in the FQH state will actually depend on what observable is being measured. For those that match the form given by (2.1) the plasma analogy can be invoked so that

$$Z_N = \int \prod_{i=1}^N d^2 z_i e^{-\beta E} = \int \prod_{i=1}^N d^2 z_i |\Psi|^2, \quad (2.13)$$

which gives the energy of some state defined by particle coordinates $\lambda_i = \{z_1, z_2, \dots, z_N\}$ to be

$$\beta E_{\lambda_i} = \sum_{i=1}^N \left(\frac{|z_i|^2}{2} - 2M \ln |z_i| \right) - 2m \sum_{i < j}^N \ln |z_i - z_j|. \quad (2.14)$$

If one goes from state $\lambda_k = \{z_1, z_2, \dots, z_k, \dots, z_N\}$ to $\lambda'_k = \{z_1, z_2, \dots, z'_k, \dots, z_N\}$ then the difference in the energy between the initial and final state will only depend on the energy contribution from the k 'th particle which is given by

$$E_{\lambda_k}(z) = \frac{|z|^2}{2} - 2M \ln |z| - 2m \sum_{i=1 \neq k}^N \ln |z - z_i|, \quad (2.15)$$

where z is the position of the k 'th electron in either the initial or final state. Therefore acceptance ratios from (2.12) are given by

$$A(\lambda_k \rightarrow \lambda'_k) = \begin{cases} e^{-\Delta E_k} & \text{for } E_{\lambda'_k} - E_{\lambda_k} > 0 \\ 1, & \text{otherwise} \end{cases} \quad (2.16)$$

where

$$\Delta E_k = \frac{1}{2} (|z'_k|^2 - |z_k|^2) + 2M \ln \left(\frac{|z_k|}{|z'_k|} \right) + 2m \sum_{i=1 \neq k} \ln \left(\frac{|z_k - z_i|}{|z'_k - z_i|} \right). \quad (2.17)$$

The difficult question to determine is just how much of a shift should be imposed on the electrons position? Moving the electron by too small amount means that the energy range of the selected states will be narrow and thus it could take a long time to reach equilibrium. Too large a shift is also counter productive since it may be impossible to ever reach the states that minimise the energy and thus the condition of ergodicity would not be satisfied. For this work the following method is used. If the initial position of the particle is $z = u + iv$ then its new position is given by

$$z' = u + K \left(\delta u - \frac{1}{2} \right) + i \left(v + K \left(\delta v - \frac{1}{2} \right) \right) \quad (2.18)$$

where δu and δv are random numbers satisfying $0 \leq (\delta u, \delta v) < 1$, and K is some constant that depends on the particulars of the program. The parameter K is chosen such that there are a sufficient number of states that are being accepted or rejected. Notice that the $-1/2$ term allows for possible moves in all direction on the complex plane from 0 to 2π . The condition of ergodicity is satisfied since it is possible for any particle to reach any position given a long enough time, and thus all states are accessible in this Markov chain from any initial state.

Taking measurements for each new state that is accepted is not very efficient since the measured value will only change a small amount for each successive particle move. Also subsequent configurations in the Markov chain will be highly correlated since only one particle position has been altered. Therefore the process of choosing a new state and either accepting/rejecting it is carried out some number n times between each measurement. After taking enough measurements when the system has reached equilibrium, the expectation value of the estimator can be calculated

via calculating the average value of all the computed measurements, as shown in Eq. (2.4). Due to the cutoff restricting the sampling to a finite number of states, there is always an error associated with the value of the estimator in a Monte Carlo simulation. Recall in the notation used here, the number of states involved in the average of the estimator in Eq. (2.4) is Λ . The more measurements taken the smaller the error becomes and eventually if it were possible to include all states so that $\Lambda \rightarrow \infty$ then $A_\Lambda \rightarrow \langle A \rangle$ where $\langle A \rangle$ is the exact value of the statistical average of some observable \hat{A} shown in (2.2). Errors are estimated from the simulation by determining the variance of the measurements recorded on the observable A . Since the variance of the sample of measurements is

$$S_\Lambda^2 = \frac{1}{\Lambda} \sum_{i=1}^{\Lambda} (A_i - \langle A \rangle)^2, \quad (2.19)$$

then the magnitude of the error is given by S_Λ and scales with the square root of the number of measurements taken $\sqrt{\Lambda}$. Eq. (2.19) holds only if the sample of measurements is uncorrelated. An empirical check to see if subsequent measurements are indeed uncorrelated is to compute nS_Λ^2 , where n is the number of configurations sampled between successive measurements. If nS_Λ^2 is independent of n , then subsequent measurements A_i are uncorrelated [83].

In this chapter, the MC method has been introduced, showing how statistical averages can be computed in accordance with the Metropolis algorithm. To compute observables for Laughlin states in particular, one can invoke the plasma analogy to obtain an effective Boltzmann probability distribution which allows statistical averages to be performed. Original work using the MC method and in particular the Metropolis algorithm as discussed in this chapter, will be presented in Chapter 3, Chapter 4 and Chapter 5.

CHAPTER 3

Edge Excitations in Laughlin-Type States

This chapter is devoted to the representations of edge excitations in Laughlin's theory of FQH states with filling factors $\nu = 1/m$, where m is an odd integer. To begin, in Section 3.1 we introduce the microscopic formalism for the description of edge states and show the difficulties experienced when working analytically with this representation. This leads onto a phenomenological description of the FQH edge states pioneered by Wen [46] who proposed that the edge states can be described by a chiral Luttinger liquid which has many similarities to a conventional Luttinger liquid. This will be the subject of Section 3.2. In the final section of this chapter, original work is presented for the overlaps of Laughlin states supporting low-energy edge excitations.

3.1 Microscopic Representation of Edge Excitations

In the introductory chapter of this thesis, it was pointed out that the Laughlin wavefunction was a zero energy eigenstate for a short range, two-particle interaction. It was originally shown by Haldane [84] that there are a whole range of additional states that are also zero energy eigenstates of this type of interaction and they can be generated by multiplying the Laughlin state by a symmetric polynomial $P_k(z_i)$ of the electron coordinates. The same findings have also been found for other short range interactions like $U(\mathbf{r}) = \nabla^2 \delta^2(\mathbf{r})$ [85, 86]. In this section we will follow the Haldane pseudopotential argument to show that in general any holomorphic function of electron coordinates describes a Laughlin-type state in the LLL and also that these states correspond to the addition of excitations to the edge states of a Laughlin-type FQH droplet.

Haldane pseudopotentials v_m are defined as the expectation value of some potential V that is dependent only on the relative angular momentum m' of a pair of particles. In the LLL the kinetic energy term can be neglected and one can write the interaction part of the Hamiltonian in terms of these Haldane pseudopotentials,

$$V = \sum_{m'=0}^{\infty} \sum_{i<j} v_{m'} P_{m'}(ij), \quad (3.1)$$

where $P_{m'}(ij)$ is a projection operator which selects states of relative angular momentum m' . Angular momentum contributions come from the polynomial part of Laughlin's wavefunction, so for now work is carried out in the holomorphic representation of Laughlin's wavefunction, which for a FQH droplet (the disk geometry will be returned to later) with filling factor $\nu = 1/m$ is given by

$$\Psi_N = \prod_{i < j}^N (z_i - z_j)^m. \quad (3.2)$$

The angular momentum operator in complex coordinates is given by $z_i \partial_{z_i}$. Applying this operator to the state (3.2) for all particle coordinates gives the total angular momentum $M_0 = mN(N - 1)/2$ in units of \hbar . From the polynomial in (3.2) one can see that the minimum, relative angular momentum between any two electrons is $m = \nu^{-1}$. Therefore if we define a short range interaction such that the Haldane pseudopotentials are non-zero only for relative angular momentum values less than m ($v_{m'} = 0$ for $m' \geq m$) then the Laughlin state (3.2) is a zero-energy eigenstate to the Hamiltonian (3.1). According to this potential, there also exist an excitation gap allowing the observation of the plateaus in the Hall resistivity. If, for example, two particles are forced to have a relative angular momentum of $m' = 1$ instead of m , then there will be a cost of energy v_1 . The state in Eq. (3.2) however, is not the only eigenstate of this potential and generally, the states

$$\Psi_N^k = P_k(z_1, z_2, \dots, z_N) \Psi_N \quad (3.3)$$

all have zero eigenvalues of the Hamiltonian (3.1) where $P_k(\{z_i\})$ are symmetric polynomials with k denoting the degree of the polynomial. An introduction to symmetric polynomials is given in the Appendix A.1. If the total angular momentum of the Laughlin state (3.2) is given by $M_0 = mN(N - 1)/2$, then the total angular momentum of the Laughlin state multiplied by a symmetric polynomial of degree k is $M = M_0 + k$; thus multiplying the Laughlin state by symmetric polynomials increases the total angular momentum of the state via moving electrons to higher angular momentum orbitals.

Any symmetric polynomial can be generated by the addition and/or the multiplication of power sum polynomials which take the form $S_n = \sum_{i=1}^N z_i^n$. Power sum

polynomials therefore provide a good basis for the description of edge excitations. The degree of the polynomial labelled as k in Eq. (3.3) determines the degeneracy for the momentum eigenvalue $M = M_0 + k$. It is given by the number of partitions $\lambda = \{\lambda_1, \lambda_2, \dots, \lambda_N\}$, which have the same weight $|\lambda| = \lambda_1 + \lambda_2 + \dots + \lambda_N = k$. A partition, λ is a set of integers, λ_i , that are ordered in decreasing size; $\lambda_1 \geq \lambda_2 \geq \dots \geq \lambda_N$. Partitions are described in more detail in Appendix A.1. For $k = 0$ and $k = 1$ the degeneracy is 1 and for $k = 2$ the degeneracy is 2. The important point to make here however, is that each unique partition has a one-to-one correspond with the configurations of boson edge excitations in the system. Each partition also corresponds to a unique symmetric polynomial. If we consider the power sum polynomials as a representation of the microscopic states, then we see that S_k can be thought of as a creation operator of the k 'th orbital and $k\partial_{S_k}$ as an annihilation operator also acting on the k 'th orbital. It can be shown that such ladder operators follow bosonic algebra [87].

To highlight the points made so far, consider a state of the type shown in (3.3) with the angular momentum contribution from the multiplication of the symmetric polynomial given by $k = 3$. There are three unique partitions that satisfy $|\lambda| = 3$. These are $\lambda_1 = \{3, 0^{N-1}\}$, $\lambda_2 = \{2, 1, 0^{N-2}\}$ and $\lambda_3 = \{1, 1, 1, 0^{N-3}\}$. For a general partition of the form $\lambda = \{\lambda_1, \lambda_2, \dots, \lambda_N\}$ the configuration of edge excitations can be extracted as follows; the number of integers with the value $\lambda_k = 1$ in the partition corresponds to the number of excitations in the angular momentum orbital $l = 1$, the number of integers of the value $\lambda_k = 2$ corresponds to the number of excitations in the angular momentum orbital $l = 2$ and so on until the maximum possible integer which is $\lambda_k = N$, corresponding to an excitation in the angular momentum orbital $l = N$. According to the theory of symmetric polynomials, there are only allowed N orbitals and thus this provides the maximum angular momentum contribution of the edge excitations. For more details on the reasoning for this statement, see Appendix A.2.

Back to the example for $|\lambda| = 3$, then the partition λ_1 corresponds to a state with a single excitations added to the $l = 3$ orbital, λ_2 corresponds to the state with a single edge excitation added to the $l = 2$ orbital and the $l = 1$ orbital, and finally λ_3 corresponds to the addition of three edge excitations to the $l = 1$ orbital. The microscopic wave functions for these three degenerate states are generated by multiplying the Laughlin state by a product of power sum polynomials of degree corresponding to the integers in the partition. Therefore, for a general partition of the form $\lambda = \{\lambda_1, \lambda_2, \dots, \lambda_N\}$ the corresponding microscopic state is

$$\Psi = \prod_{k>0}^N S_{\lambda_k} \prod_{i<j}^N (z_i - z_j), \quad (3.4)$$

where $S_{\lambda_i} = \sum_{j=1}^N z_j^{\lambda_i}$ and only non-zero integers are included from the partition ($\lambda_i \neq 0$). For our example where $|\lambda| = 3$, the three degenerate states are

$$\begin{aligned} \Psi_1 &= S_3 \prod_{i<j}^N (z_i - z_j) \\ \Psi_2 &= S_2 S_1 \prod_{i<j}^N (z_i - z_j) \\ \Psi_3 &= S_1^3 \prod_{i<j}^N (z_i - z_j) \end{aligned} \quad (3.5)$$

So far we have considered a simple Laughlin FQH droplet with a single edge. Now the partition formalism will be extended to the two-edged, disk-shape geometry described by the state

$$\Psi_N^M = \prod_{i<j}^N (z_i - z_j)^m \prod_{n=1}^N z_n^M. \quad (3.6)$$

The additional factor which creates the macroscopic hole at $z = 0$ is itself a

symmetric polynomial and as a consequence is also a zero-energy eigenstate of the Hamiltonian (3.1). The total angular momentum for this state however is $M_0 = NM + (mN(N - 1)/2)$. Excitations to the outer boundary of the fluid are added in the same way as in (A.15). Excitations for the inner boundary however are added by multiplying the state (3.6) by power sum polynomials of the inverse variable $1/z_i$. So, for example, a state labelled in terms of the number of excitations n_k in the k 'th orbital on the outer boundary and in terms of n_{-k} , the number of excitations in the k 'th orbital on the inner boundary is

$$\begin{aligned} |\{n_{\pm k}\}\rangle &= \prod_{i<j}^N (z_i - z_j)^m \prod_{n=1}^N z_n^M \prod_{k>0} S_k^{n_k} S_{-k}^{n_{-k}} \\ &= \prod_{i<j}^N (z_i - z_j)^m \prod_{n=1}^N z_n^M \prod_{k>0} \left(\sum_{i=1}^N z_i^k \right)^{n_k} \left(\sum_{i=1}^N \frac{1}{z_i^k} \right)^{n_{-k}}, \end{aligned} \quad (3.7)$$

where, to shorten notation the power sum polynomials of variables z_i and z_i^{-1} have been represented as

$$\begin{aligned} S_k &= \sum_{i=1}^N z_i^k \\ S_{-k} &= \sum_{i=1}^N \frac{1}{z_i^k} \end{aligned}$$

The angular momentum contribution from the inner boundary is therefore negative (a result from the excitations being represented by power sum polynomials of the inverse variable) as compared to the angular momentum from the outer boundary. This sets a cutoff for the maximum number of boson momentum orbitals occupied for the inner boundary. The magnitude of the maximum total angular momentum allowed for the inner boundary excitations is NM , where N is the number of

electrons and M is the number of quasiholes inserted at the position $z = 0$. A higher value than this result gives a total angular momentum of the system less than the value of $M_0 = mN(N - 1)/2$, which physically does not make sense.

Power sum polynomials of the inverse variable z_i^{-1} can then be converted into a partition formalism for the inner boundary. Thus for a two-edge system one will have two separate partitions, one for each edge. To calculate observables of the system, it is first of all important to consider the overlap of two states;

$$\begin{aligned} \langle \{n'_{\pm p}\} | \{n_{\pm k}\} \rangle &= \int \prod_{n=1}^N d^2 z_i |z_i|^{2M} e^{\frac{|z_i|^2}{2}} \prod_{i < j}^N |z_i - z_j|^{2m} \\ &\times \prod_{k > 0} S_k^{n_k} S_{-k}^{n_{-k}} \prod_{p > 0} \bar{S}_p^{n'_p} \bar{S}_{-p}^{n'_{-p}}. \end{aligned} \quad (3.8)$$

As far as this author is aware, there are no analytic solutions for such integrals in the large N limit except in the free fermion case where $m = 1$. In the free fermion case the problem becomes trivial since the overlap integrals can be represented as a series of overlap of Schur functions which have known solutions. This process is detailed in Appendix A.2. For $m > 1$, then the Vandermonde determinant is replaced instead by some determinant to the power m , which is much more difficult to work with since the Schur function technique can no longer be applied.

So far in this chapter we have introduced how edge excitations can be represented microscopically and the difficulty with calculating expectation values of these excited states for filling factors $\nu < 1$ in the large N limit has also been noted. The calculation of expectation values however can be computed numerically using the Monte Carlo technique introduced in Chapter 2. The next section of this chapter will focus on a phenomenological theory of how edge excitations can be represented in the edge states of Laughlin-type systems. This theory is a powerful tool used to make many predictions about transport properties of the FQHE.

3.2 Phenomenological Theory Representation of Edge Excitations

The phenomenological theory discussed here was originally conceived by Wen [46] who described the edge states of a FQH system as a chiral Luttinger liquid. As already hinted in the introduction of this thesis, the model for the edge states is loosely based on the model of a conventional Luttinger liquid [88, 89], which was originally formulated due to the break-down of Fermi liquid theory for interacting fermions in one dimension. The Luttinger liquid model is exactly solvable using the technique of bosonisation first introduced by Tomonaga [89] and extended in other works [90–92]. The key to the solubility of the model is linearising the dispersion about the Fermi energy which introduces massless Dirac fermions. The bosonisation procedure then allows the Hamiltonian for a 1D system of interacting fermions to be expressed as a system of non-interacting Bosons. The elementary excitations of this model can then be considered as collective boson modes, a similar result to what has been found in the microscopic picture presented in Section 3.1. Fermion operators in the original theory can then be expressed in terms of the Boson fields that describe the low-energy excitations of the system.

The most distinct property of a Luttinger liquid is the occurrence of power-law behaviours, where the exponent is dependent on the type of interaction and the geometry of the system. The chiral Luttinger liquid system of the FQH edges also have this property except, as will be shown later in this chapter, the exponents are now universal and dependent only on the filling factor ν of the state [93]. Due to the chiral nature of the system and the universality of the power-law exponent, the FQHE is one of the best systems for observing Luttinger liquid-like behaviour. In the remainder of this chapter the formalism for the chiral Luttinger liquid will be introduced. As discussed in Section 1.5 there are subtle differences in the phenomenological theory of the chiral Luttinger liquid and the theory of the

conventional Luttinger liquid.

3.2.1 Chiral Luttinger Liquid Formalism

The formalism used here to describe the chiral Luttinger liquid is based on the works [94, 95] in which operators are projected onto the subspace of edge excitations in order to define the zero mode operators and Boson creation and annihilation operators for quasiparticles. It was shown in the previous section that microscopically, the edge excitations can be represented by power sum polynomials of the variables z_i for an excitation on the outer boundary, or z_i^{-1} on the inner boundary. Again we consider a disk shape geometry for the FQH system as shown in Figure 1.5. These edge excitations are small incompressible deformations of the boundary and generally they can be described by a set of parameters; t_k for the outer boundary and t_{-k} for the inner boundary. Consider the following wavefunction;

$$\Psi = \Psi_N^M \prod_{k=1}^N e^{mw(z_k)} = \prod_{i<j}^N (z_i - z_j)^m \prod_{k=1}^N z_k^M e^{-\frac{|z_k|^2}{4t_B^2} + mw(z_k)} \equiv |N, M, \{t_{\pm k}\}\rangle \quad (3.9)$$

where,

$$w(z) = \sum_{k>0} \left(t_k z^k + \frac{t_{-k}}{z^k} \right). \quad (3.10)$$

The bra-ket notation has been introduced here for later calculations. This wavefunction is identical to the Laughlin wavefunction for the ground state system of a disk-type geometry except for the additional function $w(z)$ in the exponent. Differentiating the state Ψ with respect to $t_{\pm k}$ brings down a power sum polynomial $S_{\pm k}$ from the function $w(z)$ in the exponent. Thus the states $|\{n_{\pm k}\}\rangle$ can be gen-

erated by Ψ in Eq. (3.9) by applying differential operators in accordance with the angular momentum orbitals that are occupied.

$$|\{n_{\pm k}\}\rangle = \prod_{k>0} S_{\pm k}^{n_{\pm k}} \Psi_N^M = \prod_{k>0} \frac{1}{m^{n_{\pm k}}} \frac{\partial^{n_{\pm k}} \Psi}{\partial t_{\pm k}^{n_{\pm k}}} \Big|_{t_{\pm k}=0} \quad (3.11)$$

The normalisation coefficient of the wavefunction (3.9) is given by the square-root of the tau function of analytic curves $\tau_N^\nu(t_{\pm k}, \bar{t}_{\pm k})$, which in the semi-classical limit takes the form

$$\int \prod_{i=1}^N d^2 z |\Psi|^2 = \tau_N^\nu(t_{\pm k}, \bar{t}_{\pm k}) \rightarrow \tau^\nu(N, M, t_{\pm k}, \bar{t}_{\pm k}). \quad (3.12)$$

where,

$$\tau^\nu(N, M, t_{\pm k}, \bar{t}_{\pm k}) = D(N, M) \times \exp \left\{ m \sum_{k>0} k R_O^{2k} |t_k|^2 + k \frac{|t_{-k}|^2}{R_I^{2k}} + k t_{-k} t_k + k \bar{t}_k \bar{t}_{-k} \right\}, \quad (3.13)$$

and $D(N, M) \equiv \tau(N, M, t_{\pm k}, \bar{t}_{\pm k})|_{t_{\pm k}=0}$ is a function independent of t_{\pm} and \bar{t}_{\pm} . The tau-function has been studied in detail [96] and in Appendix B.2 it is calculated explicitly using a field theory approach. In general, the overlap for two states of the form (3.9) in the large N -limit is given by

$$\langle N, M, t_{\pm k} | N', M', t'_{\pm k} \rangle = \tau^\nu(N, M, t_{\pm k}, \bar{t}_{\pm k}) \delta_{N, N'} \delta_{M, M'}. \quad (3.14)$$

where the Kronecker delta terms represents that states of different N and M are orthogonal in the large N limit. With the tau-function known, along with equations (3.11) and (3.12), the overlap of states describing different sets of bosonic

edge excitations can be calculated. For excitations constrained on either the outer boundary or the inner boundary,

$$\begin{aligned}
\langle \{n_{\pm k}\} | \{n_{\pm p}\} \rangle &= \prod_{k,p>0} \frac{1}{m^{n_{\pm k}+n_{\pm p}}} \frac{\partial^{n_{\pm k}+n_{\pm p}} \tau^\nu(N, M, t_{\pm p}, \bar{t}_{\pm k})}{\partial \bar{t}_{\pm k}^{n_{\pm k}} \partial t_{\pm p}^{n_{\pm p}}} \Bigg|_{t_{\pm k}=0} \\
&= D(N, M) \prod_{k>0} \left(\frac{k R_{\pm}^{\pm 2k}}{m^2} \right)^{n_{\pm k}} n_{\pm k}! \delta_{pk}, \tag{3.15}
\end{aligned}$$

where $R_- \equiv R_I$ is the inner boundary radius and $R_+ \equiv R_0$ is the outer boundary radius. The formula for the overlap of states was originally obtained by Cheianov *et al.* [94] for a single edged FQH droplet. For this thesis the overlap formula (3.15) has been extended to a two edged system for the disk geometry FQHE. In Section 3.3, overlap integrals of states supporting low-energy edge excitations are computed microscopically and compared to the predictions from Eq. (3.15).

As expected, such overlaps are reminiscent of bosonic algebra, thus our next step is to define raising and lowering operators to act on the states as follows;

$$\begin{aligned}
a_{\pm p}^\dagger |n_{\pm p}\rangle &= \sqrt{n_{\pm p} + 1} |n_{\pm p} + 1\rangle, \\
a_{\pm p} |n_{\pm p}\rangle &= \sqrt{n_{\pm p}} |n_{\pm p} - 1\rangle. \tag{3.16}
\end{aligned}$$

In accordance with previous notation $+p$ corresponds to a ladder operator acting on the p bosonic mode of the outer boundary and $-p$ corresponds to the same value mode but on the inner boundary. Using (3.11) and (3.12), and choosing a representation in terms of $\bar{t}_{\pm k}$ as in [94], these operators take the form

$$\begin{aligned}
a_p &= \frac{1}{R_O^p \sqrt{mp}} \left(\frac{\partial}{\partial \bar{t}_p} - mp \bar{t}_{-p} \right), & a_p^\dagger &= R_O^p \sqrt{mp} \bar{t}_p. \\
a_{-p} &= \frac{R_I^p}{\sqrt{mp}} \left(\frac{\partial}{\partial \bar{t}_{-p}} - mp \bar{t}_p \right), & a_{-p}^\dagger &= \frac{\sqrt{mp}}{R_I^p} \bar{t}_{-p}.
\end{aligned} \tag{3.17}$$

The mixture of inner and outer boundary terms for the annihilation operators (i.e. they contain both \bar{t}_p and \bar{t}_{-p}) is a consequence of the mixed inner and outer boundary $t_{\pm k}$ in the tau-function (3.13). Even with the mixture of inner and outer boundary terms, it is a straightforward calculation to show that operators on opposing boundaries commute with each other $[a_{\pm k}, a_{\mp k}^\dagger] = 0$ and the commutation relations for operators acting on the same boundaries follow the usual bosonic algebra $[a_{\pm k}, a_{\pm p}^\dagger] = \delta_{pk}$. In the chiral Luttinger liquid theory, zero-mode operators must also be defined. For the outer boundary these are denoted as θ_N which extracts the number of particles from a state, and $e^{i\varphi_N}$ which is its conjugate operator. There also exist similar operators for the inner boundary θ_M and $e^{i\varphi_M}$ that act on the quasihole number M . Using the state notation introduced in (3.9);

$$\begin{aligned}
e^{i\varphi_N} |N, M, \{t_{\pm k}\}\rangle &= |N + 1, M, \{t_{\pm k}\}\rangle, \\
\theta_N |N, M, \{t_{\pm k}\}\rangle &= N |N, M, \{t_{\pm k}\}\rangle, \\
e^{i\varphi_M} |N, M, \{t_{\pm k}\}\rangle &= |N, M + 1, \{t_{\pm k}\}\rangle, \\
\theta_M |N, M, \{t_{\pm k}\}\rangle &= M |N, M, \{t_{\pm k}\}\rangle.
\end{aligned} \tag{3.18}$$

These operators satisfy the commutation relations; $[\theta_x, e^{i\varphi_y}] = e^{i\varphi_x} \delta_{x,y}$ where x or $y = N$ or M . With objects defined in (3.17) and (3.18), we are now in a position to construct bosonised forms of the fermion field operators. In this construction, it is assumed that the edges are sufficiently far apart such that they are completely independent of each other, thus one must define an electron operator for both

the outer boundary $\psi_{m,O}$ and the inner boundary $\psi_{m,I}$. Only the outer boundary operator $\psi_{m,O}$ will be explicitly constructed, the method used is identical for the inner boundary and so it will not be repeated. The final expression for $\psi_{m,I}$ will be stated at the end of the construction of $\psi_{m,O}$. Consider the matrix element

$$\langle N, M, \{t_{\pm k}\} | \psi_{m,O}^\dagger(\bar{\zeta}) | N', M', \{t'_{\pm k}\} \rangle. \quad (3.19)$$

Since the bosonic operators a_p and a_p^\dagger have been defined in terms of the \bar{t} -representations, rather than seeing the fermion operator $\psi_{m,O}^\dagger$ in (3.19) as a creation operator acting on the state to the right, it can instead be thought of as an annihilation operator acting on the left-state. This choice is convenient since from Laughlin's work discussed in the introductory chapter of this thesis, we know the microscopic expression for a hole created in a Laughlin state is given by

$$\begin{aligned} \langle N, M, \{t_{\pm k}\} | \psi_{m,O}^\dagger(\bar{\zeta}) | N', M', \{t'_{\pm k}\} \rangle &= \bar{\zeta}^M e^{-\frac{|\zeta|^2}{4}} e^{m\bar{w}(\bar{\zeta})} \\ &\times \int \prod_{i=1}^N d^2 z_i (\bar{\zeta} - \bar{z}_i)^m e^{m(w(z_i) + \bar{w}(\bar{z}_i))} |\Psi_N^M|^2 \delta_{N, N'+1} \delta_{M, M'}, \end{aligned} \quad (3.20)$$

where Ψ_N^M is the ground state Laughlin wave function when no edge excitations have been added to the system (see Eq. (1.31)) and the Kronecker delta terms follow from (3.14). To project this operation on the low energy edge states, (3.20) is expected to be equivalent to

$$\langle N, M, \{t_{\pm k}\} | \psi_{m,O}^\dagger(\bar{\zeta}) | N', M', \{t'_{\pm k}\} \rangle = \psi_{m,O}^\dagger(\bar{\zeta}) \tau^\nu(t_{\pm k}, \bar{t}_{\pm k}) \delta_{N, N'} \delta_{M, M'}, \quad (3.21)$$

where, in this representation $\psi_{m,O}^\dagger$ is now the effective, low energy electron opera-

tor. The aim of what follows is to manipulate (3.20) to be in the form (3.21) and thus obtain an expression for the low-energy effective electron operator. Since the fermion operator must act on the outer boundary, it is safe to assume $\bar{\zeta} > \bar{z}_i$ so the following expansion can be used in (3.20),

$$\prod_{i=1}^N (\bar{\zeta} - \bar{z}_i)^m = \bar{\zeta}^{mN} \exp \left(m \sum_{i=1}^N \ln \left(1 - \frac{\bar{z}_i}{\bar{\zeta}} \right) \right) = \bar{\zeta}^{mN} \exp \left(-m \sum_{k>0} \frac{1}{k \bar{\zeta}^k} \sum_{i=1}^N \bar{z}_i^k \right).$$

The sum over the coordinates z_i in the exponent of the above expression has the form of the power sum polynomial. It has already been discussed how power sum polynomials can be extracted from states $|N, M, \{t_{\pm k}\}\rangle$ by differentiating the state with respect to \bar{t}_k (e.g., see Eq. (3.11)). Using this argument and Eq. (3.14) allows the expression in (3.20) to be written as,

$$\begin{aligned} \langle N, M, \{t_{\pm k}\} | \psi_{m,O}^\dagger(\bar{\zeta}) | N', M', \{t'_{\pm k}\} \rangle &= \bar{\zeta}^{mN+M} e^{-\frac{|c|^2}{4}} e^{m\bar{w}(\bar{\zeta})} e^{-\sum_{k>0} \frac{1}{k \bar{\zeta}^k} \frac{\partial}{\partial \bar{t}_k}} \\ &\times \delta_{N,N'+1} \delta_{M,M'} \tau^\nu(N, M, \{\bar{t}_{\pm k}\}, \{t'_{\pm k}\}). \end{aligned} \quad (3.22)$$

The matrix element of $\psi_{m,O}^\dagger$ is now in a similar form to its effective, low energy representation in (3.21); all that remains is to sort out the zero-mode parts of the operator. According to (3.18), the zero mode operators appear in the effective field representation of the electron operator as a consequence of the following contributions:

$$\begin{aligned} \bar{\zeta}^{mN+M} &\rightarrow \bar{\zeta}^{m\theta_N + \theta_M}, \\ \delta_{N,N'+1} &\rightarrow e^{i\varphi_N} \delta_{N,N'}. \end{aligned}$$

To finish the calculation, the final expression for the electron effective field operator is expressed in terms of the boson ladder operators a_p and a_p^\dagger using (3.17), since this representation is the most familiar and easy to work with as compared to the \bar{t} -representation. Our electron field operator is thus,

$$\psi_{m,O}^\dagger(\xi) = e^{i\varphi_N} e^{m\phi_O(\xi)}, \quad (3.23)$$

where ϕ_O is the bosonised part of the operator given by

$$\begin{aligned} \phi_O(\xi) &= -\frac{i\xi}{R}(\theta_N + \frac{\theta_M}{m}) + \sum_{k>0} \sqrt{\frac{1}{mk}} \left(e^{-ik\frac{\xi}{R}} a_k^\dagger - e^{ik\frac{\xi}{R}} a_k \right) \\ &= \phi_O^0(\xi) + \phi_O^+(\xi) + \phi_O^-(\xi), \end{aligned} \quad (3.24)$$

where we have decomposed the field ϕ_O in terms of its zero mode contribution ϕ_O^0 , its creation operator part ϕ_O^+ and its annihilation operator part ϕ_O^- . This notation will be used to shorten expressions in later calculations. It is noted that a non-trivial coordinate transformation has been made in Eqs. (3.23) and (3.24). The coordinate ξ is now the longitudinal coordinate along the edges of the system where $\xi \in [0, 2\pi R]$ and R is the radius of the ring of FQH fluid. This is because in the effective theory of edge states we assume that the edge states are one-dimensional. As a consequence, terms in (3.23) that are dependent only on the transverse direction to the ring of fluid (such as $e^{-\frac{|\xi|^2}{4}}$) have also been dropped. Conjugating the field the field $\psi_{m,O}^\dagger(\xi)$ gives the bosonised representation of the electron annihilation operator,

$$\psi_{m,O}(\xi) = e^{-m\phi_O(\xi)} e^{-i\varphi_N}, \quad (3.25)$$

where $\phi_0(\xi)$ is given in (3.24). In general one can write the bosonisation formulae for general field operators $\psi_{p,O}$ in the low-energy effective theory, where p is some integer. The operator $\psi_{p,0}$ corresponds to the annihilation operator of particle with charge $e^* = (p/m)e$ in the Laughlin state $\nu = (1/m)$. Therefore $\psi_{p=1,O}$ corresponds to the field for a single Laughlin quasiparticle with charge $e^* = (1/m)e = \nu^{-1}e$ and $\psi_{p=m,O}$ corresponds to the field describing m quasiparticles, or equivalently a single electron. These general operators for the outer boundary take the form

$$\begin{aligned}\psi_{p,O}^\dagger(\xi) &= e^{i\frac{p}{m}\varphi_N} e^{p\phi_O(\xi)}, \\ \psi_{p,O}(\xi) &= e^{-p\phi_O(\xi)} e^{-i\frac{p}{m}\varphi_N}.\end{aligned}\tag{3.26}$$

Carrying out an equivalent calculation as shown here but now for the inner boundary, the field operators $\psi_{p,I}, \psi_{p,I}^\dagger$ corresponding to creating or annihilating a particle of charge $e^* = (p/m)e$ respectively are given by

$$\begin{aligned}\psi_{p,I}^\dagger(\xi) &= e^{i\frac{p}{m}\varphi_N} e^{ip\varphi_M} e^{p\phi_I(\xi)}, \\ \psi_{p,I}(\xi) &= e^{-p\phi_I(\xi)} e^{-i\frac{p}{m}\varphi_N} e^{-ip\varphi_M},\end{aligned}\tag{3.27}$$

where now the boson field $\phi_I(\xi)$ takes the form

$$\begin{aligned}\phi_I(\xi) &= -\frac{i\xi}{mR} t_M + \sum_{k>0} \sqrt{\frac{1}{mk}} \left(e^{ik\frac{\xi}{R}} a_{-k}^\dagger - e^{-ik\frac{\xi}{R}} a_{-k} \right) \\ &= \phi_I^0(\xi) + \phi_I^+(\xi) + \phi_I^-(\xi).\end{aligned}\tag{3.28}$$

Similar to the outer boundary Bose field, the inner boundary boson field has

been decomposed in terms of the zero mode part ϕ_I^0 , creation part ϕ_I^+ and the annihilation part ϕ_I^- . What is missing from our discussion so far is the convention of the ordering of the fermion fields. In fact this is a difficult point to comment on because changing the type of operator ordering used alters the normalisation coefficient of the fields. Without any microscopic calculations to compare to, the normalisation coefficient cannot be determined in this theory alone. This problem will be analysed in detail in Chapter 4, for now we define the ordering of the operators to be

$$e^{\phi_X(\xi)} = e^{\phi_X^0(\xi)} e^{\phi_X^+(\xi)} e^{-\phi_X^-(\xi)} e^{\frac{1}{2}[\phi_X^+(\xi), \phi_X^-(\xi)]}, \quad (3.29)$$

where $X = I/O$ and the following commutation relations have been used $[\phi_X^0, \phi_X^+] = [\phi_X^0, \phi_X^-] = 0$. The commutation relation for the operators ϕ_X^+ and ϕ_X^- is given by,

$$[\phi_X^+(\xi), \phi_X^-(\xi)] = \sum_{k,p>0} \frac{[a_{\pm k}^\dagger, a_{\pm p}]}{m\sqrt{pk}} = -\sum_{k>0} \frac{1}{mk}. \quad (3.30)$$

To complete the calculation the sum over k needs to be performed. There are two natural cutoffs that can be considered for the low-energy limit of the system. The first is related to the breakdown of the Boson creation and annihilation operators in the Luttinger liquid theory, which are only independent operators for $k \leq N$, this cutoff is a consequence of the theory of symmetric polynomials mentioned in the previous section of this chapter. Therefore N could be a valid cutoff for the sum. However there is also an obvious limit on the energy of the edge excitations which is related to the bulk energy gap. If quasiparticles have an energy larger than the bulk gap energy Δ then they are able to travel through the bulk destroying the representation of the chiral Luttinger liquid edge states in the FQHE. The dispersion relation for the Bose excitations is linear at the edge and so the maximum momentum for a quasiparticle is $p = \Delta/v$ where v is the quasiparticle

velocity. The momentum corresponding to a given edge orbital k is also given by $p = \hbar k/R$ and therefore the maximum value of the orbital according to the bulk energy gap is $k \leq R\Delta/(v\hbar) \equiv \Lambda$. The value of the radius R is on the order of N in the large N limit. Thus the two cutoffs are essentially equivalent. In this work we use $\Lambda \sim R$ as the cutoff, which has a more apparent meaning in terms of the physics of the system.

The sum over k in (3.31) is performed using $\Lambda \sim R \equiv |b|$ as a soft cutoff such that $\sum_{k>0} k^{-1} \rightarrow \sum_{k>0} k^{-1} e^{-k/R} = -\ln(1 - e^{-1/R})$. Therefore,

$$[\phi_X^+(\xi), \phi_X^-(\xi)] = -\frac{1}{m} \ln(1 - e^{-1/R}). \quad (3.31)$$

The result in (3.31) only holds when the variable of the two boson fields is the same. It is because of the form of the commutators of the boson fields such as (3.31) that power law behaviours are observed in the transport properties of the FQHE. For an example see Chapter 4, where matrix elements are calculated for particles tunnelling across the bulk of a FQH device. The exponent of the power law for Laughlin state FQH systems is related to m which is a universal parameter defined from the bulk states of the system.

The Hamiltonian for this system is then equivalent to the Hamiltonian for a conventional Luttinger liquid except the charge carriers move only in one direction, as imposed by the magnetic field acting on the system. In terms of the boson fields, the Hamiltonian for the chiral Luttinger liquid describing both the inner and outer boundary edge states is

$$H = \hbar v \int_0^{2\pi R} dx [(\partial_x \phi_I(x))^2 + (\partial_x \phi_O(x))^2] \quad (3.32)$$

where v is the velocity of the inner and outer boundary edge excitations. In this

chapter both the microscopic representation and the phenomenological description of the edge states has been presented. In the microscopic picture it has been shown that the edge excitations can be added to the system by multiplying Laughlin's wavefunction by a symmetric polynomial. Such new states are zero energy eigenstates of a short-range interaction Hamiltonian, however the total angular momentum is changed and depends on the configuration of the excitations at the FQH droplet boundaries. The phenomenological approach based on the work by Wen shows how the edge states of the FQHE have close behaviour to a conventional Luttinger liquid and allows predictions to be made on transport properties of the FQHE. As discussed in the introductory chapter to this thesis, there is work supporting this theory and the Luttinger liquid-like behaviour of the edge states. The next, and final section of this chapter presents computations for overlaps of Laughlin states supporting edge excitations, from a microscopic perspective.

3.3 Numerical Verification of Analytic Formulas for Overlap Integrals

In this section, numerical data will be presented for the overlap integrals of states containing both inner and outer boundary edge excitations. The overlap integrals in the microscopic picture are computed using the MC method. This work validates the analytic formula for the overlap integrals originally obtained in the work by Cheianov *et al.* for a single edge FQH droplet [94]. In Section 3.2 the formula was extended to include two edges in the FQH droplet as depicted in Figure 1.5. The equation is restated below for convenience.

$$\langle \{n_{\pm k}\} | \{n_{\pm p}\} \rangle = \prod_{k,p>0} \frac{1}{m^{n_{\pm k}+n_{\pm p}}} \frac{\partial^{n_{\pm k}+n_{\pm p}} \tau^\nu(N, M, t_{\pm p}, \bar{t}_{\pm k})}{\partial \bar{t}_{\pm k}^{n_{\pm k}} \partial t_{\pm p}^{n_{\pm p}}} \Bigg|_{t_{\pm k}=0}, \quad (3.33)$$

where $R_- \equiv R_I$ is the inner boundary radius and $R_+ \equiv R_O$ is the outer boundary radius and,

$$\tau(N, M, t_{\pm k}, \bar{t}_{\pm k}) = D(N, M) \times \exp \left\{ m \sum_{k>0} k R_O^{2k} |t_k|^2 + k \frac{|t_{-k}|^2}{R_I^{2k}} + k t_{-k} t_k + k \bar{t}_k \bar{t}_{-k} \right\}, \quad (3.34)$$

is calculated explicitly in Appendix B. The function,

$$D(N, M) \equiv \tau(N, M, t_{\pm k}, \bar{t}_{\pm k})|_{t_{\pm k}=0} \quad (3.35)$$

is independent of $t_{\pm k}$ and $\bar{t}_{\pm k}$ and will be referred to as the zero mode part. The microscopic computation of the overlap of states is important for two reasons. Firstly, it provides a good test of the MC method for computing observables in the FQHE. Secondly, the microscopic computations provide a good method to check the form of the tau-function. See Appendix B for more details.

There are an infinite number of possible configurations of the boson occupied orbitals $\{n_{\pm k}\}$. Since it is an impossible task to verify all states satisfy the analytic formula for the overlap integrals, the test is carried out for states satisfying the total edge state contribution to the orbital angular momentum of $|l_I| = 0$, or $|l_I| = 2$ for the inner boundary and $l_O = 0$ or $l_O = 2$ for the outer boundary. With this angular momentum cutoff, the highest possible orbital that can be occupied corresponds to the power sum polynomial $S_{\pm 2}$ with a single excitation. Therefore, to perform the microscopic computations using the MC method, we seek states of the form,

$$\begin{aligned}
|n_{-1}n_{-2}n_1n_2\rangle &= \left[\sum_{k=1}^N \frac{1}{z_k} \right]^{n_{-1}} \left[\sum_{k=1}^N \frac{1}{z_k^2} \right]^{n_{-2}} \left[\sum_{k=1}^N z_k \right]^{n_1} \left[\sum_{k=1}^N z_k^2 \right]^{n_2} \\
&\times \prod_{i<j}^N (z_i - z_j)^m \prod_{i=1}^N z_i^M e^{-\frac{|z_i|^2}{4}} \\
&= \prod_{k=-2}^2 S_k^{n_k} \prod_{i<j}^N (z_i - z_j)^m \prod_{i=1}^N z_i^M, \tag{3.36}
\end{aligned}$$

which has been obtained from Eq. (3.6) from Section 3.1. All possible states using the notation in (3.36) are given in the left-hand column of Table 3.1, excluding the trivial case $\langle 0|0\rangle$. These combinations of states were obtained using $|l_I| = n_{-1} + 2n_{-2} = 2$ or 0 and $l_O = n_1 + 2n_2 = 2$ or 0 for the total angular momentum contribution for the inner and outer boundaries, respectively. More information related to the array of states that correspond to certain angular momentum values is given in Appendix A. The overlap integrals for the states given in Eq. (3.36) are difficult to calculate in the large N limit for $m \neq 1$, as discussed in Section 3.1. Therefore to check the analytic formula for the overlap integrals given in (3.34), the MC method is used. The MC method works by calculating statistical averages and therefore ratios of the overlaps of states are computed which have the following form,

$$\frac{\langle n'_{-1}n'_{-2}n'_1n'_2 | n_{-1}n_{-2}n_1n_2 \rangle}{\langle 0|0 \rangle} = \frac{\int_N |\Psi_N^M|^2 \prod_{p=-2}^2 \bar{S}_p^{n'_p} \prod_{k=-2}^2 S_k^{n_k}}{\int_N |\Psi_N^M|^2}, \tag{3.37}$$

where the following shorthand notation has been used: $\int_N \equiv \int \prod_{i=1}^N d^2z_i$ and Ψ_N^M is the Laughlin wave function for the disk geometry FQH fluid. In total there are 8 states that correspond to the angular momentum cutoffs that have been imposed. This results in a total of 8×8 MC simulations run to compute overlap integrals of the form (3.37). The overlaps were calculated for a system with $N = 60$ electrons

in the quantum fluid and $M = 56$ quasiholes in the center of the droplet to create the inner boundary of the system. To compute the overlap integrals, FQH systems were chosen that correspond to the filling factor $\nu = m^{-1} = 1/3$.

All off-diagonal overlap integrals (i.e., where the occupation numbers in the left state were different to those in the right state) were decreasing in magnitude as compared to the diagonal elements and thus these results are not listed here. It is noted however that the analytic expression for the overlap integrals (3.33) also predicts zero for these off-diagonal elements in the large system size limit. The results for the diagonal overlap integrals have been listed in Table 3.1 along with the corresponding analytic values predicted by Eq.(3.33).

According to the analytic expression for the overlap integrals, all results will be proportional to the zero-mode part of the tau-function, $D(N, M)$. The form of this function is unknown and therefore results in each of the rows listed in Table 3.1 correspond to ratios of overlap integrals of the form

$$\frac{\langle 2000|2000 \rangle}{\langle n_{-1}n_{-2}n_1n_2|n_{-1}n_{-2}n_1n_2 \rangle}, \quad (3.38)$$

where the denominator corresponds to the state listed in the left-hand column of Table 3.1.

It is clear that the MC data in Table 3.1 is in complete agreement with the analytic expression for the overlap integrals, originally derived by Cheianov *et al.* This is something that has never been microscopically checked before. The results also show that the form of the tau-function calculated in Appendix B accurately represents bosonic excitations contained in the microscopic states. In this section it has been shown that the MC method is a useful tool for performing microscopic computations for Laughlin type systems for large system sizes. The overlap integrals in Eq. (3.37) were straightforward integrals for the MC method to han-

$\langle n_{-1}n_{-2}n_1n_2 n_{-1}n_{-2}n_1n_2 \rangle$	Analytic prediction	MC Result
$\langle 2000 2000 \rangle$	1.00	1.00 ± 0.02
$\langle 0100 0100 \rangle$	0.333	0.333 ± 0.006
$\langle 2020 2020 \rangle$	1.01×10^{-5}	$(1.05 \pm 0.05) \times 10^{-5}$
$\langle 2001 2001 \rangle$	6.7×10^{-6}	$(6.8 \pm 0.2) \times 10^{-6}$
$\langle 0120 0120 \rangle$	6.7×10^{-6}	$(6.7 \pm 0.2) \times 10^{-6}$
$\langle 0101 0101 \rangle$	2.2×10^{-6}	$(2.1 \pm 0.1) \times 10^{-6}$
$\langle 0020 0020 \rangle$	3.58×10^{-10}	$(3.55 \pm 0.09) \times 10^{-10}$
$\langle 0001 0001 \rangle$	1.19×10^{-10}	$(1.19 \pm 0.03) \times 10^{-10}$

Table 3.1: This table compares the analytic predictions for the overlap of states containing edge excitations on the inner and outer boundary of a two-edged FQHE. The second column lists the analytic predictions for the ratio of the overlap $\langle 2000 | 2000 \rangle$ with the overlap integral shown in the first column of the table. The third column lists the MC data for the same ratio of integrals.

dle. In the remaining chapters of this thesis the MC method will be applied for more complicated computations in the microscopic theory of Laughlin-type FQH systems.

Zero-Mode Tunnelling Matrix Elements

From the discussion in the introductory chapter of this thesis, tunnelling measurements are an important transport property to observe and test the Luttinger liquid-like behaviour of the FQHE. The theoretical description of tunnelling uses the phenomenological theory of edge states proposed by Wen to create an effective tunnelling Hamiltonian which is analysed by using a renormalization group (RG) approach [52]. However since there are no microscopic calculations to compare the calculations to, there are questions about how accurate a description this is. The question which we would like to answer in this chapter is whether the effective tunnelling Hamiltonian makes predictions that can be verified microscopically? Also, is the tunnelling Hamiltonian a local operator? The RG analysis provides flow equations for the tunnelling parameters; however without any initial conditions from a microscopic model with which to compare, the flow equations cannot provide answers to questions such as at which scales certain tunnelling processes become irrelevant? To investigate these problems a microscopic model for tunnelling between edge states using the geometry of the FQH disk shown in Figure 1.5 is developed. It has already been discussed in Chapter 3 that in the microscopic theory the matrix elements of Laughlin states cannot be solved analytically

by any methods known to this author and therefore tunnelling matrix elements will be computed numerically using the MC method.

The microscopic tunnelling matrix elements can then be compared to the effective theory predictions where the tunnelling Hamiltonian is constructed using the bosonised operator formalism introduced in Section 3.2 of Chapter 3. Only the simplest possible matrix elements are considered initially; these are referred to as the zero mode matrix elements and correspond to a system absent of any low-energy boundary excitations in the FQH device. The computations presented in this chapter are based on work by this author and V. Cheianov [45].

To begin, the representation of the zero mode tunnelling matrix elements is given for the microscopic theory. Also in Section 4.1 the methods of calculating the tunnelling matrix elements using MC are discussed. In Section 4.2 the low-energy projection of the tunnelling Hamiltonian matrix elements are derived using the bosonised formulae for the fermion operators derived in Chapter 3. In the Section 4.3 a comparison is made between the effective theory predictions and the microscopic calculations for the size dependence of the tunnelling matrix elements. The final section presents a conclusion and summary for the work covered in this chapter.

4.1 Microscopic Computation of the Zero Mode Tunnelling Matrix Elements

In this chapter, only FQH states occupying the lowest Landau level are considered. Since the exact ground state of a FQH system is not known, we instead use the Laughlin wavefunction. To consider tunnelling across the bulk of a FQH device, a disk-shaped Laughlin system is used consisting of an inner and outer edge as shown in Figure 4.1. To create a second edge in our system such that tunnelling

across the bulk can be observed, a macroscopic hole is inserted in the centre of the droplet. This macroscopic hole is created by inserting M quasiholes at $z = 0$, as discussed in the introduction of this thesis. For convenience the Laughlin state for this system is repeated below.

$$\Psi_N^M = \prod_{k=1}^N \left(e^{-\frac{|z_k|^2}{4l}} z_k^M \right) \prod_{i<j}^N (z_i - z_j)^m \equiv |N, M\rangle \quad (4.1)$$

The bra-ket notation has been introduced to simplify expressions in future calculations where $|N, M\rangle$ represents the ground state system. The electrons are confined to a domain D^M on the complex plane. The hole created at $z = 0$ has an inner radius $R_I = \sqrt{2M}$ and outer radius given by $R_O = \sqrt{2mN + 2M}$ as calculated in the Chapter 1 (see Eqs. (1.32) and (1.33)). At the interfaces of D^M there is a sharp decrease of particle density to zero in the large N limit.

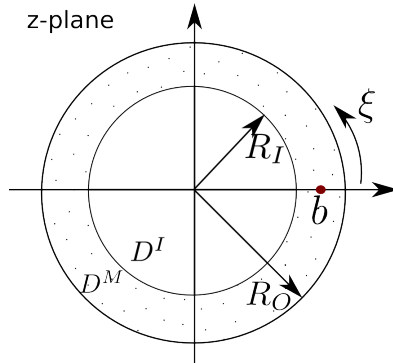


Figure 4.1: Schematic diagram for the FQH device. Charges are confined to the domain D^M on the complex plane. The radii of the inner and outer edge of D^M are given by R_I and R_O . The width of domain D^M is such that $R_O - R_I \sim 4$. Domain D^I corresponds to the area of the macroscopic hole created by inserting Laughlin quasiholes at $z = 0$. An impurity is placed at position b along the positive real axis.

To encourage tunnelling between the edges of the system, an impurity is placed inside the bulk at position b . The potential \hat{V} of this impurity has the form

$$\hat{V} = u \sum_{i=1}^N \delta^{(2)}(z_i - b). \quad (4.2)$$

The parameter u corresponds to the strength of the potential which will be set to unity and we assume that $|b| = (R_O + R_I)/2$. If the ring of the bulk is sufficiently thick then adding the impurity to the system will have no effect on the edges due to a finite correlation length in the bulk on the order of the magnetic length. Therefore it is assumed that for all N the width of the system ($R_O - R_I$) is constant and narrow enough such that both edges are affected by the impurity.

The microscopic expression for the zero mode tunnelling matrix elements due to the impurity inserted into the bulk are given by

$$\begin{aligned} \langle V \rangle_\chi &\equiv \frac{\langle N, M | V | N, M + \chi \rangle}{\sqrt{\langle N, M | N, M \rangle \langle N, M + \chi | N, M + \chi \rangle}} \\ &= \frac{\int_{N-1} |\Psi_N^M|^2 \prod_{i=1}^{N-1} z_i^\chi \sum_{n=1}^N \delta^{(2)}(z_n - b)}{\sqrt{\int_N |\Psi_N^M|^2 \cdot \int_N |\Psi_N^{M+\chi}|^2}} \end{aligned} \quad (4.3)$$

where, to shorten notation inside the integrals, $|\Psi_N^M|^2$ is used to denote the absolute value of Laughlin's wavefunction squared and the integration variables are shortened to $\int_N \equiv \int \prod_{k=1}^N d^2 z_k$. This matrix element describes a process in which a number χ of quasiparticles are transferred from the inner boundary to the outer boundary due to the impurity potential \hat{V} given in Eq. (4.2). Therefore $\chi = 1$ corresponds to quasiparticle tunnelling and $\chi = m$ to electron tunnelling for some Laughlin state $\nu = 1/m$. Note that the denominator in (4.3) is needed to correctly normalize the elements.

The delta-function in the numerator of Eq. (4.3) allows one of the variables in

the integral to be integrated out. Using the fact that the integrals appearing in each term of the sum are symmetric with respect to the exchange of integration variables, $\langle V \rangle_\chi$ can be written as

$$\langle V \rangle_\chi = \frac{N e^{-\frac{|b|^2}{2}|b|^{2M}} b^\chi \int_{N-1} |\Psi_{N-1}^M|^2 \prod_{i=1}^{N-1} z_i^\chi |z_i - b|^{2m}}{\sqrt{\int_N |\Psi_N^M|^2 \cdot \int_N |\Psi_N^{M+\chi}|^2}}. \quad (4.4)$$

The overlap integrals in Eq. (4.3) for the free fermion case can be calculated analytically and thus provides a good check for the numerical methods developed in this chapter. An effective numerical method to calculate these overlap integrals is by using Monte Carlo (MC) simulations. As already discussed, this method seems quite natural since the norm of the wavefunction can be considered as a partition function for a 2D Coulomb plasma allowing statistical averages of operators to be calculated with a probability distribution analogous of the Boltzmann distribution of the plasma. All the MC simulations in the present work were carried out using the Metropolis algorithm (see Chapter 2).

To directly use the MC method on the integral in the numerator of (4.3) is difficult due the product over all particles of the form z_i^χ . This product introduces a phase problem to the calculation since the MC measurements on the phase part of this product will have significant fluctuations between successive measurements and the convergence of the simulation will be slow. Two successful methods to overcome this phase problem have been found. The effectiveness of each method depends on the value of χ and the first of the methods to be discussed is appropriate for small values of χ whereas the second method can only be used for $\chi = m$, i.e., for the case of an electron tunnelling across the bulk.

4.1.1 Phase Problem Solution: Method 1 for $\chi \leq 1$

The first method of overcoming the phase problem in the integral (4.3) is by using the cumulant expansion. It will be seen later that only for a small value of χ can the particular cumulant expansion of interest be calculated reliably. First the integral in the numerator should be expressed in a more convenient way. To do this it is noted that part of the numerator of Eq. (4.4) can be re-written as;

$$\prod_{i=1}^{N-1} |z_i - b|^{2m} z_i^\chi = \left(\frac{-b}{|b|} \right)^{\chi(N-1)} \prod_{i=1}^{N-1} |z_i - b|^{2m} |z_i|^\chi \Theta_\chi(z_i, b)$$

where

$$\Theta_\chi(z_i, b) = \left[\frac{\left(1 - \frac{z_i}{b}\right) \left(1 - \frac{\bar{b}}{\bar{z}_i}\right)}{\left|1 - \frac{z_i}{b}\right| \left|1 - \frac{\bar{b}}{\bar{z}_i}\right|} \right]^\chi. \quad (4.5)$$

The advantage of the function $\Theta_\chi(z, b)$ is that its cumulant expansion can be calculated with respect to some probability distribution using a MC simulation with a relatively quick convergence. Indeed if we choose the probability distribution such that

$$\left\langle \prod_{i=1}^{N-1} \Theta_\chi(z_i, b) \right\rangle_\varphi = \frac{\int_{N-1} |\Psi_{N-1}^M|^2 \prod_{i=1}^{N-1} |z_i|^\chi |z_i - b|^{2m} \Theta_\chi(z_i, b)}{\int_{N-1} |\Psi_{N-1}^M|^2 \prod_{i=1}^{N-1} |z_i|^\chi |z_i - b|^{2m}} \quad (4.6)$$

then the average over $\Theta(z, b)$ in (4.6) can be related the tunnelling matrix elements in (4.3) via

$$\langle V \rangle_\chi = \left(\frac{-|b|}{b} \right)^{\chi(N-1)} \left\langle \prod_{i=1}^{N-1} \Theta_\chi(z_i, b) \right\rangle_\varphi N e^{\frac{|b|^2}{2}} |b|^{2M} b^\chi \sqrt{h_1 h_2}, \quad (4.7)$$

where

$$h_1 = \frac{\int_{N-1} |\Psi_{N-1}^M|^2 \prod_{i=1}^{N-1} |z_i|^\chi |z_i - b|^{2m}}{\int_N |\Psi_N^M|}, \quad (4.8)$$

$$h_2 = \frac{\int_{N-1} |\Psi_{N-1}^M|^2 \prod_{i=1}^{N-1} |z_i|^\chi |z_i - b|^{2m}}{\int_N |\Psi_N^{M+\chi}|}. \quad (4.9)$$

Integrals h_1 and h_2 are relatively trivial MC integrals to compute. Even though the number of particles is different in the numerator and the denominator, it is observed that the form of h_1 and h_2 is similar to the definition of the average of the density operator (e.g., see Eq. (1.18)) and therefore

$$h_1 = \frac{\langle \rho \rangle_M e^{\frac{|b|^2}{2}}}{N|b|^{2M}} \frac{\int_{N-1} |\Psi_N^M|^2 \prod_{k=1}^{N-1} |z_k - b|^{2m}}{\int_{N-1} |\Psi_N^M|^2 \prod_{k=1}^{N-1} |z_k - b|^{2m} |z_k|}, \quad (4.10)$$

$$h_2 = \frac{\langle \rho \rangle_{M+1} e^{\frac{|b|^2}{2}}}{N|b|^{2(M+1)}} \frac{\int_{N-1} |\Psi_N^{M+1}|^2 \prod_{k=1}^{N-1} |z_k - b|^{2m}}{\int_{N-1} |\Psi_N^M|^2 \prod_{k=1}^{N-1} |z_k - b|^{2m} |z_k|}. \quad (4.11)$$

Now the integrals in the numerator and denominator of both h_1 and h_2 have the same number of integration variables and therefore the ratio of integrals can be calculated using MC. Since it is assumed that the impurity is placed deep within the bulk; $\langle \rho(b) \rangle_M = \langle \rho(b) \rangle_{M+1} = (2\pi m)^{-1}$. As already mentioned it is the cumulant expansion of $\Theta(z, b)$ in (4.6) that gets rid of the phase problem in the MC computations for the tunnelling matrix elements. In order to see why this is so, consider $\Theta(z, b)$ written in terms of an exponential function.

$$e^{\ln \Theta(z,b)} = \exp \left(i\chi \text{Arg} \left[\left(1 - \frac{z}{b} \right) \left(1 - \frac{\bar{b}}{\bar{z}} \right) \right] \right) \quad (4.12)$$

The first couple of terms for the cumulant expansion of some function $\langle e^G \rangle$ is

$$\langle e^G \rangle = e^{\langle G \rangle + \frac{1}{2!} (\langle G^2 \rangle - \langle G \rangle^2) + \frac{1}{3!} (2\langle G \rangle^3 - 3\langle G \rangle \langle G^2 \rangle + \langle G^3 \rangle) + \dots} \quad (4.13)$$

After substituting Eq. (4.12) into the expansion of Eq. (4.13) we notice the following; the mean field of G is essentially an average over an angle, which is zero. Secondly, sequential terms in the expansion increase by a factor of χ . For the cumulant expansion to be used reliably, the higher order terms must quickly decay to zero. For $\chi > 1$, this is not the case and the cumulant expansion converges too slowly considering only a small, finite number of terms can be computed numerically. However for $\chi = 1$ the cumulant expansion of $\langle \prod \Theta(z_i, b) \rangle$ is well behaved and can be used to calculate the matrix elements in Eq. (4.3) reliably.

4.1.2 Phase Problem Solution: Method 2 for $\chi = m$

The second method of avoiding the phase problem in (4.3) relies on the fact that for the special case $\chi = m$, then (4.3) can be written in terms of real valued functions. The numerator of (4.3) (sticking to general χ for the moment) can be written as follows,

$$\langle N, M | V | N, M + \chi \rangle = N e^{-\frac{b^2}{2}} b^{2M+\chi} \int_{N-1} |\Psi_{N-1}^M|^2 \prod_{i=1}^{N-1} z_i^\chi |z_i - b|^{2m}$$

$$= N e^{-\frac{b^2}{2}} b^{2M+\chi} \int_{N-1} |\Psi_{N-1}^M|^2 \prod_{i=1}^{N-1} |z_i|^{2\chi} z_i^{m-\chi} (z_i - b)^m \left(1 - \frac{\bar{b}}{z_i}\right)^m. \quad (4.14)$$

The only non-zero terms of this integral are terms that conserve total angular momentum; the remainder of the terms will be angle dependent and will go to zero after performing the integration over the angle variables. To see what terms do conserve angular momentum, a global transformation can be performed such that $\{z_i\} \rightarrow \{z_i e^{i\theta}\}$, where θ is some constant. From performing this transformation it can be deduced that for $\chi > m$ there are no terms in the polynomials that conserve angular momentum and thus the tunnelling matrix elements $\langle V \rangle_{\chi > m}$ are zero for Laughlin wave functions. Under a similar global rotation argument when $\chi = m$, the numerator of $\langle V \rangle_m$ takes the particularly simple form

$$\langle N, M | V | N, M + m \rangle = N e^{-b^2/2} b^{2M+m} (-b)^{m(N-1)} \int_{N-1} |\Psi_{N-1}^{M+m}|^2. \quad (4.15)$$

Therefore one can write the matrix element for the electron tunnelling as

$$\langle V \rangle_m = N e^{-\frac{b^2}{2}} (-b)^{m(N-1)} b^{2M+m} \sqrt{\frac{\Xi^2}{\tau}}. \quad (4.16)$$

The integrals have all been symbolised by Ξ and τ to shorten notation and they have the form

$$\Xi = \frac{\int_{N-1} |\Psi_{N-1}^{M+m}|^2}{\int_N |\Psi_N^{M+m}|^2}, \quad (4.17)$$

$$\tau = \frac{\int_N |\Psi_N^M|^2}{\int_N |\Psi_N^{M+m}|^2}. \quad (4.18)$$

Functions Ξ and τ are simply ratios of the overlap of the ground state functions (4.1) for various N and M values. The function τ is a relatively trivial MC calculation, where Ξ is not so trivial due to the differing number of integration variables in the numerator and the denominator. To form a method to compute Ξ , consider the following average

$$\langle F \rangle_{N,M+m} = \frac{\int_N |\Psi_N^{M+m}|^2 \sum_{i=1}^N f(z_i)}{\int_N |\Psi_N^{M+m}|^2} = N \frac{\int_N |\Psi_N^{M+m}|^2 f(z_N)}{\int_N |\Psi_N^{M+m}|^2} \quad (4.19)$$

The explicit form of $f(z)$ is chosen to be

$$f(z_i) = \Theta(|z_i| - (R_O + d)) = \begin{cases} 1 & \text{for } |z_i| \geq R_O + d \\ 0 & \text{otherwise,} \end{cases} \quad (4.20)$$

where d is some distance added to the outer radius and will be defined later. By multiplying and dividing the average $\langle F \rangle_{N,M+m}$ by $\int_{N-1} |\Psi_{N-1}^{M+m}|^2$ then (4.19) can be manipulated in such a way as to contain the function Ξ . I.e.,

$$\langle F \rangle_{N,M+m} = N \cdot \Xi \cdot \frac{\int_N |\Psi_N^{M+m}|^2 f(z_N)}{\int_{N-1} |\Psi_{N-1}^{M+m}|^2} = N \Xi I_N. \quad (4.21)$$

The remaining integrals in the expression (4.21) have been labelled by I_N .

$$\begin{aligned}
I_N &= \frac{\int d^2 z_N e^{-|z_N|^2/2} |z_N|^{2(M+m)} f(z_N) \int_{N-1} \left| \Psi_{N-1}^\beta \right|^2 \prod_{i=1}^{N-1} |z_i - z_N|^{2m}}{\int_{N-1} \left| \Psi_{N-1}^\beta \right|^2} \\
&= 2\pi \int_{R_O+d}^{\infty} dr_N e^{-r_N^2/2} r_N^{2(M+m)+2m(N-1)} \left\langle \prod_{i=1}^{N-1} \left| 1 - \frac{z_i}{z_N} \right|^{2m} \right\rangle_{N-1, M+m} \\
&= 2\pi \int_{R_O+d}^{\infty} dr_N e^{-r_N^2/2} r_N^{2(M+m)+2m(N-1)} \gamma(z_N) \tag{4.22}
\end{aligned}$$

The average over $N - 1$ particles is labelled as γ , which is a function of the N 'th particle coordinate. Since it will be real valued the angle integration over the N 'th coordinate has been performed. The function $e^{-r_N/2} r_N^{2(M+m)+2m(N-1)}$ is a rapidly decaying function away from the outer boundary and thus if the lower integration limit of r_N is sufficiently larger than R_O , then one can use the following asymptotic approximation $\gamma(z_N) \sim \gamma(R_O + d)$. This substitution makes the function $\gamma(R_O + d)$ trivial to calculate using a MC simulation. Once $\gamma(R_O + d)$ is known, the integral I_N is a straightforward two-dimensional integral.

Alongside the γ -function, the average $\langle F \rangle$ must also be calculated using an MC simulation. This average is also dependent on d , the distance from the outer boundary. Since $\langle F \rangle$ simply counts the number of particles beyond the point $R_O + d$ there is a trade-off as to how large d should be. The larger the value of d the fewer particles there will be to count since the particle density decreases sharply from the outer boundary, but also for larger values of d , the more accurate the asymptotic approximation, $\gamma(z_N) \sim \gamma(R_O + d)$, thus a trade off must be made. With Ξ now define in terms of computable MC integrals,

$$\Xi = \frac{\langle F \rangle_{N, M+m}}{N I_N}, \tag{4.23}$$

then the zero mode tunnelling matrix elements satisfying $\chi = m$ can be expressed

in terms of these MC integrals as follows,

$$\langle V \rangle_m = e^{-|b|^2/2} (-b)^{m(N-1)} b^{2M+m} \frac{\langle F \rangle_{N,M+m}}{I_N \sqrt{\tau}}. \quad (4.24)$$

Therefore the zero mode tunnelling matrix elements due to an impurity in the bulk can be computed for the two special cases; $\chi = m$ given in terms of MC averages in (4.24) and, for $\chi = 1$ which has also been expressed in terms of MC averages in the previous part of this section (4.7). In the next section, analogous expressions for the tunnelling matrix elements will be formulated in the effective theory.

4.2 Zero Mode Tunnelling Matrix Elements Using the Effective Hamiltonian

As implied in the introduction, it is the edges of the device, consisting of two counter propagating chiral Luttinger liquids that are of most interest for tunnelling calculations. A successful method for describing the effective low-energy physics of a chiral Luttinger liquid uses the method of bosonisation which has been discussed in Chapter 3 where the bosonised fields for quasiparticle operators were derived. For convenience they are stated below.

$$\begin{aligned} \psi_{p,O}^\dagger(\xi) &= e^{i\frac{p}{m}\varphi_N} e^{p\phi_O(\xi)} \\ \psi_{p,O}(\xi) &= e^{-p\phi_O(\xi)} e^{-i\frac{p}{m}\varphi_N} \\ \psi_{p,I}^\dagger(\xi) &= e^{i\frac{p}{m}\varphi_N} e^{ip\varphi_M} e^{p\phi_I(\xi)} \\ \psi_{p,I}(\xi) &= e^{-p\phi_I(\xi)} e^{-i\frac{p}{m}\varphi_N} e^{-ip\varphi_M} \end{aligned} \quad (4.25)$$

The subscript ‘‘I’’ corresponds to an inner boundary operator and ‘‘O’’ to an outer boundary operator. The fields $\phi_{O/I}$ are bosonic and are given by

$$\begin{aligned}
\phi_O(\xi) &= -\frac{i\xi}{R}\left(\theta_N + \frac{\theta_M}{m}\right) + \sum_{k>0} \sqrt{\frac{1}{mk}} \left(e^{-ik\frac{\xi}{R}} a_k^\dagger - e^{ik\frac{\xi}{R}} a_k \right) \\
&= \phi_O^0 + \phi_O^+ - \phi_O^- \\
\phi_I(\xi) &= -\frac{i\xi}{mR}\theta_M + \sum_{k>0} \sqrt{\frac{1}{mk}} \left(e^{ik\frac{\xi}{R}} a_{-k}^\dagger - e^{-ik\frac{\xi}{R}} a_{-k} \right) \\
&= \phi_I^0 + \phi_I^+ - \phi_I^-.
\end{aligned} \tag{4.26}$$

In the effective theory of low-energy excitations the transverse positions to the edges of the FQH device are unimportant since we assume that the domain D^M is a very narrow ring in comparison to the size of its outer radius R_O , therefore our particle fields depend only on the longitudinal coordinate ξ , where $\xi \in [0, 2\pi R]$ and R is the radius at which the transfer of charges between the edges takes place. I.e., $R \equiv |b|$. In (4.25), ψ_p corresponds to the annihilation operator of particle with charge $e^* = (p/m)e$ in the Laughlin state $\nu = (1/m)$. Therefore $\psi_{p=1}$ corresponds to the field for a single Laughlin quasiparticle with charge $e^* = (1/m)e$ and $\psi_{p=m}$ corresponds to m quasiparticles, or equivalently a single electron field.

With the low-energy, effective theory field operators defined, one can now discuss the effect of the impurity placed in the bulk. The tunnelling operator takes the form

$$H_T = \sum_{p=1}^{\infty} A_p(\xi), \tag{4.27}$$

where ξ is the longitudinal position at which tunnelling occurs along the boundaries and the operators A_p transfer a number of p quasiparticles from the inner to the outer boundary. From the form of H_T one can see it is possible for the tunnelling

of any number of quasiparticles across the bulk. For $p = 1$, A_P describes the tunnelling process for a single quasiparticle and for $p = m$ the tunnelling process is for that of an electron in FQH state $\nu = 1/m$. For Laughlin states, however, it was shown (see Eq. (4.14)) that the transfer of $p > m$ quasiparticles is identically zero. Whether this behaviour should be extended to the exact wave functions of quantum Hall states is unknown and, thus experiments on FQH systems that observe a $p > m$ tunnelling process would be extremely interesting and a good measure for the preciseness of the Laughlin wavefunction as a microscopic description of the FQHE.

Here two types of tunnelling processes across the bulk are considered, the first being a single quasiparticle tunnelling and the second will be electron tunnelling or equivalently m quasiparticles tunnelling. These processes are described by $A_{p=1}$ and $A_{p=m}$ respectively. In general operators A_p have the form;

$$A_p(\xi) = t_p \left(\psi_{p,O}^\dagger(\xi) \psi_{p,I}(\xi) + \text{h.c.} \right), \quad (4.28)$$

where ξ is the longitudinal position at which the tunnelling occurs on the boundaries and t_p is a parameter that cannot be calculated analytically given the microscopic theory. In this work the scaling behaviour of the parameters t_p will be investigated as system size N is varied. This can be achieved by looking at the zero mode matrix elements of the tunnelling operator.

$$\begin{aligned} \langle A_p(\xi) \rangle &= \langle N, M | A_p(\xi) | N', M' \rangle \\ &= t_p \langle N, M | \psi_{p,O}^\dagger(\xi) \psi_{p,I}(\xi) | N', M' \rangle + \text{h.c.} \\ &= t_p \langle N, M | e^{i\frac{p}{m}\varphi_N} e^{p\phi_O(\xi)} e^{-p\phi_I(\xi)} e^{-i\frac{p}{m}\varphi_N} e^{-ip\varphi_M} | N', M' \rangle + \text{h.c.} \end{aligned} \quad (4.29)$$

The first term in (4.29) describes a process where p particles move from the inner boundary to the outer boundary and for the second term this process is reversed.

Only one term is needed here so the Hermitian conjugate term can be neglected. Next the ordering of the operators is considered which will in turn affect the behaviour of the parameter t_p . Here, two types of ordering are considered with the first being the usual definition of normal ordering defined by

$$e^\phi \rightarrow : e^\phi := e^{\phi^0} e^{\phi^+} e^{-\phi^-}. \quad (4.30)$$

The matrix element calculated using this ordering is denoted by $\langle : A_p(\xi) : \rangle$ and is straightforward to calculate.

$$\begin{aligned} |\langle : A_p(\xi) : \rangle| &= \left| \left\langle N, M \left| e^{i\frac{p}{m}\varphi_N} : e^{p\phi_O(\xi)} e^{-p\phi_I(\xi)} : e^{-i\frac{p}{m}\varphi_N} e^{-ip\varphi_M} \right| N', M' \right\rangle \right| \\ &= |t_p| \delta_{N,N'} \delta_{M,M'-p} \end{aligned} \quad (4.31)$$

The absolute values of matrix elements are taken to get rid of unnecessary phase terms. Therefore if normal ordering is used, only t_p contributes to system size dependence. On the other hand, a different result is obtained by choosing the following ordering for the operators,

$$e^\phi = e^{\phi^0} e^{\phi^+} e^{-\phi^-} e^{-\frac{1}{2}[\phi^0, \phi^+ - \phi^-]} e^{-\frac{1}{2}[\phi^+, -\phi^-]} = e^{\phi^0} e^{\phi^+} e^{-\phi^-} e^{-\frac{1}{2}\sum_k (\frac{m}{k})}, \quad (4.32)$$

where the following commutation relations have been used; $[\phi_x^0(\xi), \phi_x^+(\xi) - \phi_x^-(\xi)] = 0$ and $[\phi_x^+(\xi), \phi_x^-(\xi)] = -\sum_k (m/k)$ where $x = I$ or, $x = O$. These relations are straightforward to calculate using the commutators listed in Chapter 3 for the zero mode operators and $a_{\pm k}$, $a_{\pm k}^\dagger$. Proceeding with the matrix element (4.29),

$$|\langle A_p(\xi) \rangle| = |t_p| \exp \left(- \sum_{k>0} \frac{p^2}{mk} \right) \delta_{N,N'} \delta_{M,M'-p} \quad (4.33)$$

The sum over k in (4.33) has already been calculated in Chapter 3, see Eq. (3.31). It was calculated using a soft cutoff $\Lambda \sim R \equiv |b|$ to give $\sum_{k>0} k^{-1} \rightarrow \sum_{k>0} k^{-1} e^{-k/R} = -\ln(1 - e^{-1/R})$. To get an approximate idea of the behaviour of this sum in the large N , or equivalently large R limit, the exponential in the logarithm can be expanded to give $-\ln(1 - e^{-1/R}) \sim \ln R$. Thus for a log-log plot of the amplitude of (4.33) versus particle number, one would expect the gradient to be $\sim -p^2/m$ for large enough $R \equiv |b|$. For now we will keep the exact form of the sum so that the final expression of the tunnelling matrix elements is,

$$|\langle A_p(\xi) \rangle| = |t_p| \left(1 - e^{-\frac{1}{R}} \right)^{\frac{p^2}{m}} \delta_{N,N'} \delta_{M,M'-p}. \quad (4.34)$$

From (4.34); the zero mode tunnelling matrix elements have a dependence on the system size N , which for non-normal ordering of operators given by (4.32) is not from the parameter t_p . If the operator A_p for ordering (4.32) is local then we can assume all the system size dependence originates from the sum $\sum_k k^{-1}$ and t_p is constant for all N . Ideally the tunnelling operators should remain local since the impurity placed between the edges in the FQH device should only affect charges in its vicinity and not the remainder of the system. The correlator of a local operator $\langle A_p(\xi) A_p(\xi') \rangle$ should be independent of system size for ξ and ξ' sufficiently far apart, also ξ, ξ' should be sufficiently far away from the edges of the system.

$$\begin{aligned} \langle A_p(\xi) A_p(\xi') \rangle &= \langle N, M | A_p(\xi) A_p(\xi') | N', M' \rangle \\ &= 2 \exp \left\{ \frac{2p^2}{m} \sum_{k>0} k^{-1} \left(\cos \left[\frac{k}{R} (\xi' - \xi) \right] - 1 \right) \right\} \\ &\quad \times \cos \left[\frac{p}{R} \left(N - \frac{p}{m} \right) (\xi' - \xi) \right] \end{aligned} \quad (4.35)$$

Only matrix elements that are kept in the above expression are those with $M' = M$ and $N' = N$ which satisfies the definition of the tunnelling operator A_p .

To finish the calculation, a soft cutoff is used ($\Lambda \equiv R$) to calculate the sum in (4.35), which is the same approach as was used to calculate similar sums earlier for the tunnelling matrix elements. Using this cutoff and taking the limit $|\xi - \xi'|/R \ll 1$ gives the final result for the correlator calculation in Eq. (4.36). There is no system size independence as required for the correlator of the tunnelling operator using the operator ordering defined in Eq. (4.32).

$$\langle A_p(\xi)A_p(\xi') \rangle = \frac{2}{(1 + (\xi' - \xi)^2)^{\frac{p^2}{m}}} \cos \left[\frac{p}{R} \left(N - \frac{p}{m} \right) (\xi' - \xi) \right] \quad (4.36)$$

The correlator of the tunnelling operator for normal ordering, $\langle : A_p(\xi) :: A_p(\xi') : \rangle$ does have system size dependence and therefore tunnelling operators A_p defined by ordering (4.32) are preferred. To summarise this section; expressions for the zero mode matrix tunnelling elements have been calculated for both normal ordered operators (4.31) and for non-normal ordered operators (4.34). In the normal ordered case there is system size dependence which must be encoded in the parameter t_p . For the non-normal ordered tunnelling operators, this size dependence comes from the calculation of the matrix elements and the operator algebra itself. Since the non-normal ordered tunnelling matrix elements show explicit size dependence and were obtained from local tunnelling operators, it is expected that these results should manifest from the microscopic theory also. Therefore we would expect to see the same system size dependence from $\langle A_p(\xi) \rangle$ and the microscopic matrix elements $\langle V \rangle_p$. In the next section the details, and the results of the MC computations will be discussed.

4.3 Results for Zero Mode Tunnelling Matrix Elements

After showing the formulation for the microscopic computations, the results of the simulations can now be discussed. They are shown in the later parts of this section. To begin, details for the particular states and system sizes of MC simulations are presented.

4.3.1 Simulation Details

To run the MC simulations for the zero mode tunnelling matrix elements, the filling factors chosen for the computations were $\nu = m^{-1} = 1/3$ and $\nu = m^{-1} = 1$. The free fermion case provides a good check for the numeric methods used since for this state, all matrix elements of form (4.3) can be calculated analytically. See the Appendix A for a more detailed discussion.

When considering tunnelling across the bulk in a FQH device, there are two particularly interesting cases. According to the literature discussed in the introduction to this thesis, for Laughlin states the most favourable form of tunnelling is for a single quasiparticle ($\chi = 1$). The other interesting case is for when an electron tunnels across the bulk. In most other systems, as well as in the FQH system in the strong back scattering regime, charge is usually transported by electrons. For these reasons, MC simulations have been run for $\chi = 1$ and $\chi = 3$.

Equations (4.7) and (4.24) give the forms for the tunnelling operators in terms of MC integrals for the tunnelling of a single quasiparticle and three quasiparticles respectively. It is noted that in the free fermion case where $\nu = 1$, electrons are transported across the bulk rather than Laughlin quasiparticles and for $\chi > 1$, all the matrix elements in Eq. (4.3) are zero. Therefore both methods presented

in the previous two sections to overcome the phase problem are equivalent to one another in the free fermion case $\nu^{-1} = \chi = 1$. The results listed for the free fermion case in the next section were obtained using method 1.

For the less trivial state $\nu = 1/3$, MC calculations according to method 1 were used to calculate the zero mode tunnelling matrix elements for a single quasiparticle and method 2 was used for three quasiparticles/one electron tunnelling. In method 1, for both $\nu = 1$ and $\nu = 1/3$ the cumulant expansion (4.13) was computed up to the tenth cumulant. For method 2; there is an additional value d that appears in the integrals (4.19) and (4.22), which was defined as some length away from the outer boundary. An appropriate value (found via a numerical calculation in the free fermion state) to minimise systematic errors was found to be $d = 3$ magnetic lengths.

It is the system size dependence of the matrix elements given by (4.3) that is of interest and so multiple simulations were performed for various values of N ranging from 20 to 200 electrons. For all values of N , the width of the system between the two edges was always kept constant such that $R_O - R_I \sim 4$ units of magnetic length. This was achieved by varying the value of M accordingly with the number of electrons, N . The only important statement about the placement of the impurity is that it was equal distance from the inner and outer edge, i.e., $|b| = (R_O + R_I)/2$. Changing the argument of b has no physical effect on the tunnelling due to the axial symmetry of the system. For simplicity these results were obtained by choosing b to be along the positive real axis.

4.3.2 Tunnelling Results for $\nu = 1$

The zero mode tunnelling matrix elements in the free fermion case were calculated microscopically according to (4.7) where the averages were computed using MC. The only non zero matrix element (excluding the trivial $\chi = 0$ case) is when a

single electron is being transferred across the bulk corresponding to $\chi = 1$ in (4.7). These results are presented graphically on a log-log plot in Figure 4.2.

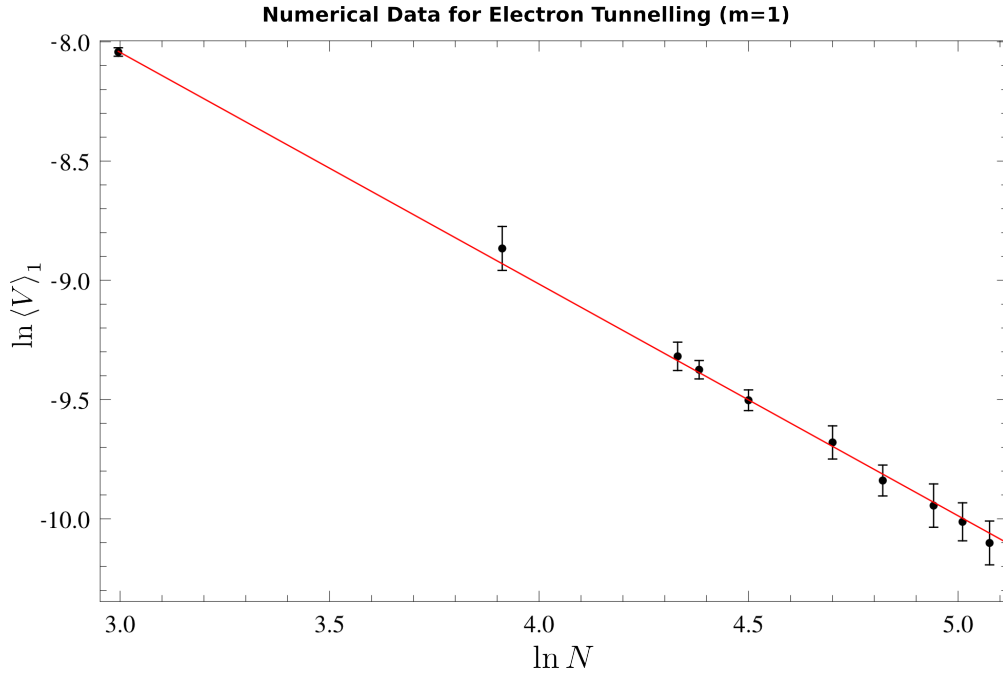


Figure 4.2: Curve for the logarithm of the zero mode quasiparticle tunnelling operator versus the logarithm of N as calculated using Monte Carlo for filling factor $\nu = m^{-1} = 1$. The points are the data from the Monte Carlo calculations, whilst the linear curve is the line of best fit as shown in Eq. (4.37).

The data set plotted on Figure 4.2 is fitted to straight a line where the gradient of the line for $\nu = 1$ is given by,

$$\frac{d \ln \langle V \rangle_1}{d \ln N} = -0.972 \pm 0.006 \quad (\text{for } \nu = 1) \quad (4.37)$$

The tunnelling matrix elements obviously have a system size dependence. Therefore when comparing these numerical results to the effective theory results for the tunnelling operator, operator ordering defined in (4.32) must be imposed for a constant t_p .

In the simulations, the impurity was placed at position b along the real axis and

so in the effective theory calculation $\xi = 0$ and $R = |b|$. These parameters allow us to drop the absolute value of the matrix elements since the phase terms drop out anyway. Setting $p = \chi = 1$ in (4.34) gives

$$\frac{d \ln \langle A_1 \rangle}{d \ln N} = -0.966 \quad (\text{for } \nu = 1). \quad (4.38)$$

Comparing (4.38) to (4.37) shows that the effective theory, when using non-normal ordered operators does match the microscopic computations for the zero mode tunnelling matrix elements.

4.3.3 Tunnelling Results for $\nu = 1/3$

For the filling factor $\nu = 1/3$ tunnelling matrix elements were computed for both a quasiparticle ($\chi = 1$) and an electron ($\chi = 3$) tunnelling across the bulk. Method 1 (4.7) was used for the quasiparticle tunnelling case and method 2 (4.24) for electron tunnelling. The data from both MC simulations is presented on a log-log plot in Figure 4.3.

The gradient of linear curve fitted to the $\chi = 1$ data set is;

$$\frac{d \ln \langle V \rangle_1}{d \ln N} = -0.308 \pm 0.003 \quad (\text{for } \nu = 1/3). \quad (4.39)$$

Following similar arguments to those given in the results section for $\nu = 1$; the effective theory prediction for the tunnelling matrix elements for a quasiparticle transferred across the bulk is

$$\frac{d \ln \langle A_1 \rangle}{d \ln N} = -0.331 \quad (\text{for } \nu = 1/3). \quad (4.40)$$

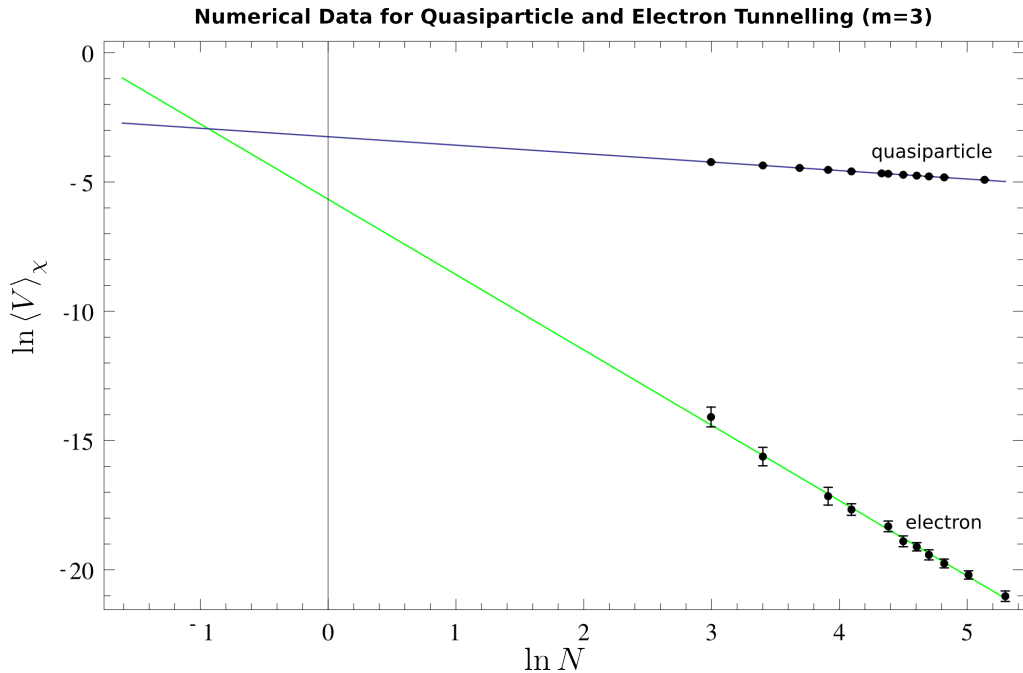


Figure 4.3: Curve for the logarithm of the zero mode tunnelling matrix elements versus the logarithm of N as calculated using MC for filling factor $\nu = m^{-1} = 1/3$. The points are the data collected from the MC computations for $\chi = 1$ and $\chi = 3$, whilst the curves are lines of best fit shown in equations (4.39) and (4.41) corresponding to a quasiparticle and electron respectively.

Comparing (4.40) to (4.39); the effective theory does not predict the correct scaling behaviour for the zero mode tunnelling matrix elements from the tunnelling Hamiltonian.

This author doubts that the difference between the effective theory and the numerical calculation for a single quasiparticle tunnelling in the $\nu = 1/3$ state is a consequence of the numerical method used. Recall, for $\chi = 1$, method 1 was used within the MC calculation to compute the tunnelling matrix element, which makes use of the cumulant expansion. Therefore there is a possibility that systematic errors have appeared as a consequence of computing only a finite number of terms for the cumulant expansion. This argument, however does not seem plausible for the following reason; this cumulant expansion method was also used to compute electron tunnelling in the free fermion case, where the results matched those of the effective theory predictions. Since higher-order terms in the cumulant expansion

for $\nu = 1/3$ go to zero much faster than for the $\nu = 1$ case, one would expect that computing up to the tenth cumulant, as was done for $\nu = 1$, would be more than sufficient to get an accurate result for the quasiparticle tunnelling matrix element.

The data for electron tunnelling ($\chi = 3$) has also been fitted to a linear curve in Figure 4.3. The gradient of the line is given by,

$$\frac{d \ln \langle V \rangle_3}{d \ln N} = -2.97 \pm 0.06 \quad (\nu = 1/3). \quad (4.41)$$

From (4.34), the effective theory prediction from the non-normal ordered tunnelling Hamiltonian can be extracted for electron tunnelling in the FQH state $\nu = 1/3$.

$$\frac{d \ln \langle A_3 \rangle}{d \ln N} = -2.97 \quad (\nu = 1/3). \quad (4.42)$$

For the case of an electron tunnelling across the bulk of a FQH device, the effective theory predictions for the scaling of the zero mode matrix elements match the microscopic computations and are well within the error range. In Figure 4.3 the curves describing the MC data set for a quasiparticle and an electron tunnelling have been extrapolated such that the point of intersection of the two curves can be seen. Interestingly, the point at which the intersect occurs is when $N < 1$ and therefore from the graph we see that for all system sizes, the electron tunnelling process is always less relevant than the quasiparticle tunnelling process.

4.4 Summary and Conclusions

Before the summary of this section is given, I would just like to make a last remark on the applicability of what has been discussed in this chapter to the addition of edge excitations in the system. In the microscopic theory described in Section 3.1,

edge excitations $\{n_{\pm k}\}$, where $n_{\pm k}$ are the occupation numbers of the k 'th orbital on the inner “-” or outer “+” boundary are described by Laughlin’s wavefunction multiplied by a series of power sum polynomials $S_{\pm k}^{n_{\pm k}}$.

$$|\{n_{\pm k}\}, N, M\rangle = \prod_{k>0} S_{\pm k}^{n_{\pm k}} \Psi_N^M \quad (4.43)$$

Similarly in terms of the chiral Luttinger liquid formalism, the same set of occupied orbitals can be obtained by applying the boson creation operator $a_{\pm k}^\dagger$ to the ground state.

$$|\{n_{\pm k}\}\rangle = \prod_{k>0} a_{\pm k}^\dagger |N, M\rangle \quad (4.44)$$

Therefore a similar procedure to the one described in this chapter can also be used to numerically check the effective Hamiltonian for more complicated states where not only has charge been transferred between edges, but also the occupation configuration of excited orbitals has also been altered. If the effective Hamiltonian does match the microscopic model then it is expected

$$\langle \{n'_{\pm k}\} | V | \{n_{\pm k}\} \rangle_{M \rightarrow M+\chi} \equiv \left\langle N', M' \left| \prod_{p>0} a_{\pm p} A_\chi(\xi) \prod_{k>0} a_{\pm k}^\dagger \right| N, M \right\rangle, \quad (4.45)$$

where V is the potential of the impurity inserted into the bulk and $A_\chi(\xi)$ is the effective tunnelling operator in Eq. (4.28).

This work has investigated the zero mode tunnelling matrix elements due to an impurity in the bulk, which have been computed as a function of system size, N and then compared to the effective theory predictions for the effective tunnelling operators. In Section 4.2, the effective theory predictions were discussed. The

quasiparticle operators from the Luttinger liquid theory of FQH edge states were used to calculate the zero mode matrix elements of the tunnelling operators A_p , where p corresponded to the number of quasiparticles tunnelling at the impurity. These matrix elements were calculated using two types of ordering of quasiparticle operators. The first type was the usual definition of normal ordering defined in Eq. (4.30), where it was found that only the tunnelling parameter t_p could contain system size dependence. The second type of ordering considered was when the operators were not normal ordered, as defined in Eq. (4.32). These matrix elements did show signs of system size dependence. To investigate which scaling of the tunnelling parameters t_p best describes the tunnelling events in a FQH system, a microscopic calculation was performed.

This microscopic calculation was based on the Laughlin states of the FQHE and was the subject of Section 4.1. The microscopic formula that describes the process for the tunnelling of χ particles due to the impurity inserted in to the bulk is given by $\langle V \rangle_\chi$ in (4.3). The only known way of calculating such integrals in (4.3) was by using numerical methods. The MC method was chosen for the computation of $\langle V \rangle_\chi$, though to directly calculate this average would not be very efficient due to a phase problem encountered in the simulation. This phase problem manifest itself by causing a slow convergence of the simulation whilst computing the tunnelling matrix elements.

Two methods were found to overcome this problem. Method 1. used MC to calculate the cumulant expansion of a function related to $\langle V \rangle_\chi$ and was suitable only for $\chi \leq 1$. Method 2. to overcome the phase problem was applicable only for $\chi = \nu^{-1}$, in which case the matrix elements in $\langle V \rangle_\chi$ could be written in terms of real valued functions, thus avoiding any phase problems.

Finally, the results of the MC calculations for $\langle V \rangle_\chi$ were presented and compared to the effective theory predictions of the tunnelling behaviour. It was found that the electron tunnelling Hamiltonian predicted by the effective theory is an accurate

representation of the effects on the zero modes of the edges when an impurity is inserted into the bulk of a $\nu = 1/3$ Laughlin state. The predictions from quasiparticle tunnelling Hamiltonian however, were significantly different to the microscopically computed result. Emphasised in Section 4.3.3, there is no obvious cause of an error arising from the microscopic computation.

For future work, I think there are two possible avenues of investigation to look more closely at possible discrepancies of the effective theory for the tunnelling matrix elements in the Laughlin states. The most obvious one would be to test quasiparticle tunnelling for other Laughlin filling fractions, such as $\nu = 1/5$. Initial tests for such a calculation were conducted (using method 1, i.e. cumulant expansion method) and it was found that numerically, this would be a time consuming computation since the size of the cumulants are so small, many measurements would need to be taken for an accurate result for the matrix elements. The second potentially interesting avenue of investigation would be to investigate two quasiparticles tunnelling at the impurity and see how the results would match up to the predictions from the effective theory tunnelling operator. Again, to calculate these matrix elements numerically would be time consuming compared to the calculations computed so far in this chapter, namely because method 1 and method 2, introduced in Sections 4.1.1 and 4.1.2, could not be applied to the case when two quasiparticle tunnel across the FQH bulk states.

There can be some agreement found between the microscopic computations and the effective theory, shown in Figure 4.3 for filling fraction $\nu = 1/3$. When increasing the system sizes of the FQH device the electron operator plays a less important role than that of the quasiparticle operator. This can be seen for all system sizes and supports previous works mentioned in the introduction when the the electron tunnelling term is dropped in comparison to the quasiparticle tunnelling process.

It is unfortunate that the behaviour of the most predominant tunnelling channel (i.e. that of the quasiparticle) is the one in which there is a possibility of a

discrepancy in effective theory. Such computations involving tunnelling at an impurity are an important link to experiments which use point contacts to measure quasiparticle charge and the type of statistics they obey. In particular, shot noise experiments involving measurements on the back scattered current (and therefore will be dependent on the tunnelling matrix elements at the point contact) should shed some light onto the correct scaling behaviour of the the tunnelling matrix elements with system size. These experimental measurements would also need to be accurate enough to distinguish between the numbers of magnitudes given in (4.40) and (4.39).

The final conclusion for this section is that there is a possible discrepancy between the tunnelling matrix elements calculated microscopically and the tunnelling matrix elements predicted for the effective quasiparticle tunnelling Hamiltonian in the Laughlin state $\nu = 1/3$. It is unlikely that this discrepancy is a consequence of the cumulant expansion method used to obtain the microscopic theory and thus it is concluded there is possibly an error arising from the effective theory itself. There has previously been some experimental work measuring quasiparticle charge where the result did not agree with the predictions from the effective theory. This supports the claim that the effective tunnelling Hamiltonian may not be a complete theory in describing the tunnelling of quasiparticles between two edges in the FQHE. A discussion of these works were given in Section 1.5 of the introduction to this thesis. The effective theory however, for an electron tunnelling across the bulk of a FQH device was shown to be in good agreement with the microscopic computations of the tunnelling matrix elements.

Numerical Testing for the Free Energy Expansion in the Semi-classical Limit

In the previous chapter, it was shown that at a quantum point contact (QPC) in the FQHE, there is a possible error with the formulation of the effective theory Hamiltonian describing the tunnelling process of a Laughlin quasiparticle. There is also some experimental evidence suggesting that tunnelling processes in Laughlin states may not be accurately described by the effective tunnelling Hamiltonian [60]. This cited work was based on a shot noise experiment, involving measurements on the back scattered current at a QPC. It was proposed that some differences between the predictions of the effective theory and the experimental measurements could be a consequence of the electrostatic reconstruction caused by the gates creating the QPC. Therefore it is natural to want a description of the effects an external electric field has on the surrounding charge density of the point contact. However, in literature, the description of how the equilibrium density of the electrons in the QH fluid behaves as a result of an applied external field is open to debate.

In fact there has been two differential equations derived, using completely different

methods, and each gives different functions of the equilibrium QH charge density as a function of the external field. Therefore, to further shed light on the nature of electrostatic reconstruction at a QPC in the future, one must first determine which one of the two expressions for the charge density is accurate.

These differential equations for the equilibrium charge density in a QH droplet will be referred to as Liouville-type equations, since their forms are similar to a Liouville differential equation, the only difference being a non-zero term on the right-hand-side. The first Liouville-type equation to be introduced was derived by Zabrodin *et al.* in the semi-classical limit using Ward identities, the formula taken from the work [97] is quoted below.

$$-\frac{\hbar(2-m)}{8\pi}\Delta\ln\rho_0(z)+m\rho_0(z)=\sigma(z), \quad (5.1)$$

where m is the inverse filling factor of the quantum Hall state, \hbar is a function of magnetic length, the explicit relation will be given later, and $\sigma(z)$ is related to the background charge density due to the external potential. The notations used in the works by Zabrodin *et al.* are explained in detail in the next section of this chapter. A similar Liouville equation has been derived by Cheianov *et al.* [98]. This calculation was carried out by reformulating Laughlin-type systems to a boson field theory using the grand partition function. The method is discussed in Appendix B where this Liouville-type equation is given in (B.17); it is restated below to make a comparison with (5.1),

$$\frac{1}{4\pi}\Delta\ln\rho_0(z)+m\rho_0(z)=m\rho_{\text{bg}}(z). \quad (5.2)$$

The terms on the right of Eqs. (5.2) and (5.1) are equivalent since in Zabrodin *et al.*'s notation, $\sigma(z)=m\rho_{\text{bg}}(z)$. There is however a difference in the coefficient of the terms containing the Laplacian. Eq. (5.1) appears to have an extra term

proportional to $m\Delta \ln \rho_0$ that does not appear in (5.2).

To attempt to resolve the issue of which Liouville-type equation is most accurate, Zabrodin *et al.*'s equation will be tested indirectly by a microscopic calculation using the MC technique. This indirect test can be done by noting that in the literature by Zabrodin *et al.* [97, 99–101], they use the plasma analogy to define an effective free energy for the QH system. The authors then derive the free energy expansion in the large N limit, and the method in which they use to do this, is the same as the method used to derive the Liouville-type equation in (5.1). Thus testing the free energy expansion will give some insight into the accuracy of the different methods used to derive both (5.1) and (5.2).

The next section contains a brief introduction to the work carried out by Zabrodin *et al.* [97, 99–101]. In Section 5.2 the analytic form of the Free energy expansion is calculated; Sections 5.3 and 5.4 discuss how the Free energy expansion can be computed numerically using MC. The results for this work are presented in Section 5.5 and the chapter ends with a summary and conclusion given in Section 5.6.

5.1 Introduction to the Formalism Used in the Free Energy Expansion

The notations that are used in the work by Zabrodin *et al.* are quite different to the notations used in the previous chapters and thus this chapter starts with an introduction to the formalism used to obtain the free energy expansion of a quantum fluid with the same interactions as described in the plasma analogy of the Laughlin states. Note that here the geometry considered is a simple droplet with a single boundary; there are no quasiholes inserted into the system. Using Laughlin's plasma analogy, the norm of Laughlin's wavefunction can be considered effectively as a partition function of the form

$$Z_N = \int \prod_{k=1}^N (d^2 z_k e^{W(z_k)/\hbar}) \prod_{i<j}^N |z_i - z_j|^{2m}, \quad (5.3)$$

where $\hbar = 2l_B^2$. When the external potential $W(z)$ takes the form $W(z) = -\bar{z}z$, the partition function is related to the absolute ground state of Laughlin's wavefunction. Following the cited work [97, 99–101], we assume that the radius of the quantum fluid is kept constant for any value of N . This is only possible if the magnetic length, l_B becomes a function of particle number N . Recall that Laughlin's wavefunction describes a circular quantum fluid with radius $R = l_B \sqrt{2mN}$ and so, for this radius to be kept constant, $l_B = R/(\sqrt{2mN})$. In accordance with the cited work, rather than referring to the magnetic length we use the variable $\hbar = R^2/(mN)$. An important result obtained by Zabrodin *et al.* is that in the large- N limit (or equivalently in the limit $\hbar \rightarrow 0$) the effective free energy of the 2D Coulomb plasma has the expansion

$$\frac{F}{\hbar^2} = \ln Z_N = c(N) + \frac{F_0}{\hbar^2} + \frac{F_{\frac{1}{2}}}{\hbar} + \mathcal{O}(\hbar^0). \quad (5.4)$$

It is emphasised that the limit is taken in such a way that $\hbar \rightarrow 0$, $N \rightarrow \infty$ whilst $N\hbar$ is kept constant. Before writing the expression for each of the terms in the expansion we first introduce some terminology used in the description of the system. To take into account the obvious increase in density as N increases, the particle density is now defined as

$$\rho(z) = \hbar \sum_{i=1}^N \delta^{(2)}(z - z_i). \quad (5.5)$$

Therefore the constant value in the large- N expansion is defined by

$$N\hbar = \int d^2z \rho(z). \quad (5.6)$$

The 2D Coulomb potential of the plasma is

$$\begin{aligned} \Phi(z) &= -\hbar \sum_{i=1} \ln |z_i - z|^{2m} \\ &= -m \int d^2\zeta \ln |z - \zeta|^2 \rho(\zeta), \end{aligned} \quad (5.7)$$

where the transformation to an integral in the second line holds in the large N limit considered here and the density is defined in the following manner,

$$\rho(z) = -\frac{1}{4\pi m} \Delta \Phi(z) = \hbar \sum_{i=1}^N \delta^2(z - z_i). \quad (5.8)$$

When the charges are in their equilibrium position, denoted by $\langle \rho(z) \rangle \equiv \rho_0(z)$, the 2D Coulomb plasma potential is denoted as

$$\Phi_0(z) = -m \int d^2\zeta \ln |z - \zeta|^2 \rho_0(\zeta). \quad (5.9)$$

The condition for the equilibrium charge distribution is such that the energy ε is maximised. The energy can be extracted from the partition function (5.3) using $Z_N = \int_N e^{-\hbar^{-1}\varepsilon}$.

$$-\frac{\varepsilon}{\hbar} = m \sum_{i \neq j}^N \ln |z_i - z_j| + \frac{1}{\hbar} \sum_{i=1}^N W(z_i), \quad (5.10)$$

where it is a double sum in the first term following from $\sum_{i < j} \ln |z_i - z_j| =$

$(1/2) \sum_{i \neq j} \ln |z_i - z_j|$. By taking the continuum limit for the energy in (5.10), which holds for scales much larger than the average spacing between particles, a general expression for the free energy can be obtained,

$$F = \hbar^2 \ln Z_N = m \int d^2z d^2z' \rho(z) \rho(z') \ln |z - z'| + \int d^2z \rho(z) W(z). \quad (5.11)$$

The first term in the free energy expansion, F_0 in (5.4), is given by (5.11) when the density corresponds to the equilibrium density of charges $\rho_0(z)$.

$$F_0 = \hbar^2 \ln Z_N = m \int d^2z d^2z' \rho_0(z) \rho_0(z') \ln |z - z'| + \int d^2z \rho_0(z) W(z) \quad (5.12)$$

A convenient method to find ρ_0 is to note that when the system of charges is in an equilibrium distribution, the energy ε is maximised. The maximum energy is given by

$$\frac{\partial \varepsilon}{\partial z_i} = -m\hbar \sum_{j=1 \neq i} \frac{1}{z_i - z_j} - \frac{\partial W(z_i)}{\partial z_i} = 0 \quad (5.13)$$

Therefore when this condition holds, the density is given by ρ_0 . Taking the expression (5.13) to the continuum limit we have

$$\frac{\partial}{\partial z} (\Phi_0(z) - W(z)) = 0, \quad (5.14)$$

where $\Phi_0(z)$ is given by (5.9). Differentiating (5.14) with respect to \bar{z} allows the equilibrium density to be expressed in terms of the Laplacian of the external potential which provides a trivial calculation for ρ_0 :

$$\rho_0(z) = \begin{cases} -\frac{1}{4\pi m}\Delta W(z) & \text{for } |z| \leq R \\ 0 & \text{for } |z| > R. \end{cases} \quad (5.15)$$

Also from (5.14), the 2D Coulomb potential at equilibrium density ρ_0 must be equal to the the external potential plus some constant. I.e.,

$$\Phi_0(z) = W(z) + \eta. \quad (5.16)$$

Setting $z = 0$ in this relationship gives the value of the constant η to be

$$\eta = -2m \int d^2\xi \rho_0(\xi) \ln |\xi|. \quad (5.17)$$

Equation (5.16) can be used to simplify the expression for F_0 defined in (5.12) in terms of only the external potential $W(z)$ and the constant η .

$$\begin{aligned} F_0 &= -\frac{1}{2} \int d^2z \rho_0(z) \Phi_0(z) + \int d^2z \rho_0(z) W(z) \\ &= m \int d^2z \rho_0(z) \int d^2z \rho_0(z) \ln |z| + \frac{1}{2} \int d^2z \rho_0(z) W(z) \\ &= mN\hbar \int d^2z \rho_0(z) \ln |z| + \frac{1}{2} \int d^2z \rho_0(z) W(z) \\ &= R^2 \int d^2z \rho_0(z) \ln |z| + \frac{1}{2} \int d^2z \rho_0(z) W(z). \end{aligned} \quad (5.18)$$

The next highest order term in the free energy expansion has been calculated by Zabrodin *et al.* and is given by

$$F_{\frac{1}{2}} = -\frac{(2-m)}{2} \int d^2z \rho_0(z) \ln \rho_0(z). \quad (5.19)$$

Higher orders of the expansion have been calculated in the cited works [97, 99–101], though these are not taken into account for the computations carried out in this Thesis. The aim of the remainder of this chapter is to test via a numerical computation if the free energy expansion in the large- N limit does display the behaviour described, in particular by the term $F_{\frac{1}{2}}$. The numerical method used in this work is Monte Carlo and it is convenient for this method to calculate the difference of the free energy expansions for two similar systems rather than calculating the free energy expansion directly. To do this we consider three different potentials, W_0 , W_1 and W_2 for which the free energy expansion can be calculated analytically using the model by Zabrodin *et al.* This is discussed in Section 5.2. These free energy expansions can then be compared to numeric computations of the differences in the free energy expansions of W_1 with W_0 and also W_2 with W_0 , which is described in Section 5.3 in more detail.

5.2 Analytic Expressions for the Free Energy Expansions for Particular Choices of $W(z)$

In this section the free energy expansions in the large N limit are calculated for particular choices of potential $W(z)$ according to the model by Zabrodin *et al.* The first choice of external potential, $W_0(z)$ is chosen such that the partition function (5.3) is equivalent to the magnitude squared of the Laughlin wavefunction. For this system, the equilibrium particle density is simply a constant $\rho_0^{(0)}$ inside the domain confining the charges. Since this is the simplest choice of external potential, this system will be discussed first in Subsection 5.2.1. External potentials W_1 and W_2 will correspond to systems where the density of charges has been slightly deformed from the constant value $\rho_0^{(0)}$. In particular, the later two external potentials have been chosen to reproduce relatively straight forward expressions to be computed numerically.

5.2.1 Free Energy Expansion with Potential $W_0(z)$

Following the terminology introduced in the previous section, here the free energy expansion in the large N limit is calculated for the FQH system described by the effective partition function in (5.3) when the external potential has the form,

$$W_0(z) = -z\bar{z}. \quad (5.20)$$

The density of charges when in equilibrium is known to be constant in the FQHE (see, for example Eq. (1.25)) and the value can be calculated using (5.15) where $\Delta = 4\partial_z\partial_{\bar{z}}$, which gives

$$\rho_0^{(0)}(z) = \begin{cases} \frac{1}{\pi m} & \text{for } |z| \leq R \\ 0 & \text{otherwise.} \end{cases} \quad (5.21)$$

Substituting in the external potential $W_0(z) = -z\bar{z}$ and the value for $\rho_0^{(0)}$ into the Eqs. (5.18) and (5.19) give the first two highest order terms of the free energy expansion to be

$$\begin{aligned} F_0^{(0)} &= \frac{R^4}{m} \left(\ln R - \frac{3}{4} \right), \\ F_{\frac{1}{2}}^{(0)} &= \frac{(2-m)}{2m} R^2 \ln(\pi m). \end{aligned} \quad (5.22)$$

The value for $N\hbar = \int d^2z \rho_0(z) = R^2/m$ has also been substituted into the above expressions. This completes the calculation for the FQH free energy expansion and in the next part a similar calculation is completed for $W_1(z)$.

5.2.2 Free Energy Expansion with Potential $W_1(z)$

For the FQH system, the equilibrium density was constant inside the domain confining the charges. Since it is convenient to calculate the difference of the free energy expansions within the confines of the numerical method used, here we will discuss the free energy expansion for a slightly more complicated equilibrium density profile which will in turn affect the form of the external potential $W_1(z)$. The density profile considered here is one which is still radially symmetric, however it has a maximum value at $z = 0$ and decreases linearly to the radius of the droplet of charges:

$$\rho_0^{(1)}(z) = \begin{cases} \kappa + (\rho_0^{(0)} - \kappa) \frac{|z|}{R_1} & \text{for } |z| \leq R_1 \\ 0 & \text{otherwise,} \end{cases} \quad (5.23)$$

where $\rho_0^{(0)} = 1/(\pi m)$ is the value of the equilibrium distribution of charges for potential $W_0(z)$ as discussed in the previous subsection and κ is a constant with a value slightly increased from $\rho_0^{(0)}$. A sketch of this density profile is shown in Figure 5.1.

The difference in free energy between the system with the density as described in (5.23) and the FQH system is taken for a given value of particle number N . Since the density will be overall larger for this system than the FQH system, this implies that if we wish for the constant $N\hbar$ to be the same value for the two systems, the radius for the droplet with density $\rho_0^{(1)}(z)$ will be different to the radius for the FQH droplet described by potential W_0 . To calculate the radius of the new system R_1 we use the definition (5.6).

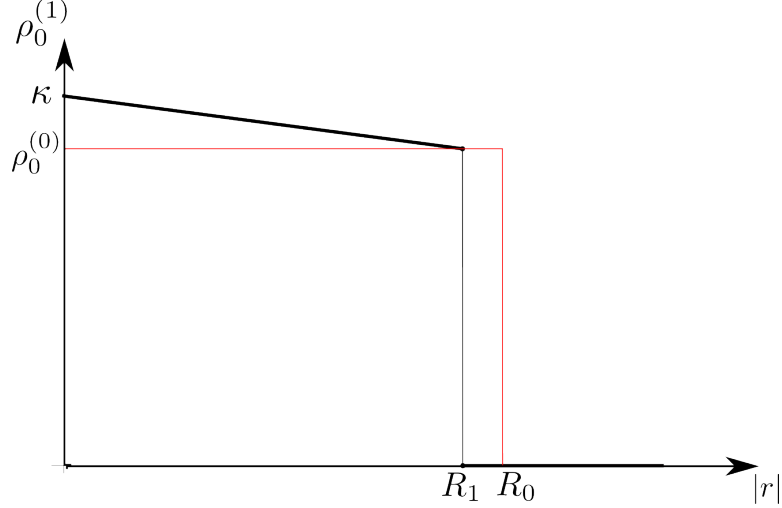


Figure 5.1: Sketch of density profile, $\rho_0^{(1)}(r)$, shown in black. The uniform, homogeneous density $\rho_0^{(0)}$ corresponding to the external potential W_0 is shown in red as a comparison. Since the total number of electrons in each fluid described by density profiles; $\rho_0^{(1)}$ and $\rho_0^{(0)}$ are equal, the radius of the droplet described by the inhomogeneous density profile, R_1 must be less than the radius of the homogeneous density profile R_0 . The number κ denotes the maximum value of $\rho_0^{(1)} - \rho_0^{(0)}$.

$$\begin{aligned}
 N\hbar &= \int d^2z \rho_0^{(1)}(z) = 2\pi \int_0^{R_1} dr r \left(\kappa + (\rho_0^{(0)} - \kappa) \frac{|z|}{R_1} \right) \\
 &= 2\pi R_1^2 \left(\frac{\kappa}{6} + \frac{\rho_0^{(0)}}{3} \right) \tag{5.24}
 \end{aligned}$$

For the FQH system, the value of the constant is $N\hbar = R^2/m$ and therefore

$$R_1 = R \sqrt{\frac{3}{2\pi(\kappa + 2\rho_0^{(0)})}}. \tag{5.25}$$

Before continuing with the calculation for the first two terms in free energy expansion for this new system, the external potential $W_1(z)$ must first be found which describes the density profile given in (5.23). This is done by solving the 2D Poisson equation. From Gauss's Law the electric field due to the charge distribution with

density $\rho_0^{(1)}(z)$ is

$$\begin{aligned} |E_1| \cdot 2\pi|z| &= 4\pi m \int dA \rho_0'(z) \\ \mathbf{E}_1 &= 4\pi|z| \left[\kappa + \frac{2|z|}{3R_1} (\kappa - \rho_0^{(0)}) \right] \hat{\mathbf{r}} \end{aligned} \quad (5.26)$$

for $|z| \leq R_1$. Since it is only the potential $W_1(z)$ inside the droplet that is needed, the calculation for the electric field outside the droplet is neglected. Since $\mathbf{E}_1 = -\nabla W_1(z) = -\hat{\mathbf{r}} (dW_1(z)/d|z|)$, integrating the electric field in the radial direction gives the external potential $W_1(z)$.

$$W_1(z) = -2\pi|z|^2 \left[\kappa + \frac{4|z|}{9R_1} (\rho_0^{(0)} - \kappa) \right] \quad (5.27)$$

Substituting the expressions for $W_1(z)$ and $\rho_0^{(1)}(z)$ into (5.18) and (5.19) allows the first two highest order terms in the free energy expansion to be calculated.

$$\begin{aligned} F_0^{(1)} &= R^2 \int d^2z \rho_0^{(1)}(z) \ln |z| + \frac{1}{2} \int d^2z \rho_0^{(1)} W_1(z), \\ F_{\frac{1}{2}}^{(1)} &= \frac{(m-2)}{2} \int d^2z \rho_0^{(1)} \ln \rho_0^{(1)}, \end{aligned} \quad (5.28)$$

where the integral over the radius coordinate runs from 0 to R_1 . The integrals in (5.28) are straight forward to calculate but their final form is not listed here since they are quite long expressions. This completes the calculation for the free energy expansion in the large- N limit for the system described by external potential $W_1(z)$ given in equation (5.27).

5.2.3 Free Energy Expansion with Potential $W_2(z)$

In this section, the free energy expansion is calculated analytically for some configuration of charges of a one-component plasma described by the external potential $W_2(z)$. The charges are confined to some droplet originating in the center of the complex plane. This region of charge is denoted as the domain D_2 . The external potential $W_2(z)$ is related to the density of charges when the system is in its equilibrium configuration; this density is denoted as $\rho_0^{(2)}(z)$. This density is chosen to be convenient when performing a MC simulation on the system and has the form

$$\rho_0^{(2)}(z) = \kappa + \left(\rho_0^{(0)} - \kappa\right) \sqrt{\frac{|z|}{R_2}}. \quad (5.29)$$

Again $\rho_0^{(0)} = 1/(\pi m)$ and κ is a small deviation of this value. This density profile is sketched in Figure 5.2.

The radius of the droplet of charges R_2 confined to domain D_2 is calculated such that

$$\int d^2z \rho_0^{(0)}(z) \equiv \int d^2z \rho_0^{(2)}(z), \quad (5.30)$$

which gives the radius R_2 in terms of the of the radius R for the uniform charge distribution,

$$R_2 = R \sqrt{\frac{5}{2\pi \left(\kappa + 4\rho_0^{(0)}\right)}}. \quad (5.31)$$

Following the method to extract the form of the external potential as described in Section 5.2.2 the external potential $W_2(z)$ is calculated to be

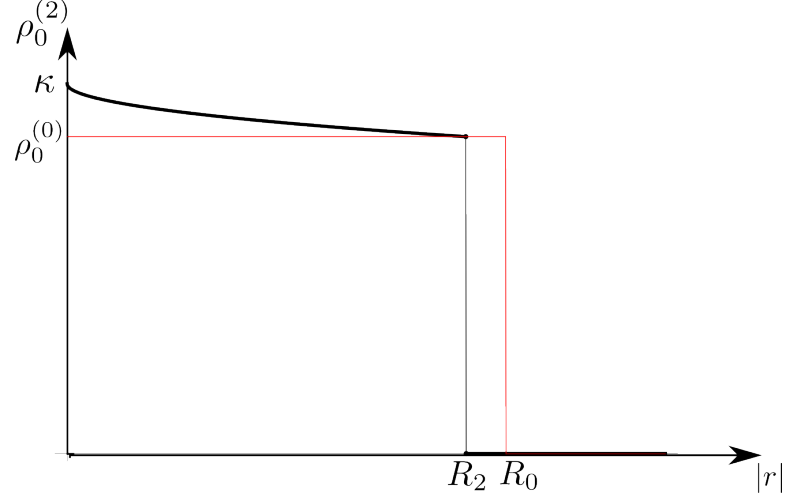


Figure 5.2: Sketch of density profile, $\rho_0^{(2)}(r)$, shown in black. The uniform, homogeneous density $\rho_0^{(0)}$ corresponding to the external potential W_0 is shown in red as a comparison. Since the total number of electrons in each fluid described by density profiles; $\rho_0^{(2)}$ and $\rho_0^{(0)}$ are equal, the radius of the droplet described by the inhomogeneous density profile, R_2 must be less than the radius of the homogeneous density profile R_0 . The number κ denotes the maximum value of $\rho_0^{(2)} - \rho_0^{(0)}$.

$$W_2(z) = -2\pi|z|^2 \left[\kappa + \frac{16}{25} \sqrt{\frac{|z|}{R_2}} (\rho_0^{(0)} - \kappa) \right]. \quad (5.32)$$

With the form of the density $\rho_0^{(2)}$ and external potential $W_2(z)$ the integrals for the terms in the free energy expansion can be calculated.

$$\begin{aligned} F_0^{(2)} &= R^2 \int d^2z \rho_0^{(2)}(z) \ln |z| + \frac{1}{2} \int d^2z \rho_0^{(2)} W_2(z) \\ F_{\frac{1}{2}}^{(2)} &= \frac{(m-2)}{2} \int d^2z \rho_0^{(2)} \ln \rho_0^{(2)} \end{aligned} \quad (5.33)$$

To summarise this section, the free energy expansion has been obtained using the model by Zabrodin *et al.* for three different external potentials; $W_0(z)$, $W_1(z)$ and $W_2(z)$. The remainder of this work will focus on developing a method to calculate

the free energy exactly for each of these potentials such that the first couple of terms in the free energy expansion by Zabrodin *et al.* can be compared. The numerical procedure used for the exact free energy expansion will be discussed in Section 5.3.

5.3 Numerical Calculation of the Free Energy

In Eq. (5.4) the free energy expansion is shown to be related to the partition function Z_N in the following way,

$$\frac{F}{\hbar^2} = \ln Z_N = C(N) + \frac{F_0}{\hbar^2} + \frac{F_{\frac{1}{2}}}{\hbar}. \quad (5.34)$$

To test the accuracy of this expansion a MC calculation can be used by computing the ratio of the partition functions of the two systems for various values of N .

$$e^{\tau_{\text{mc}}^{(i)}} = \frac{Z_N^{(i)}}{Z_N^{(0)}} = \frac{\int \prod_{k=1}^N (d^2 z_k e^{W_i(z_k)/\hbar}) \prod_{i<j}^N |z_i - z_j|^{2m}}{\int \prod_{k=1}^N (d^2 z_k e^{W_0(z_k)/\hbar}) \prod_{i<j}^N |z_i - z_j|^{2m}}, \quad (5.35)$$

where $W_0 = -z\bar{z}$ and $i = 1, 2$ which corresponds to either the potential W_1 or W_2 . Therefore the formula (5.4) is tested by comparing the difference of two different free energy expansions in the large N limit.

It is straightforward to see that the numerically computed value of $\tau_{\text{mc}}^{(i)}$ in Eq. (5.35) should be equivalent to the value of $\tau_{\text{wz}}^{(i)}$ given by

$$\tau_{\text{wz}}^{(i)} = \ln Z_N^{(i)} - \ln Z_N^{(0)}(W) = \left(\frac{mN}{R^2}\right)^2 (F_0^{(i)} - F_0^{(0)}) + \frac{mN}{R^2} (F_{\frac{1}{2}}^{(i)} - F_{\frac{1}{2}}^{(0)}), \quad (5.36)$$

where $i = 1, 2$ depending on whether we are comparing the expansions from potential W_1 and W_0 or W_2 and W_0 . For the numerical calculation of (5.35) it is noted that the cumulant expansion of $e^{\tau_{\text{mc}}^{(i)}}$ is calculated for a finite number of terms rather than the exact value of the function itself. The reason for this is because the values of $e^{\tau_{\text{mc}}^{(i)}}$ are sometimes too large to be computed numerically, since the sizes are frequently larger than the length of a double precision floating point number. If (5.35) is calculated for a range of values for N then the data can be fitted to a quadratic function of N ,

$$\tau_{\text{mc}}^{(i)} = A_{\text{mc}}N^2 + B_{\text{mc}}N + C_{\text{mc}}, \quad (5.37)$$

where A_{mc} and B_{mc} corresponds to the values of the first and second terms in (5.35) respectively. The value of C is not of interest here since we consider only the first two terms of the free energy expansion by Zabrodin *et al.*. The term in the expansion that is of most interest is related to $F_{\frac{1}{2}}$ in (5.36), in particular we are interested in testing the coefficient of the integral. This coefficient is of the same form of the coefficient in the Liouville-type equation (5.1) that differs from the Liouville-type equation obtained by Cheianov *et al.* (5.2). Rewriting the $F_{\frac{1}{2}}$ term as

$$F_{\frac{1}{2}} = \frac{m-2}{2} \int d^2z \rho_0(z) \ln \rho_0(z) = \Delta(m)I_{\frac{1}{2}}, \quad (5.38)$$

where the coefficient to the integral is given by

$$\Delta(m) = \frac{m-2}{2}. \quad (5.39)$$

This coefficient is independent of the potential and density, which we have chosen to calculate the free energy expansion and therefore it will be interesting to extract

this value from the numerical data computed from the MC simulation. According to (5.37) and (5.38) the numerical value of $\Delta(m)$ is given by

$$\Delta_{\text{mc}}(m) = \frac{B_{\text{mc}}R^2}{m(I_{\frac{1}{2}}^{(1)} - I_{\frac{1}{2}}^{(0)})}. \quad (5.40)$$

In this section we have described a method in which the large N , free energy expansion predicted by Zabrodin *et al.* can be tested and in particular we are interested in testing the value of $\Delta(m)$ which according to the model has a value given by Eq. (5.39).

5.4 Simulation Details

In total, 12 MC computations have been performed; for convenience each computation is denoted as $\tau_{\text{mc}}^{(i)}(\kappa, m)$. The symbol i represents whether the difference in the free energy expansion is between $W_1(z)$ and $W_0(z)$ ($i = 1$) or $W_2(z)$ and $W_0(z)$ ($i = 2$). κ denotes the magnitude of the density $\rho_0^{(i)}$ at the value $z = 0$ and can have the value $\kappa_1 = \rho_0^{(0)} + 1/4\pi m$ or $\kappa_2 = \rho_0^{(0)} + 1/10\pi m$, where $\rho_0^{(0)} = 1/(\pi m)$. Then m corresponds to the value of the inverse filling in the FQHE terminology for which $\tau_{\text{mc}}^{(i)}(\kappa, m)$ was computed for $m = 1, 2, 3$. The MC simulations to calculate (5.35) were run for different particle number N , starting at $N = 50$ particles all the way to $N = 140$ particles and the value of the constant radius R was chosen to be $R = \sqrt{2m50}$ and is therefore chosen to be dependent on the value of m . The reason for testing the expansions for two different values of κ was to investigate if the behaviour of the cumulant expansion strongly depended on the magnitude of the alteration of the density from the uniform density value, i.e., $|\kappa - \rho_0^{(0)}|$. In the next section the results of all simulations listed here are presented and then compared to the predicted results from the analytic model of the free energy expansion.

5.5 Results for MC Computations for the Free Energy Expansion

In this section the results are listed in tabular form for the 12 different expansions of the free energies $\tau_{\text{mc}}^{(i)}(\kappa, m)$ listed in Section 5.4. The numerical data was fitted to a quadratic function in N with the coefficients

$$\tau_{\text{mc}}^{(i)}(\kappa, m) = A_{\text{mc}}N^2 + B_{\text{mc}}N. \quad (5.41)$$

One can also analytically calculate coefficients of a similar quadratic equation for Zabrodin *et al.*'s free energy expansion given in Eq. (5.36). These analytically calculated coefficients in the quadratic equation for N are symbolised as

$$\tau_{\text{wz}}^{(i)}(\kappa, m) = A_{\text{wz}}N^2 + B_{\text{wz}}N. \quad (5.42)$$

The results for $\tau^{(1)}(\kappa, m)$ are given in Table 5.1 and the results for $\tau^{(2)}(\kappa, m)$ are given in Table 5.2.

κ	m	A_{wz}	A_{mc}	B_{wz}	B_{mc}
κ_1	1	-0.075524	-0.075520 ± 0.000004	-0.0408	-0.0408 ± 0.0003
κ_2	1	-0.0313793	-0.0313792 ± 0.0000003	-0.01652	-0.01654 ± 0.00003
κ_1	2	-0.15105	-0.15106 ± 0.00001	0	0.003 ± 0.002
κ_2	2	-0.0627586	-0.0627584 ± 0.000002	0	0.0005 ± 0.0004
κ_1	3	0.22657	-0.22658 ± 0.00003	0.041	0.045 ± 0.005
κ_2	3	-0.094138	-0.094141 ± 0.000002	0.0165	0.0178 ± 0.0003

Table 5.1: Table showing data for $\tau^{(1)}(\kappa_1)$ and $\tau^{(1)}(\kappa_2)$ which denote the difference of two free energy expansions corresponding to the external potentials $W_1(z)$ and $W_0(z)$. The first column κ corresponds to the size of the alteration of the density from the uniform density, the second column corresponds to the values of the inverse filling factor m in each simulation. Columns A_{mc} and B_{mc} are numerically calculated coefficients in the large N limit of the free energy expansion and columns A_{wz} and B_{wz} are the analytically calculated coefficients.

κ	m	A_{wz}	A_{mc}	B_{wz}	B_{mc}
κ_1	1	-0.051707	-0.051707 ± 0.000001	-0.02477	-0.02477 ± 0.00008
κ_2	1	-0.0211961	-0.0211961 ± 0.000001	-0.00997	-0.00997 ± 0.00001
κ_1	2	-0.103413	-0.103410 ± 0.000008	0	0.000 ± 0.001
κ_2	2	-0.0423922	-0.0423928 ± 0.0000007	0	0.0004 ± 0.0001
κ_1	3	-0.155120	-0.155125 ± 0.000007	0.025	0.027 ± 0.001
κ_2	3	-0.0635883	-0.0635899 ± 0.0000005	0.00997	0.01070 ± 0.00008

Table 5.2: Table showing data for $\tau^{(2)}(\kappa_1)$ and $\tau^{(2)}(\kappa_2)$ which denote the difference of two free energy expansions corresponding to the external potentials $W_2(z)$ and $W_0(z)$. The structure of this table is identical to Table 5.1.

From the results in Table 5.1 and Table 5.2, there is a good fit for the free energy expansion model formulated by Zabrodin *et al.* and the numerical simulations for the free fermion case. The results for $m = 2$ and $m = 3$ however are questionable. In general the coefficient of the quadratic term in N , A_{wz} can be matched to the numerical data in the $m = 2$ case, though there is some deviance from the expected value for $m = 3$. For the coefficient of the linear term in N , labelled B_{wz} , there could be a fit for the $m = 2$ case, since the magnitude of the error in the MC simulations is the same order of the measurement of B_{wz} , implying that this result is zero within the confines of the simulation. The results which show a clear deviance from the predicted values of the free energy model are measurements on B_{wz} for $m = 3$. In Table 5.3 the values for $\Delta(m)$ have been listed for all of the 12 simulations carried out so far. From the free energy expansion model, the value of $\Delta(m)$ is given in (5.39) and it can be extracted from the numerical data as described in (5.40).

As expected, the data for the free fermion case $m = 1$ agree with the model values for $\Delta(1)$. The results for $m = 2$ are unclear, and this is a consequence of attempting to measure an observable whose value is obviously very small. Results for $\Delta(3)$ appear not to match the predicted value from the model, in particular all the numerical values from the four simulations run for this FQH filling factor point at the value $\Delta(3) = 0.54$ rather than 0.50, which is the model value.

m	Model	$\tau^{(1)}, \kappa_1$	$\tau^{(1)}, \kappa_2$	$\tau^{(2)}, \kappa_1$	$\tau^{(2)}, \kappa_2$
1	$-\frac{1}{2}$	-0.500 ± 0.004	-0.5004 ± 0.0009	-0.50 ± 0.01	-0.5003 ± 0.0007
2	0	0.04 ± 0.02	0.02 ± 0.01	0.00 ± 0.02	0.020 ± 0.005
3	$\frac{1}{2}$	0.55 ± 0.06	0.54 ± 0.01	0.54 ± 0.02	0.537 ± 0.004

Table 5.3: Table summarising the values calculated for $\Delta(m)$. The first column corresponds to the value for the inverse filling factor m . The second column is the value of $\Delta(m)$ from the analytic free energy expansion. The last four columns corresponds to the numerical $\Delta(m)$ values from all simulations; $\tau^{(1)}(\kappa_1)$, $\tau^{(1)}(\kappa_2)$, $\tau^{(2)}(\kappa_1)$ and $\tau^{(2)}(\kappa_2)$.

5.6 Summary and Conclusion

Clearly, the results listed in the previous section do not all match the prediction by Zabrodin *et al.* for the free energy expansion in the large N limit. For FQH filling factor $m = 1$, there is a good match between the analytic data and numerical simulations which is not surprising since the free fermion case can be solved exactly using analytic methods. What the numerical results do show for this case, is that the method used in the MC simulations can work for this model. For $m = 2$, the results are generally inconclusive due the values of the observables measured in the MC simulation being small in magnitude. MC obviously struggles to calculate such small observables due to the errors produced by the simulation. For the $m = 3$ case there is certainly a deviance from the model predictions of the value for $\Delta(m)$, this is clear since all four simulations run for this filling factor tend to the same value of 0.54.

In general the numerical results do agree with the behaviour of $\Delta(m)$ in the sense that for $m = 1$, the value is negative, gets closer to zero for $m = 2$, then becomes larger and positive for $m = 3$. Further testing needs to be carried out to accurately pinpoint what has caused the differences between the numerical data and the model values of the free energy expansion in the large N limit. A possibility to account for these discrepancies is that they are caused by boundary effects that are not taken into consideration in the work by Zabrodin *et al.* For example in the two

systems where the free energy expansion has been numerically tested, described by the external potentials $W_1(z)$ and $W_2(z)$, the density profile has been altered such that the radius of these systems has been shifted by an amount as compared to the radius of the FQH system described by the external potential $W_0(z) = \bar{z}z$. Also close to the boundary, the value of the density is different from the value of the FQH system where the density is $\rho_0^{(0)} = 1/(\pi m)$.

Such boundary effects can be removed by considering a potential $W_3(z)$ such that $R_3 = R$ and for a few magnetic lengths from the boundary, $\rho_0^{(3)} = \rho_0^{(0)}$. This investigation is ongoing. Another avenue of investigation is by directly testing the forms of the Liouville-type equations themselves. In particular both Cheianov *et al.*'s equation (5.2) and Zabrodin *et al.*'s equation (5.1) can be solved for $\rho_0(z)$ analytically for some external potential $W(z)$. These solutions can then be compared to numerical computations of the density $\rho_0(z)$ from a MC simulation.

In summary, the analytic formula for the large N expansion obtained by Zabrodin *et al.* has been tested via a microscopic computation. The numerical method of performing the calculation is MC. To carry out the tests, specific systems were chosen, where the density profile has been purposefully manipulated to deviate from the constant, homogeneous density profile of charges observed in systems such as the FQHE. This allowed the difference of the free energy expansions to be calculated for the perturbed density profile and the constant density profile using MC. The predictions for the free energy expansion obtained by Zabrodin *et al.* does not match numerical data for $m = 3$, and, possibly $m = 2$. Further testing is being carried out to identify the causes of these differences between the numerical computations and the analytic model.

Even though there is not an exact match between Zabrodin *et al.*'s predictions and the free energy expansion, what the results in this chapter do imply is that Zabrodin *et al.*'s Liouville-type equation is more likely to predict more accurate description of the equilibrium charge density of a QH fluid subject to an external

potential, rather than the Liouville-type equation derived by Cheianov *et al.* This statement can be made in light of the behaviour of $\Delta(m)$ as shown in Table 5.3, though a more thorough investigation is needed before any definite conclusions can be stated. Experimentally accurate measurements at QPC's in the FQHE could also potentially help to resolve which description of the equilibrium charge density works best. The main technicality here, from the theoretical perspective, would be finding an external potential to solve the Liouville-type equations that matches the external potential in the experiment to sufficient accuracy.

Summary, Conclusions, and Future Work

The aim of the work covered in this thesis was to microscopically verify effective theory predictions with regards to the FQHE. Throughout this thesis only FQH states described by the Laughlin wavefunction have been considered. These states were introduced in Chapter 1; they lie in the LLL and have filling factors of the form $\nu = 1/m$, where m is an odd integer. The edge states in FQH systems support low-energy excitations and they determine how charge is transported throughout the system. There exists a phenomenological description of these edge states provided by Wen. This is the chiral Luttinger liquid theory and it has been successful in making predictions on transport behaviour, which can be tested and verified experimentally. The chiral Luttinger liquid was discussed in detail in Chapter 3 where the bosonised formula for the electron fields were formulated by performing a projection onto the low-energy space of excitations.

Original work was also presented in Chapter 3, Section 3.3 with regards to the overlap of Laughlin states supporting low-energy excitations. An analytic formula for the overlap of states for a single edge system was originally derived by Cheianov *et al.* [94], as discussed in Section 3.2. This formula uses the tau-

function $\tau^\nu(N, M, t_k, \bar{t}_k)$ to calculate overlap matrix elements. In Appendix B this tau-function was derived for a two-edged system following a boson field theory method originally discussed in [98]. Using the tau-function, $\tau^\nu(N, M, t_{\pm k}, \bar{t}_{\pm k})$ for both inner and outer boundary edge excitations, allows the formula for the overlap of states derived by Cheianov *et al.* to be extended to a two-edged FQH system.

This formula was important to verify since, firstly; the microscopic calculations in the large N limit have never been extensively investigated. Secondly, the method used to obtain the tau-function in Appendix B relies on a boson field theory created using the grand partition function. Therefore the states that are averaged over in this field theory, not only are dependent on the energy of the system, but also the number of particles. Such an average for bulk properties of the FQH system should not be affected by including states of varying number of particles, however boundary specific properties such as the tau-function, could possibly be affected. The microscopic definition of the tau-function (i.e. the norm of the Laughlin wavefunction with the addition of edge excitations) is for a constant particle number. By verifying the formula for the overlap of states, the form of the tau-function is also checked.

To verify the analytic formula for the overlap of Laughlin states containing edge excitations, the microscopic formulas were computed using the Monte Carlo method. The space of states used in the computation were restricted such that the angular momentum contributions from the edge excitations on the inner and outer boundary were given by 2 or 0 in units of \hbar . The Monte Carlo procedure was the subject of Chapter 2 and it was shown that the numerical method could be used effectively for computing FQHE observables due to the correspondence between the Laughlin state and the partition function of a one component plasma. The MC data for the microscopic computations for the overlap integrals were in good correspondence to the predictions from the analytic formula, and thus also the form of the tau-function for a two-edged system was also verified.

A particular transport property of the FQHE that was studied in this thesis was the tunnelling of charge particles across the incompressible bulk states of a two-edged FQH device. The motivation for such an investigation was the lack of a microscopically derived theory. The description of tunnelling that is commonly used in the FQHE is an effective tunnelling operator built up from the bosonised operators defined in the chiral Luttinger liquid theory. Existing literature using the effective tunnelling Hamiltonian was discussed in detail in Section 1.5. The main concerns about the effective theory tunnelling operator was that it was taken from the description of tunnelling for a conventional Luttinger liquid and directly applied to a chiral Luttinger liquid describing the edge states of the FQHE.

Such an assumption has possible issues because, firstly, in a conventional Luttinger liquid, the bosonised fermion fields can be microscopically derived unlike for similar fields in the chiral Luttinger liquid, which are obtained from a projection onto the FQH low-energy edge states. This can lead to an issue with locality of the tunnelling operator in the FQHE. The second potential issue is that in a conventional Luttinger liquid, interactions can be treated as perturbations whereas switching off interactions in the FQHE is impossible because the system only exists in the presence of strongly correlated electrons.

The need to describe the tunnelling process in the FQHE with an effective theory is a consequence of the microscopic picture being difficult to analytically solve for large system sizes. This was discussed in Section 3.1; therefore for microscopic computations concerning tunnelling in the FQHE, the MC method would have to be used.

The comparison of the effective theory and the microscopic representation of tunnelling in the FQHE was carried out In Chapter 4. To make the comparison, the zero mode tunnelling matrix elements in the microscopic picture were first formulated. These tunnelling matrix elements corresponded to some amount of charge being transferred from the outside edge of a disk of FQH fluid to the inside

edge due to an impurity inserted into the bulk of the quantum fluid. To compute these microscopic matrix elements using MC, a phase problem had to first be resolved. In this thesis two methods were found to solve this problem. The first method was to calculate the cumulant expansion of the matrix elements rather than the exact function itself. This method was appropriate when considering a single quasiparticle tunnelling between the edge states. The second method found was for an electron tunnelling across the bulk states. In this special case, due to angular momentum considerations the integrals describing the tunnelling process of an electron could be transformed purely in terms of real functions, thus removing any phase problems encountered in the MC simulations. The details of these methods were given in Section 4.1.

The effective theory zero mode tunnelling operators were then calculated in Section 4.2 using the operators from the chiral Luttinger liquid theory. It was found that one specific type of ordering of the operators in the effective tunnelling Hamiltonian lead to a local tunnelling operator. The results for the local tunnelling operators were chosen to be compared with the microscopically computed tunnelling matrix elements. The comparison between the effective and microscopic theories was made by comparing the size dependence of the zero mode tunnelling matrix elements. The specific Laughlin states that were considered in this work correspond to the filling factors $\nu = 1$ and $\nu = 1/3$.

The calculations using the local tunnelling operator were found to be in good agreement with the MC data for electron tunnelling in both the $\nu = 1$ and $\nu = 1/3$ QH state. However, the effective theory tunnelling Hamiltonian for a Laughlin quasiparticle did not predict the same scaling behaviour as computed microscopically for the tunnelling matrix elements. This result was found for FQH filling factor $\nu = 1/3$ and could hint at there being an error within the effective theory. To confirm this assertion, the scaling behaviour for the quasiparticle tunnelling matrix elements in other Laughlin states, such as $\nu = 1/5, 1/7$, etc., should also

be investigated, as well as the tunnelling processes for multiple quasiparticles at the impurity. Such findings will hint as to where possible sources of the errors occur in the effective theory of tunnelling across the bulk FQHE.

Definite conclusions that were drawn from Chapter 4 was that the bosonised operator ordering in the tunnelling Hamiltonian is important and must be considered when performing calculations related to tunnelling in the FQHE. Changing the ordering of the bosonised operators effects the locality of the tunnelling operator. Another important finding from the microscopic computations of both the quasiparticle and electron tunnelling matrix elements for $\nu = 1/3$ was that the electron tunnelling process is less relevant than the quasiparticle tunnelling process for all system sizes. This validates tunnelling calculations, which disregard the electron tunnelling operator in the effective tunnelling Hamiltonian in favour of only considering the quasiparticle tunnelling process.

With the success of the MC method to perform microscopic computations in the FQHE, in Chapter 5 a similar numerical procedure was performed, but now measuring the effective free energy of the system. The motivation for this project is related to the fact that there exists conflicting results between the work by Zabrodin *et al.* and Cheianov *et al.* Both have derived a Liouville-type equation in the semi-classical limit for the equilibrium density in terms of some background potential. The methods used are quite different, and as a consequence the Liouville equation derived by Cheianov *et al.* differs to the equivalent equation derived by Zabrodin *et al.* Therefore the aim of the work discussed in Chapter 5 was to check which Liouville equation most accurately described the behaviour of the FQH fluid. The method used by Cheianov *et al.* is discussed in Appendix B.1.

To perform a check for the two different Liouville equations, it was noticed that Zabrodin *et al.* had also derived a free energy expansion in the large N limit, where N corresponds to the number of electrons. The free energy is just the logarithm of the partition function or, using the plasma analogy, the magnitude squared of

the wavefunction. From Chapter 2 and Chapter 4 objects such as the norm of the Laughlin wavefunction are easily computed using MC, thus the free energy expansion was chosen to be tested microscopically, which in turn would shed light on the accuracy of the Liouville equation derived by Zabrodin *et al.* In particular, the two Liouville equations differ only in a single coefficient. For the Liouville equation derived by Zabrodin *et al.* this coefficient is denoted $\Delta(m)$ and the same coefficient also appears in the free energy expansion. Therefore it is of particular interest to compute the value of $\Delta(m)$ from the MC simulations.

In Section 5.2 analytic expressions for the free energy expansions were calculated for two background potentials in accordance with the formulae from Zabrodin *et al.*'s work. These expressions could in turn be compared to the MC data, which were obtained using the cumulant expansion method. The FQH states used in the MC simulations corresponded to filling factors $\nu = 1, 2$, and 3. In the free fermion case ($m = 1$) the MC data was in complete agreement with the large N expansion of the free energy obtain by Zabrodin *et al.* For $m = 2$, the MC data was inconclusive. The reason for the lack of clear data for this filling factor was due to the measured values from the MC simulations being small in magnitude, thus they were obscured by intrinsic statistical errors of the MC program. Finally for the inverse filling factor $m = 3$, the MC results suggest that the value of $\Delta(m)$ was not the same as the predicted value from the free energy expansion model. The numerical results consistently gave a value closer to 0.54, whereas the model predicts $\Delta(m) = 0.50$.

It was deduced that the discrepancy from the $m = 3$ simulations were not a consequence of the MC method used, I.e. it was not a systematic error of the cumulant expansion since no significant systematic error was apparent in the free fermion simulation. However it could be a result of boundary effects that are not taken into account in the model of the free energy expansion by Zabrodin *et al.* This project is still ongoing.

At the end of both the Chapters 4 and 5 there have already been proposals made for further areas of study. For Chapter 5 which was concerned with the large N expansion of the free energy, further MC tests were proposed which remove all boundary effects from the problem. Such a simulation should be a better match for the free energy expansion by Zabrodin *et al.* since their model does not take into account perturbations around the boundary.

Another proposal for further study is directly related to the Liouville equations derived by Cheianov *et al.* and Zabrodin *et al.* Both equations could be solved analytically for some background potential. To investigate which Liouville equation gives the most accurate equilibrium density distribution the analytical solutions can be compared to a MC simulation of the same background potential which calculates the density at given positions in the quantum fluid.

With regards to further work for the testing of the effective tunnelling Hamiltonian in Chapter 4, it was proposed that the occupied angular momentum orbitals could be increased such that we are no longer considering solely the zero mode matrix elements. The problem with this is the vast number of states and therefore MC simulations that would have to be included for an analysis that considers tunnelling of excitations between one occupied orbital on one boundary to a different orbital on the adjacent boundary. If an angular momentum cutoff is imposed however this is possible and some trial simulations have already been carried out for the free fermion case. These preliminary results show that the MC computation is still a good method for investigating tunnelling of higher angular momentum orbitals since the results can be checked against an exact analytic calculation for $m = 1$. The method to calculate the analytic solution is discussed in Appendix A.2.

In Chapter 4 only tunnelling for Laughlin states was considered. In reality there are many other FQH states that cannot be described by this wavefunction. An example is the state with filling factor $\nu = 5/2$. It was mentioned in Section 1.5 that not only is the microscopic wave function that describes this state unknown,

but whether the system follows Abelian or non-Abelian fractional statistics is still under debate. One proposal for a possible wavefunction for the $\nu = 5/2$ state is the Pfaffian wave function. This state supports non-Abelian fractional statistics and recently it has been indicated that there may also exist a plasma analogy for the Pfaffian state [102]. With a plasma analogy for the Pfaffian state a similar set of MC computations for tunnelling matrix elements can be carried out which, in turn can be compared to both the effective theory predictions for this wave function and also to experimental results measuring the tunnelling currents. Such simulations would shed light on the microscopic representation of this $\nu = 5/2$ state.

The final avenue to be considered for future study is related to the Klein factors, originally discussed in Section 1.5. Klein factors are extra phases added to the quasiparticle operators in the chiral Luttinger liquid theory. These phases allow multiple tunnelling operators at spatially separated multiple QPC's to commute with each other. Without these phases the tunnelling operators would not commute and thus be non-local operators. The addition of these Klein factors in literature is justified as being a manifestation of the fractional statistics followed by the quasiparticles. It is known from the chiral Luttinger liquid theory that for two quasiparticles exchanged on the same edge, a phase is obtained as a consequence of the fractional statistics. The Klein factors are obtained from the conjecture that a similar phase should also be picked up from exchanging quasiparticles on two disconnected edges (such as the inner and outer boundary of the FQH disk geometry considered in this thesis). An investigation to see if these Klein factors manifest from the microscopic theory would be extremely interesting. They have not been explicitly probed in the work presented in Chapter 4, concerned with the zero mode tunnelling matrix elements for the disk FQH device since it can be reasoned that for a two-edged system, the Klein factors do not contribute to observables [63]. Thus a system of three or more disconnected edges would have to be modelled microscopically.

In this thesis the MC method has been used to test the accuracy of effective theories for Laughlin FQH fluids. For MC simulations to be accurate and have a quick convergence, two solutions have been proposed to overcome phase problems that occur whilst considering tunnelling in Laughlin FQH systems. In particular using the results obtained from MC computations, it has been shown that the effective theory of electron tunnelling is an accurate description of the processes computed microscopically. This result is only true for a specific ordering of the chiral Luttinger liquid operators in the effective tunnelling Hamiltonian. Using this operator ordering also makes the Hamiltonian a local operator. The agreement between the microscopic computation and effective tunnelling Hamiltonian does not extend however, for a quasiparticle tunnelling across the bulk of the QH fluid, in the state $\nu = 1/3$. The cause of this disagreement may possibly be caused by an inaccuracy in the effective quasiparticle tunnelling Hamiltonian. The MC method has also been used to attempt to resolve the accurate form of the Liouville-type equation for the equilibrium density of a Laughlin quantum fluid. Overall the data was inconclusive possibly due to boundary effects in the simulation that were not considered in the analytic model, which the numerical data was compared to. Proposals have been made to overcome these boundary effects and work is still ongoing to resolve which Liouville-type equation best describes the equilibrium density distribution of a FQH system.

Theory of Symmetric Functions and the Free Fermion QHE

In Section A.1 of this appendix, a brief overview of the theory of symmetric polynomials is given. This material is complimentary to discussions in Section 3.1 of Chapter 3. Section A.2 contains information for analytically calculating exact overlap integrals for the free fermion QHE. Such methods have been used as a check for all MC programs discussed in this thesis.

A.1 Introduction to the Theory of Symmetric Polynomials

Good references for the theory of symmetric polynomials can be found in books [103] and [104]. This section introduces some definitions of the theory of symmetric polynomials. A polynomial $P(z_1, z_2, \dots, z_N)$ is symmetric if it is left invariant under any transformation permuting any of the z_i variables. Symmetric polynomials can be expressed as a sum of monomial symmetric functions defined via;

$$m_\lambda = \sum_{\mathcal{P}} z_1^{\lambda_1} z_2^{\lambda_2} z_3^{\lambda_3} \dots z_N^{\lambda_N} \quad (\text{A.1})$$

where the sum is over all permutations \mathcal{P} of the coordinates $\{z_i\}$. Therefore monomial symmetric functions form a linear basis for all symmetric polynomials. Different monomial symmetric functions can be distinguished from one another via their relationship to a partition. A partition is an ordered set of integers which can be written as,

$$\lambda = \{\lambda_1, \lambda_2, \lambda_3, \dots, \lambda_N\}, \quad (\text{A.2})$$

where λ_i are all integers and $\lambda_1 \geq \lambda_2 \geq \dots \geq \lambda_N$. Therefore the monomial given in Eq. (A.1) has the subscript λ , which refers to the partition, and the powers of the coordinates in the right-hand-side of the expression correspond to the integers in the partition itself. For example, for the number of variables $N = 3$, the symmetric monomial function corresponding to the partition $\lambda = \{3, 2, 1\}$ is

$$m_\lambda = z_1^3 z_2^2 z_3^1 + z_1^3 z_2^1 z_3^2 + z_1^2 z_2^3 z_3^1 + z_1^2 z_2^1 z_3^3 + z_1^1 z_2^3 z_3^2 + z_1^1 z_2^2 z_3^3. \quad (\text{A.3})$$

and we see from (A.3), the symmetric monomial functions are permanents.

The weight of a partition $|\lambda|$ is defined as $|\lambda| = \lambda_1 + \lambda_2 + \lambda_3 + \dots + \lambda_N$ and the length $l(\lambda)$ is the number of parts, or integers the partition contains. For example in (A.2), we have $l(\lambda) = N$. For meaningful partitions with regards to FQH systems, it is required that $l(\lambda)$ is less than or equal to the number of variables z_i . Another notation that is frequently used inside the partition is, k^{m_k} where m_k denotes the multiplicity, or frequency with which the integer k occurs. For example;

$$\lambda = \{3^1, 2^1, 1^3\} = \{3, 2, 1, 1, 1\}. \quad (\text{A.4})$$

It will be shown that these two representations of the partition correspond to either the boson or fermion representation of the low-energy excitations in the Laughlin wavefunction. There are three main types of symmetric polynomials that we are concerned with initially, these are;

1. Elementary symmetric functions,
2. Homogeneous product sums,
3. Power sums.

1. Elementary Symmetric Functions

For a total of N variables, the elementary symmetric functions are defined as follows;

$$\begin{aligned}
 a_1 &= \sum_{\mathcal{P}} z_1 \\
 a_2 &= \sum_{\mathcal{P}} z_1 z_2 \\
 a_3 &= \sum_{\mathcal{P}} z_1 z_2 z_3 \\
 &\vdots \\
 a_n &= \sum_{\mathcal{P}} z_1 z_2 z_3 \dots z_n
 \end{aligned} \quad (\text{A.5})$$

where the sum is over all permutations of the N variables. For example, when $N = 3$ the first three elementary symmetric functions are the following.

$$\begin{aligned}
a_1 &= z_1 + z_2 + z_3 \\
a_2 &= z_1 z_2 + z_2 z_3 + z_1 z_3 \\
a_3 &= z_1 z_2 z_3
\end{aligned} \tag{A.6}$$

The generators of the elementary symmetric functions are;

$$f(x) = \prod_{i=1}^n (1 - z_i x) = 1 - a_1 x + a_2 x^2 - a_3 x^3 + \dots + (-1)^n a_n x^n. \tag{A.7}$$

2. Homogeneous Product Sums

The generator for the homogeneous product sums h_i is simply the inverse of $f(x)$ in Eq. (A.7);

$$\begin{aligned}
\frac{1}{f(x)} &= \frac{1}{1 - a_1 x + a_2 x^2 \dots + (-1)^n a_n x^n} \\
&= 1 + h_1 x + h_2 x^2 + h_3 x^3 + \dots + h_n x^n + \dots
\end{aligned} \tag{A.8}$$

where the last equality arises from an expansion of x . To obtain an expression for the homogeneous product sums in terms of the variables z_i , one can expand the inverse of the product in (A.7) to give,

$$\frac{1}{f(x)} = \prod_{i=1}^n (1 + z_i x + z_i^2 x^2 + z_i^3 x^3 + \dots). \tag{A.9}$$

Comparing the expressions in (A.8) and (A.9) we see that the homogeneous power sums are simply the sum of all monomial symmetric functions of the same degree.

The first three homogeneous product sums are given below, where the sum is taken over all permutations of the variables index.

$$\begin{aligned}
h_1 &= \sum_{\mathcal{P}} z_1 \\
h_2 &= \sum_{\mathcal{P}} z_1^2 + \sum_{\mathcal{P}} z_1 z_2 \\
h_3 &= \sum_{\mathcal{P}} z_1^3 + \sum_{\mathcal{P}} z_1^2 z_2 + \sum_{\mathcal{P}} z_1 z_2 z_3
\end{aligned} \tag{A.10}$$

3. Power Sums

Power sums, S_k are the sum over all variables to the power k .

$$S_k = \sum_{\mathcal{P}} z_1^k \tag{A.11}$$

The generating function for the power sum polynomials is obtained by differentiating $f(x)$ with respect to x in (A.7) then dividing the resulting function by $f(x)$ itself, i.e.

$$\frac{f'(x)}{f(x)} = \sum_i \frac{-z_i}{1 - z_i x} = -S_1 - S_2 x - S_3 x^2 - \dots - S_n x^{n-1} - \dots \tag{A.12}$$

It is the power sum polynomials of the form (A.11) that can be multiplied by the Laughlin states to describe excitations in QH edge states. To see how this is achieved we first consider a circular droplet of Laughlin's incompressible fluid in the free fermion state with $m = 1$.

One of the first papers to highlight the advantages of describing FQH states in terms of symmetric polynomials was written by Stone [87, 105]. This work focused

on the free fermion picture corresponding to filling factor $\nu = 1$. The holomorphic representation (where exponential factors are omitted) of the Laughlin wavefunction in the free fermion state is

$$\Psi_{GS} = \prod_{i < j}^N (z_i - z_j). \quad (\text{A.13})$$

The wavefunction in (A.13) is actually the Vandermonde determinant which, in matrix form is given by,

$$\Psi_{GS} = \begin{vmatrix} z_1^{N-1} & z_1^{N-2} & \dots & 1 \\ z_2^{N-1} & z_2^{N-2} & \dots & 1 \\ \vdots & \vdots & \ddots & \vdots \\ z_N^{N-1} & z_N^{N-2} & \dots & 1 \end{vmatrix} = \det |z_s^{N-t}|. \quad (\text{A.14})$$

Excited edge states in the quantum Hall effect are obtained by multiplying the ground state wavefunction by a series of power sum polynomials given in (A.11). A general wavefunction describing low-level excitations in the edge states for the system of free fermions is given by

$$\Psi = \prod_{k>0} \left(\sum_i^N z_i^k \right)^{n_k} \prod_{i < j}^N (z_i - z_j), \quad (\text{A.15})$$

where k denotes the level of the excitation and n_k is the number of excitations in the k 'th level. Thus creating low-level excitations increases the powers of the z_i in the polynomial part of the wavefunction. In general these excited states should be able to be expressed in terms of a Slater determinant, where the extra powers due to the additional edge excitations are denoted by a set of integers $\lambda = \{\lambda_1, \lambda_2, \lambda_3, \dots, \lambda_N\}$.

$$\Psi_\lambda = \begin{vmatrix} z_1^{\lambda_1+N-1} & z_1^{\lambda_2+N-2} & \dots & z_1^{\lambda_N} \\ z_2^{\lambda_1+N-1} & z_2^{\lambda_2+N-2} & \dots & z_2^{\lambda_N} \\ \vdots & \vdots & \ddots & \vdots \\ z_N^{\lambda_1+N-1} & z_N^{\lambda_2+N-2} & \dots & z_N^{\lambda_N} \end{vmatrix} = \det|z_s^{\lambda_t+N-t}| \quad (\text{A.16})$$

The set of integers, λ is a partition of length $l(\lambda) = N$ satisfying the usual condition $\lambda_1 \geq \lambda_2 \geq \dots \geq \lambda_N$. Zero is a valid integer entry in a partition and in particular, the Vandermonde determinant is obtained for $\lambda = \{0, 0, \dots, 0\}$. Therefore the representation of the partition function $\lambda = \{\lambda_1, \lambda_2, \lambda_3, \dots, \lambda_N\}$ corresponds to a fermion basis since the integers in the partition are related to the increased orbital values occupied by the electrons in the fluid. In the bosonic formalism, states such as (A.16) are represented by the same partition but using the multiplicity notation for the integers as in Eq. (A.4). To see this equivalence of notation more explicitly we consider an example, starting from the boson formalism. In this formalism the low-energy excitations are denoted in terms of angular momentum orbitals, where the bosonic occupation number of a given angular momentum orbital k is denoted n_k . The total angular momentum can be summed as follows,

$$l = L_{total} - L_{GS} = n_1 + 2n_2 + 3n_3 + \dots \quad (\text{A.17})$$

For this example we consider only excited states that satisfy $l = 3$. There are three possible states which satisfy this condition,

$$\begin{aligned} \textbf{State 1:} \quad & n_1 = 3, n_2 = n_3 = \dots = 0, \\ \textbf{State 2:} \quad & n_1 = 1, n_2 = 1, n_3 = n_4 \dots = 0, \\ \textbf{State 3:} \quad & n_1 = n_2 = 0, n_3 = 1, n_4 = n_5 = \dots = 0. \end{aligned} \quad (\text{A.18})$$

To each unique state corresponds a unique partition. The integers in the partition are given by k , where k corresponds to the occupied level of the excitation and if $n_k \geq 1$, the multiplicity of k in the partition is equal n_k . In general,

$$\lambda = \{r^{n_r}, \dots, 3^{n_3}, 2^{n_2}, 1^{n_1}\} \quad (\text{A.19})$$

Thus our bosonic basis can be written in terms of the partitions;

$$\begin{aligned} \lambda_{B,1} &= \{1^3\} \\ \lambda_{B,2} &= \{2^1, 1^1\} \\ \lambda_{B,3} &= \{3^1\} \end{aligned} \quad (\text{A.20})$$

For each bosonic excitation, the Laughlin wavefunction gets multiplied by a power sum polynomial of degree corresponding to the momentum orbital occupied in this representation. Thus the corresponding wavefunctions of the partitions in (A.20) written in terms of the occupation numbers $|n_1, n_2, n_3\rangle$ in the holomorphic representation are;

$$\begin{aligned} |3, 0, 0\rangle &= S_1^3 \prod_{i<j} (z_i - z_j) = \left[\sum_{i=1}^N z_i \right]^3 \prod_{i<j} (z_i - z_j), \\ |1, 1, 0\rangle &= S_1 S_2 \prod_{i<j} (z_i - z_j) = \left[\sum_{i=1}^N z_i \right] \left[\sum_{i=1}^N z_i^2 \right] \prod_{i<j} (z_i - z_j), \\ |0, 0, 1\rangle &= S_3 \prod_{i<j} (z_i - z_j) = \left[\sum_{i=1}^N z_i^3 \right] \prod_{i<j} (z_i - z_j). \end{aligned} \quad (\text{A.21})$$

The corresponding fermion representation of partitions for states 1 to 3 in (A.18)

are;

$$\begin{aligned}\mathbf{State\ 1:} & \{1, 1, 1, 0, \dots, 0\}, \\ \mathbf{State\ 2:} & \{2, 1, 0, 0, \dots, 0\}, \\ \mathbf{State\ 3:} & \{3, 0, 0, 0, \dots, 0\}.\end{aligned}\tag{A.22}$$

The Slater determinants corresponding to states 1 to 3 can thus be calculated using (A.16) with the partitions given in (A.22). Therefore to summarise this section, definitions of various types of symmetric polynomials have been introduced along with the concept of a partition which can be represented using two different notations. These can be thought of as a basis in the bosonic representation, where low-energy excitations are created by multiplying the Laughlin wavefunction by a series of power sum polynomials, or in the fermion representation where integers in the partition correspond to the increase of angular momentum orbitals of the electrons in the Laughlin droplet. Although the example considered in this section was for the free fermion case, the excitation representations can be extended for any Laughlin state with filling factor $\nu = 1/m$. The fermion basis is most intuitive for the free fermion case where the holomorphic part of the Laughlin wavefunction is a Vandermonde determinant. It is for this reason the overlap integrals for the free fermion case have an exact analytic solution. This will be the subject of the next section.

A.2 Analytical Calculations for Overlap Integrals in the Free Fermion QHE

Overlap integrals for the free fermion state can be made trivial to solve by introducing another type of symmetric polynomial, called Schur functions. Schur functions are defined by the quotient of the Slater determinants with respect to the Vandermonde determinant. Each partition λ corresponds to a unique Schur function;

$$\Phi_\lambda = \frac{\Psi_\lambda}{\Psi_{GS}} = \frac{\det|z_s^{\lambda_i+n-t}|}{\det|z_s^{n-t}|}, \quad (\text{A.23})$$

where the numerator of (A.23) is a Slater determinant of the form (A.16). The inner product of two Schur functions is only non-zero when the Schur functions are equivalent. Thus expressing FQH states for the free fermion system in terms of Schur functions greatly reduces computational effort for the overlap of states. The definition for the overlap of Schur functions is;

$$\langle \Phi_{\lambda'} | \Phi_\lambda \rangle = \int \prod_{i=1}^N \left(d^2 z_i e^{-|z_i|^2/2} \right) \prod_{i < j}^N |z_i - z_j|^2 \bar{\Phi}_{\lambda'} \Phi_\lambda. \quad (\text{A.24})$$

Using the definition of the Schur function in (A.23) as a quotient, with denominator as the Vandermonde determinant, then the above overlap can be expressed in terms of the product of two determinants,

$$\langle \Phi_{\lambda'} | \Phi_\lambda \rangle = \int \prod_{i=1}^N \left(d^2 z_i e^{-|z_i|^2/2} \right) \det|\bar{z}_s^{\lambda'_i+n-t}| \det|z_s^{\lambda_i+n-t}| \delta_{\lambda'\lambda}. \quad (\text{A.25})$$

For the above integral to be non-zero there must exist terms in the product of the two determinants which depend only on the magnitude of the coordinate and

not the angle. This condition is met only when $\lambda' \equiv \lambda$. The product of the two determinants is straightforward to calculate.

$$\langle \Phi_{\lambda'} | \Phi_{\lambda} \rangle = (2\pi)^N N! \prod_{i=1}^N [2^{\lambda_i + N - i} (\lambda_i + N - i)!] \delta_{\lambda' \lambda} \quad (\text{A.26})$$

If free fermion QH states containing low-energy excitations can be expressed in terms of the Schur functions, applying (A.26) will give the overlap of states. To write the states as Schur functions one can use the conversion relations between various different types of symmetric polynomials. Since the excited states of interest are just the Vandermonde determinant multiplied by a series of power sum polynomials, the aim is to be able to write such power sum polynomials as a linear superposition of the Schur functions.

The Schur functions have a simple expression in terms of the homogeneous product of sums given by the following determinant;

$$\Phi_{\lambda} = \det |h_{\lambda_s - s + t}|. \quad (\text{A.27})$$

If one is also able to express power sum polynomials in terms of the homogeneous product of sums then (A.27) can be used to define a new basis for the low-energy excitations in the free fermion QH states. To do this an intermediate step is needed which converts power sums to elementary symmetric functions (see previous section) via the determinant of a quasi-lower triangular matrix.

$$S_r = \begin{vmatrix} a_1 & 1 & 0 & 0 & \cdots & 0 \\ 2a_2 & a_1 & 1 & 0 & \cdots & 0 \\ 3a_3 & a_2 & a_1 & 1 & \cdots & 0 \\ \vdots & \vdots & \vdots & \vdots & \ddots & \vdots \\ ra_r & \cdots & \cdots & \cdots & \cdots & a_1 \end{vmatrix} \quad (\text{A.28})$$

A similar relationship also exist between homogeneous product sums and elementary symmetric functions.

$$a_r = \begin{vmatrix} h_1 & 1 & 0 & 0 & \cdots & 0 \\ h_2 & h_1 & 1 & 0 & \cdots & 0 \\ h_3 & h_2 & h_1 & 1 & \cdots & 0 \\ \vdots & \vdots & \vdots & \vdots & \ddots & \vdots \\ h_r & \cdots & \cdots & \cdots & \cdots & h_1 \end{vmatrix} \quad (\text{A.29})$$

These are all the tools needed to express the power sum polynomials as a linear superposition of Schur functions and all that remains is a simple algebraic problem. To show an explicit example, we will continue on the example used earlier when the three states were considered with the angular momentum contribution due to the excitations, $l = 3$. These states were given in (A.21), since there are only three partitions possible for $l = 3$, there are only three Schur functions that are needed to define the basis for all states that satisfy $l = 3$. The aim is to find the following coefficients such that (A.21) is satisfied.

$$\begin{aligned}
|3, 0, 0\rangle &= (a\Phi_{\{1,1,1\}} + b\Phi_{\{2,1\}} + c\Phi_{\{3\}}) \prod_{i<j} (z_i - z_j) \\
|1, 1, 0\rangle &= (d\Phi_{\{1,1,1\}} + e\Phi_{\{2,1\}} + f\Phi_{\{3\}}) \prod_{i<j} (z_i - z_j) \\
|0, 0, 1\rangle &= (g\Phi_{\{1,1,1\}} + h\Phi_{\{2,1\}} + k\Phi_{\{3\}}) \prod_{i<j} (z_i - z_j)
\end{aligned} \tag{A.30}$$

Equation (A.27) is first used to express the Schur functions in terms of homogeneous product of sums. The results for the three Schur functions in this example are

$$\begin{aligned}
\Phi_{\{1,1,1\}} &= h_1^3 - 2h_1h_2 + h_3, \\
\Phi_{\{2,1\}} &= h_1h_2 - h_3, \\
\Phi_{\{3\}} &= h_3.
\end{aligned} \tag{A.31}$$

Using (A.28) and (A.29) the power sum polynomials expressed in terms of the homogeneous product of sums have the form;

$$\begin{aligned}
S_1^3 &= a_1^3 = h_1^3, \\
S_1S_2 &= a_1^3 - 2a_2a_1 = -h_1^3 + 2h_1h_2, \\
S_3 &= a_1^3 - 3a_2a_1 + 3a_3 = h_1^3 - 3h_1h_2 + 3h_3.
\end{aligned} \tag{A.32}$$

Comparing the above with (A.31) it can be seen that (A.30) is satisfied by the following coefficients of the Schur functions.

$$\begin{aligned}
|3, 0, 0\rangle &= (\Phi_{\{1,1,1\}} + 2\Phi_{\{2,1\}} + \Phi_{\{3\}}) \prod_{i<j} (z_i - z_j) \\
|1, 1, 0\rangle &= (-\Phi_{\{1,1,1\}} + \Phi_{\{3\}}) \prod_{i<j} (z_i - z_j) \\
|0, 0, 1\rangle &= (\Phi_{\{1,1,1\}} - \Phi_{\{2,1\}} + \Phi_{\{3\}}) \prod_{i<j} (z_i - z_j)
\end{aligned} \tag{A.33}$$

Overlaps between these three states with themselves and between each other are trivial to calculate since they can now be expressed in terms of overlaps of Schur functions, of which the result is given by (A.26). For example,

$$\langle 3, 0, 0 | 0, 0, 1 \rangle = \langle \Phi_{\{1,1,1\}} | \Phi_{\{1,1,1\}} \rangle - 2 \langle \Phi_{\{2,1\}} | \Phi_{\{2,1\}} \rangle + \langle \Phi_{\{3\}} | \Phi_{\{3\}} \rangle. \tag{A.34}$$

So far we have only dealt with a QH system with a single edge. However an extension to a two edge system with the wavefunction in the holomorphic representation given by

$$\Psi_N^M = \prod_{i<j}^N (z_i - z_j) \prod_{i=1}^N z_i^M \tag{A.35}$$

is relatively straightforward. The Schur function representation for the outer boundary still holds, the only difference being that the extra product of z_i^M increases the degree of the determinant by M , thus in the definition of the Schur functions for the outer boundary we have $N \rightarrow T = N + M$, such that,

$$\Phi_\lambda = \frac{\det |z_s^{\lambda_t + T - t}|}{\det |z_s^{T - t}|}. \tag{A.36}$$

With this definition however we can obtain an overlap for the Schur functions for the outer boundary similar to (A.26);

$$\langle \Phi_{\lambda'} | \Phi_{\lambda} \rangle = (2\pi)^N N! \prod_{i=1}^N [2^{\lambda_i + T - i} (\lambda_i + T - i)!] \delta_{\lambda' \lambda} \quad (\text{A.37})$$

Defining a basis for excitations on the inner boundary is similar to that of the outer boundary except now the power sum polynomials are a sum over the inverse electron coordinate variables. Writing occupation numbers as n_{-k} for an excitation in the k 'th orbital of the inner boundary; an example of a state containing only inner boundary low-energy excitations is;

$$|n_1, n_2, n_3\rangle = \left[\sum_{i=1}^N \frac{1}{z_i} \right]^{n_1} \left[\sum_{i=1}^N \frac{1}{z_i^2} \right]^{n_2} \left[\sum_{i=1}^N \frac{1}{z_i^3} \right]^{n_3} \prod_{i < j}^N (z_i - z_j) \prod_{i=1}^N z_i^M. \quad (\text{A.38})$$

A new variable can be defined, $w = z^{-1}$ such that the terms defining the inner-edge excitations are power sum polynomials in this new variable w ,

$$S_{-k}^{n_{-k}} = \left[\sum_{i=1}^N w_i^k \right]^{n_{-k}} = \left[\sum_{i=1}^N \frac{1}{z_i^k} \right]^{n_{-k}}.$$

Thus, the additional angular momentum acquired by inner boundary low-energy excitations is given by

$$l = L_{total} - L_{GS} = -n_{-1} - 2n_{-2} - 3n_{-3} - \dots \quad (\text{A.39})$$

The definition of the Schur functions that corresponds to the inner excitations are therefore given by;

$$\Phi_{-\lambda} = \frac{\det|w_s^{\lambda_t+N-t}|}{\det|w_s^{N-t}|}. \quad (\text{A.40})$$

This is the same definition as for the outer boundary excitations in Eq. (A.23) only now the variable has changed $z \rightarrow w$. Defining the Schur function in terms of the variable w is however not good practice since the remainder of the wavefunction is defined in terms of $z = w^{-1}$ thus we need to convert (A.40) to an expression dependant on z only. To begin this process, we first consider the denominator in (A.40) and note that,

$$\left(\prod_i w_i^{N-1} \right)^{-1} \det|w_s^{N-t}| = \det|w_s^{1-t}| = \det|z_s^{t-1}|.$$

The determinant on the right-hand-side is as follows,

$$\det|z_s^{t-1}| = \begin{vmatrix} 1 & z_1 & \cdots & z_1^{N-1} \\ 1 & z_2 & \cdots & z_2^{N-1} \\ \vdots & \vdots & \ddots & \vdots \\ 1 & z_N & \cdots & z_N^{N-1} \end{vmatrix}.$$

To calculate the overlap between inner boundary Schur functions, we would hope to be able to write the denominator in the Schur function definition (A.40) in terms of the Vandermonde determinant in the variable z , given by;

$$\det|z_s^{N-t}| = \begin{vmatrix} z_1^{N-1} & \cdots & z_1 & 1 \\ z_2^{N-1} & \cdots & z_2 & 1 \\ \vdots & \ddots & \vdots & \vdots \\ z_N^{N-1} & \cdots & z_N & 1 \end{vmatrix}.$$

From observing the above two determinants, one can see that the Vandermonde

determinant $\det|z_s^{N-t}|$ can be obtained from $\det|z_s^{t-1}|$ by simply interchanging the columns. Therefore we can now write the denominator in (A.40) in terms of the Vandermonde determinant in variable z as

$$\det|w_s^{N-t}| = (-1)^{\frac{N}{2}(N-1)} \prod_{i=1}^N (w_i^{N-1}) \det|z_s^{N-t}|. \quad (\text{A.41})$$

Now we focus our attention on the numerator of (A.40) proceeding in the same way as for denominator by considering the following relation.

$$\left(\prod_i w_i^{N-1} \right)^{-1} \det|w_s^{\lambda_t+N-t}| = \det|w_s^{\lambda_t+1-t}| = \det|z_s^{t-1-\lambda_t}|$$

The form of the determinant on the right-hand-side written out explicitly is

$$\det|z_s^{t-1-\lambda_t}| = \begin{vmatrix} z_1^{-\lambda_1} & z_1^{1-\lambda_2} & \dots & z_1^{N-1-\lambda_N} \\ z_2^{-\lambda_1} & z_2^{1-\lambda_2} & \dots & z_2^{N-1-\lambda_N} \\ \vdots & \vdots & \ddots & \vdots \\ z_N^{-\lambda_1} & z_N^{1-\lambda_2} & \dots & z_N^{N-1-\lambda_N} \end{vmatrix}.$$

One can exchange all the columns in the above determinant to completely reverse their order which will give a factor of (-1) to the $\frac{N}{2}(N-1)$ times, this will eventually cancel out with the same factor in (A.41).

$$\det|z_s^{t-1-\lambda_t}| = (-1)^{\frac{N}{2}(N-1)} \begin{vmatrix} z_1^{N-1-\lambda_N} & \dots & z_1^{1-\lambda_2} & z_1^{-\lambda_1} \\ z_2^{N-1-\lambda_N} & \dots & z_2^{1-\lambda_2} & z_2^{-\lambda_1} \\ \vdots & \ddots & \vdots & \vdots \\ z_N^{N-1-\lambda_N} & \dots & z_N^{1-\lambda_2} & z_N^{-\lambda_1} \end{vmatrix}. \quad (\text{A.42})$$

To complete the final definition for the numerator of the Schur function, the con-

jugate partition $\bar{\lambda}$ must be defined. The partition $\lambda = \{\lambda_1, \lambda_2, \dots, \lambda_N\}$ can be conjugated to give,

$$\bar{\lambda} = \{\bar{\lambda}_1, \bar{\lambda}_2, \dots, \bar{\lambda}_{N-1}, \bar{\lambda}_N\} = \{\lambda_N, \lambda_{N-1}, \dots, \lambda_2, \lambda_1\} \quad (\text{A.43})$$

i.e., the order of the partition is simply reversed. An equation relating an element of a partition to its conjugate element is

$$\bar{\lambda}_{N-i} = \lambda_{i+1}. \quad (\text{A.44})$$

Using the conjugate partition $\bar{\lambda}$ rather than the partition λ we can express the above determinant (A.45) as

$$\begin{aligned} \det|z_s^{t-1-\lambda_t}| &= (-1)^{\frac{N}{2}(N-1)} \begin{vmatrix} z_1^{N-1-\bar{\lambda}_1} & \dots & z_1^{1-\bar{\lambda}_{N-1}} & z_1^{-\bar{\lambda}_N} \\ z_2^{N-1-\bar{\lambda}_1} & \dots & z_2^{1-\bar{\lambda}_{N-1}} & z_2^{-\bar{\lambda}_N} \\ \vdots & \ddots & \vdots & \vdots \\ z_N^{N-1-\bar{\lambda}_1} & \dots & z_N^{1-\bar{\lambda}_{N-1}} & z_N^{-\bar{\lambda}_N} \end{vmatrix} \\ &= (-1)^{\frac{N}{2}(N-1)} \det|z_s^{N-t-\bar{\lambda}_t}|. \end{aligned} \quad (\text{A.45})$$

So the numerator in (A.40) can be expressed as

$$\det|w_s^{\lambda_t+N-t}| = (-1)^{\frac{N}{2}(N-1)} \prod_{i=1}^N (w_i^{N-1}) \det|z_s^{N-t-\bar{\lambda}_t}|. \quad (\text{A.46})$$

Combining (A.46) with (A.41), we can convert the definition of the Schur function as a quotient in terms of w (A.40) to a simple quotient in terms of z where we use the conjugate partition as opposed to the actual partition itself. The result

is given below.

$$\Phi_{-\lambda} = \frac{\det|z_s^{N-t-\bar{\lambda}_t}|}{\det|z_s^{N-t}|} \quad (\text{A.47})$$

All that remains is to calculate the overlap for the inner-boundary Schur functions.

$$\begin{aligned} \langle \Phi_{-\lambda'} | \Phi_{-\lambda} \rangle &= \int \prod_{i=1}^N \left(d^2 z_i e^{-|z_i|^2/2} |z_i|^{2M} \right) \prod_{i<j}^N |z_i - z_j|^2 \bar{\Phi}_{-\lambda} \Phi_{-\lambda} \delta_{\lambda'\lambda} \\ &= \int \prod_{i=1}^N \left(d^2 z_i e^{-|z_i|^2/2} |z_i|^{2M} \right) \det|\bar{z}_s^{N-t-\bar{\lambda}_t}| \det|z_s^{N-t-\bar{\lambda}_t}| \delta_{\lambda'\lambda} \\ &= \int \prod_{i=1}^N \left(d^2 z_i e^{-|z_i|^2/2} \right) \det|\bar{z}_s^{T-t-\bar{\lambda}_t}| \det|z_s^{T-t-\bar{\lambda}_t}| \delta_{\lambda'\lambda}, \end{aligned}$$

where $T = N + M$. Note that this integral can only be solved when M is greater or equal to the angular momentum contributions from the inner boundary. If this condition is not fulfilled then negative powers of z occur in the in the determinants for the overlap making the integrals diverge. Physically this condition makes sure that there exists enough available excited states inside the hole of the QH disk such that there is room for the occupancy of the inner boundary excitations.

The solution for the overlaps of the inner boundary Schur functions is as follows,

$$\langle \Phi_{-\lambda'} | \Phi_{-\lambda} \rangle = N! (2\pi)^N \prod_{i=1}^N \left(2^{T-i-\bar{\lambda}_i} (T-i-\bar{\lambda}_i)! \right) \delta_{\lambda'\lambda}. \quad (\text{A.48})$$

Thus the inner boundary low-energy excitation states can now be treated in a similar manner to the outer boundary excited states. The states that originally consist of a product of power sum polynomials of the inverse variable can be converted into a linear superposition of Schur functions defined in (A.40). The overlap integrals for inner boundary low-energy excitations are then calculated

using (A.48).

The form of the overlap of Schur functions for the outer boundary and the inner boundary allows all overlap integrals to be calculated for free fermion systems containing any configuration of inner boundary excitations or outer boundary excitations. In general, using this formalism of Schur functions in the free fermion system, the overlap calculations of FQH excited states can be generalised to include averages over operators.

Calculating the Norm of Laughlin States

Laughlin-type wavefunctions are not normalised. In this section the norm of the variational wavefunction is calculated for the generalised wavefunctions given in (3.9), which support low-energy excitations. The norm of the wavefunctions are tau-functions of analytic curves which have been studied in works of Wiegmann, Zabrodin *et al.* [96, 97, 99]. To perform this calculation, the FQH system described by Laughlin states is reformulated to a boson field theory using Laughlin’s plasma analogy. The method involves expressing the grand partition function in terms of a boson field path integral, from which an action describing the dynamics of the free boson system can be extracted. The process that is followed here was originally described in the work [98] for a Laughlin state containing a single edge, it has been extended here to include excitations on the inner and outer boundaries of the FQH device shown in Figure 1.5. The first part of this section is the field theory reformulation for the “undeformed” Laughlin state when there are no excitations present at the edges. In the second section the field theory formalism is extended to include the edge excitations which in turn allows the form of the tau-function to be calculated.

B.1 Boson Field Theory Reformulation for a Laughlin-Type System

Laughlin's plasma analogy allows one to express the magnitude squared of the ground state wavefunction (1.31) as a partition function Z_N of a classical two-component plasma with Coulomb interactions.

$$Z_N = \int \prod_i^N d^2 z_i e^{-m\varepsilon} = \int \prod_i^N d^2 z_i |\Psi_N^M|^2, \quad (\text{B.1})$$

where

$$\varepsilon = -2 \sum_{i < j}^N \ln |z_i - z_j| - \frac{1}{m} \sum_{i=1}^N \varphi_{bg}(z, \bar{z}), \quad (\text{B.2})$$

and m is the inverse temperature in the plasma analogy. The symbol φ_{bg} is used to shorten notation and encodes the background potential terms of the plasma.

$$\varphi_{bg}(z, \bar{z}) = 2M \ln |z_i| - \frac{|z_i|^2}{2} \quad (\text{B.3})$$

The mapping described in [98] is now used for the case when the only excitations in the system are the M quasiholes used to create the macroscopic hole at the center of the device. The steps are repeated below for completeness. The aim is to describe the system in terms of a field theory, to do this the partition function of the plasma (B.1) is written as a correlator in terms of the Bose field $\phi = \phi(z, \bar{z})$.

$$Z_N = \int \prod_{i=1}^N (d^2 z_i e^{\varphi_{bg}(z_i, \bar{z}_i)}) \left\langle \prod_{i=1}^N e^{i\sqrt{m}\phi} \right\rangle \quad (\text{B.4})$$

The above average is performed using the Euclidean Gaussian action of a free

massless boson. For a detailed discussion on the cutoffs for the divergences, see the original work [98]. To see that this correlator corresponds to the partition function given in (B.1), Wick's theorem is employed. This theorem states that the average value of a product of n operators, \hat{A}_i , can be written as a sum running over all distinct permutations \mathcal{P} of the n indices in the following manner,

$$\langle \hat{A}_1 \hat{A}_2 \dots \hat{A}_n \rangle = \sum_{\mathcal{P}} \langle \hat{A}_1 \hat{A}_2 \rangle \langle \hat{A}_3 \hat{A}_4 \rangle \dots \langle \hat{A}_{n-1} \hat{A}_n \rangle. \quad (\text{B.5})$$

Therefore the correlator in (B.4) can be written as

$$\begin{aligned} \left\langle \prod_j^N e^{i\sqrt{m}\phi(z_j, \bar{z}_j)} \right\rangle &= \exp \left(-m \sum_{i < j}^N \langle \phi(z_i, \bar{z}_i) \phi(z_j, \bar{z}_j) \rangle \right) \\ &= \exp \left(m \sum_{i < j}^N \ln |z_i - z_j|^2 \right), \end{aligned} \quad (\text{B.6})$$

where we have used $\langle \phi(z) \phi(z') \rangle = -\ln |z - z'|^2$ in the free boson theory. One can now write the average of $|\Psi_N^M|^2$ (or in the plasma analogy $e^{-m\varepsilon}$) as a correlator,

$$e^{-m\varepsilon} = \frac{\int \mathcal{D}\phi \left[\prod_j^N e^{i\sqrt{m}\phi(z_j)} \right] \prod_i^N e^{\varphi_{bg}(z_i)} S^{-S_0[\phi(z)]}}{\int \mathcal{D}\phi e^{-S_0}}. \quad (\text{B.7})$$

The action for a free massless boson is given by,

$$S_0[\phi] = \frac{1}{2\pi} \int d^2z \partial\phi \bar{\partial}\phi. \quad (\text{B.8})$$

The solution of this action is $\phi = 0$ and so we are assuming that our field theory has solutions that are small deviations from this value. Using the average (B.7) one can now express the partition function and thus the grand canonical ensemble

partition function in terms of this field theory. The definition of the partition function of the grand canonical ensemble in terms of the partition functions Z_N and coupling constant I is

$$\Theta(I) = \sum_{N=0}^{\infty} \frac{I^N}{N!} Z_N = \sum_{N=0}^{\infty} \frac{I^N}{N!} \int d^2 z_1 \dots d^2 z_N e^{-m\epsilon} \quad (\text{B.9})$$

Upon substitution of the field integral given in (B.7) and permuting the order of the integrals one obtains,

$$\Theta(I) = \frac{1}{\kappa} \sum_{N=0}^{\infty} \frac{I^N}{N!} \int \mathcal{D}\phi e^{-S_0[\phi]} \int d^2 z_1 \dots d^2 z_N \prod_{j=1}^N \left(e^{i\sqrt{m}\phi(z_j, \bar{z}_j)} e^{\varphi_{bg}(z_j, \bar{z}_j)} \right). \quad (\text{B.10})$$

To shorten notation, κ is simply the value of the denominator in (B.7). Since permuting any of the N indices of the particle coordinates leaves the integrals unchanged, Eq. (B.10) can be expressed as

$$\begin{aligned} \int d^2 z_1 \dots d^2 z_N \prod_{j=1}^N \left(e^{i\sqrt{m}\phi(z_j, \bar{z}_j)} e^{\varphi_{bg}(z_j, \bar{z}_j)} \right) &= \left[\int d^2 z e^{i\sqrt{m}\phi(z, \bar{z})} e^{\varphi_{bg}(z, \bar{z})} \right]^N \\ &= X^N. \end{aligned} \quad (\text{B.11})$$

The sum over the number of particles in the expression for the grand partition function can now be removed by noticing the sum is in fact an expansion of an exponential function with exponent IX . Thus,

$$\Theta(I) = \frac{1}{\kappa} \int \mathcal{D}\phi e^{IX - S_0[\phi]} = \frac{1}{\kappa} \int \mathcal{D}\phi e^{-S[\phi]}, \quad (\text{B.12})$$

where $S[\phi]$ is our new action in terms of the Bose field ϕ describing the ground state FQH system depicted in Figure 1.5 and has the corresponding wavefunction given by (1.31). The explicit form of this action is,

$$S[\phi] = \frac{1}{8\pi} \int d^2z \left[(\nabla\phi)(\nabla\phi) - 4\mu e^{i\sqrt{m}\phi(z,\bar{z}) + \varphi_{bg}(z,\bar{z})} \right], \quad (\text{B.13})$$

where μ is the fugacity and is related to the coupling constant in the following manner; $\mu = 2\pi I$. Our aim is now to obtain an expression for the field ϕ in terms of the complex variable z , from this expression one can calculate important characteristics of the system such as the particle density throughout the bulk of the FQH system.

The variational principle is employed to give the differential equation

$$\Delta\varphi(z, \bar{z}) + 2m\mu e^{-\varphi(z,\bar{z})} = 2 - 4\pi M\delta|z|, \quad (\text{B.14})$$

where the following change of variables has been used

$$\phi = \frac{i}{\sqrt{m}} (\varphi + \varphi_{bg}). \quad (\text{B.15})$$

It is noted that the solution must be angle independent as a result of the axial symmetry of the system and so $\varphi(z, \bar{z}) \equiv \varphi(r)$. Having the dependent variable φ as the exponent of an exponential function makes (B.14) particularly difficult to solve. However it was noticed that one can relate the term $e^{-\varphi}$ to the density of particles using the two-dimensional Poisson's equation given by

$$\Delta\varphi = 4\pi m(\rho - \rho_{bg}) = 4\pi m\rho - \Delta\varphi_{bg}, \quad (\text{B.16})$$

where ρ corresponds to the charge density due to the particles creating the plasma and ρ_{bg} is due to the neutralising background. Substituting this expression into (B.14) gives $2m\mu e^{-\varphi} = -4\pi m\rho$. Eq. (B.15) can therefore be written as a differential equation for the particle density;

$$\frac{1}{4\pi}\Delta \ln \rho + m\rho = m\rho_{bg}, \quad (\text{B.17})$$

where $\rho_{bg} = 4\pi m\Delta\varphi_{bg}$ denotes background density distribution. The differential equation (B.17) is a Liouville-type equation with an additional non-zero term on the right-hand side. It has been discussed in Chapter 5 of this thesis. For this section it is convenient to stick with the notation for the field $\varphi(z, \bar{z})$ as in Eq. (B.14). Since $e^{-\varphi}$ is related to density and in the semi-classical limit the bulk density is a constant $\rho = (2\pi ml_B^2)^{-1}$, the differential equation for $\varphi(z, \bar{z})$ can be re-written as

$$\Delta\varphi(z, \bar{z}) - F^2 = 2 - 4\pi M\delta|z|. \quad (\text{B.18})$$

where

$$F^2 = \begin{cases} \frac{2}{ml_B^2} & \text{for } R_I < |z| < R_O, \\ 0 & \text{otherwise.} \end{cases} \quad (\text{B.19})$$

The solution to this differential equation is not given here since we are more interested in the system that contains low energy excitations occupying the inner and the outer boundary, as discussed in the next section. However since the low energy excitations are treated as a perturbation to the ground state system the differential equation (B.18) will be referred to later.

B.2 Laughlin States Including Edge Excitations

In the remainder of this appendix, the procedure given previously for mapping the FQH system to a boson field theory is again used for the wavefunction given in (3.9). Purposefully, the distance between the inner and outer boundary is greater than the magnetic length such that the two edges do not interact with each other. For simplicity, the wavefunction parameterised by $t_{\pm k}$ is repeated below.

$$\Psi = \prod_{i=1}^N (z_i - z_j)^m \prod_{i=1}^N z_i^M e^{-\frac{|z_i|^2}{4} + w(z_i)}, \quad (\text{B.20})$$

where

$$w(z) = \sum_{k>0} \left(z^k t_k + \frac{t_{-k}}{z^k} \right). \quad (\text{B.21})$$

This wavefunction can be expressed in terms of a partition function which will now contain the parameters $t_{\pm k}$.

$$Z(t_{\pm k}, \bar{t}_{\pm k}) = \int \prod_{i=1}^N d^2 z_i e^{-m\varepsilon(t_{\pm k}, \bar{t}_{\pm k})} = \int \prod_{i=1}^N d^2 z_i |\Psi|^2, \quad (\text{B.22})$$

where the effective energy, according to (B.20) is

$$\varepsilon(t_{\pm k}, \bar{t}_{\pm k}) = 2 \sum_{i<j}^N \ln |z_i - z_j| + \sum_{i=1}^N \left(\frac{2M}{m} \ln |z_i| - \frac{|z_i|^2}{2m} + w(z_i) + \bar{w}_i(\bar{z}) \right). \quad (\text{B.23})$$

The aim for this section is to calculate the norm of the state (B.20) in the semi-classical limit, which is referred to as the tau-function.

$$\tau(N, M, t_{\pm k}, \bar{t}_{\pm k}) = e^{mF(N, M, t_{\pm k}, \bar{t}_{\pm k})}, \quad (\text{B.24})$$

where the function $F(N, M, t_{\pm k}, \bar{t}_{\pm k})$ should have no dependence on the inverse filling factor m of the state. The problem with the partition function in (B.22) is that the function contains an infinite sum over the $t_{\pm k}$ parameters which is difficult to work with. Instead, the partition function $Z(t_{\pm k}, \bar{t}_{\pm k})$ is mapped onto a new partition function $Z(a, c)$ using a transformation to Miwa variables [106]. Effectively, this new partition function describes a disk-shaped quantum fluid (absent of edge excitations) with two source charges placed at complex coordinates a and c where a is placed in the macroscopic hole inside the disk ($|a| < R_I$) and c is outside the droplet ($|c| > R_O$). This new system is described by the partition function,

$$Z(a, c) = \int \prod_{i=1}^N d^2 z_i \prod_{i < j}^N |z_i - z_j|^{2m} \prod_{k=1}^N \left(e^{\varphi_{\text{bg}}(z)_k} \frac{|z_i - a|^{2m}}{|z_i|^{2m}} |z_i - c|^{2m} \right), \quad (\text{B.25})$$

where $\varphi_{\text{bg}}(z, \bar{z}) = 2M \ln |z| - |z|^2/2$, as defined in the previous section. The extra product; $\prod |z_i|^{-2m}$ has been inserted into the above partition function as a mathematical convenience to simplify the mappings between the partition functions $Z(a, b)$ and $Z(t_{\pm k}, \bar{t}_{\pm k})$. This addition reduces the number of quasiholes in the center of the disk from M to $M - m$. This is not a problem as long as $M > m$. To find this mapping the following expansions are used in $Z(a, c)$;

$$|z - c|^{2m} = |c|^{2m} \exp \left[-m \sum_{k>0} \left(\frac{z^k}{k c^k} + \frac{\bar{z}^k}{k \bar{c}^k} \right) \right],$$

$$|z - a|^{2m} = |z|^{2m} \exp \left[-m \sum_{k>0} \left(\frac{a^k}{k z^k} + \frac{\bar{a}^k}{k \bar{z}^k} \right) \right].$$

Substituting these expansions into (B.25) and comparing $Z(a, c)$ and $Z(t_{\pm k}, \bar{t}_{\pm k})$

it is observed that the two partitions can be made equivalent with the following mapping,

$$Z(a, c) \Big|_{c^k = -\frac{1}{k\bar{t}_k}, a^k = -kt_{-k}} = \frac{Z(t_{\pm k}, \bar{t}_{\pm k})}{|c|^{2mN}}. \quad (\text{B.26})$$

Therefore we can create the field theory using the partition function $Z(a, c)$ and then use the mapping (B.26) to get back to the original system described by the wavefunction (B.20). The process of calculating the action is exactly the same as in the previous section using the the grand partition function;

$$\Theta(a, c) = \frac{1}{|a - c|^{2m}} \frac{\int \mathcal{D}\phi e^{-S'[\phi]}}{\int \mathcal{D}\phi e^{-S_0[\phi]}}, \quad (\text{B.27})$$

where $S_0 = (1/2\pi) \int d^2z \partial\phi\bar{\partial}\phi$ is the free boson action and the action $S'[\phi]$ is given by

$$S'[\phi] = \frac{1}{8\pi} \int d^2z \left[(\nabla\phi)(\nabla\phi) - 4\mu e^{i\sqrt{m}\phi + \tilde{\varphi}} - 8\pi i\sqrt{m}\phi (\delta^2(z - a) + \delta^2(z - c)) \right] \quad (\text{B.28})$$

where $\tilde{\varphi}(z) = -(|z|^2/2) + 2(M - m) \ln |z|$. The factor $|a - c|^{2m}$ in Eq. (B.27) is important since it mixes inner and outer boundary terms. The physics of most interest in the above action is the part due to the addition of the source charges (which corresponds to the edge excitations in the original partition function), therefore we consider the following action,

$$S[\chi] = S'[\phi + \chi] - S[\phi], \quad (\text{B.29})$$

where $S[\phi]$ is the action for the disk shaped fluid absent of any edge excitations

and was calculated previously in Eq. (B.13). The saddle point equation for the action $S[\chi]$ is

$$\Delta\chi + i\sqrt{m}F^2 \left(\frac{e^{i\sqrt{m}\chi}}{R_I^{2m}} - 1 \right) = -4\pi i\sqrt{m} (\delta^2(z-a) + \delta^2(z-c)) \quad (\text{B.30})$$

where F^2 is defined in Eq. (B.19). This differential equation can be solved but the solution, denoted χ_{sp} , is not presented here due to the expressions being long and untidy. With the saddle point solution, the tau-function, or the norm of the Laughlin states parameterised by $t_{\pm k}$ can be extracted via,

$$\tau(N, M, t_{\pm k}, \bar{t}_{\pm}) = \frac{e^{-S[\chi_{\text{sp}}]}}{|a-c|^{2m}} \Big|_{c^k = -\frac{1}{kt_k}, a^k = -kt_{-k}}, \quad (\text{B.31})$$

where the mapping described in Eq. (B.26) is used to get back to the original $t_{\pm k}$ variables. Remembering that we are only interested in the $t_{\pm k}$ and $\bar{t}_{\pm k}$ dependence, the final result following the above processes is given by

$$\tau(N, M, t_{\pm k}, \bar{t}_{\pm}) = D(N, M) \times \exp \left\{ m \sum_{k>0} \left(kR_O^{2k} |t_k|^2 + k \frac{|t_{-k}|^2}{R_I^{2k}} + kt_{-k}t_k + k\bar{t}_k\bar{t}_{-k} \right) \right\}, \quad (\text{B.32})$$

where $D(N, M)$ is a function of zero mode contributions. It is noted here that this function was also calculated using another method in [95] where the same $t_{\pm k}$ dependence was obtained. To finalise this section, a few remarks will be made about the types of averages performed using the field theory developed in this appendix.

This field theory was developed using the grand canonical partition, meaning that the states averaged over in this theory are not just energy dependent, but they also differ in the total number of particles. It is expected that this should not

affect any calculations for bulk properties of the FQH fluid however, measurements which are dependent on the boundaries of the FQH fluid may not be accurate in this representation. For example consider the tau-function calculated above. According to Eq. (B.24), the tau-function is defined for a constant number of particles, whereas the calculation of this function using the boson field theory in Eq. (B.31) averages over states of varying number of particles. Therefore it is not obvious that the calculation listed here is accurate for the norm of Laughlin states supporting edge excitations. In Chapter 3 however, this expression for the tau-function was verified by numerically computing overlap integrals for Laughlin states containing inner and outer boundary excitations for various cutoffs of the orbital angular momentum.

Bibliography

- [1] A. B. Fowler, F. F. Fang, W. E. Howard, and P. J. Stiles. Magneto-oscillatory conductance in silicon surfaces. *Phys. Rev. Lett.*, 16:901–903, May 1966.
- [2] K. v. Klitzing, G. Dorda, and M. Pepper. New method for high-accuracy determination of the fine-structure constant based on quantized Hall resistance. *Phys. Rev. Lett.*, 45:494–497, Aug 1980.
- [3] D. C. Tsui, H. L. Stormer, and A. C. Gossard. Two-dimensional magnetotransport in the extreme quantum limit. *Phys. Rev. Lett.*, 48:1559–1562, May 1982.
- [4] D. C. Tsui, H. L. Störmer, J. C. M. Hwang, J. S. Brooks, and M. J. Naughton. Observation of a fractional quantum number. *Phys. Rev. B*, 28:2274–2275, Aug 1983.
- [5] H. L. Stormer, A. Chang, D. C. Tsui, J. C. M. Hwang, A. C. Gossard, and W. Wiegmann. Fractional quantization of the Hall effect. *Phys. Rev. Lett.*, 50:1953–1956, Jun 1983.
- [6] A. M. Chang, P. Berglund, D. C. Tsui, H. L. Stormer, and J. C. M. Hwang. Higher-order states in the multiple-series, fractional, quantum Hall effect. *Phys. Rev. Lett.*, 53:997–1000, Sep 1984.
- [7] A. M. Chang, M. A. Paalanen, D. C. Tsui, H. L. Störmer, and J. C. M. Hwang. Fractional quantum Hall effect at low temperatures. *Phys. Rev. B*, 28:6133–6136, Nov 1983.

- [8] V. J. Goldman, M. Shayegan, and D. C. Tsui. Evidence for the fractional quantum Hall state at $\nu = \frac{1}{7}$. *Phys. Rev. Lett.*, 61:881–884, Aug 1988.
- [9] P. Bonderson, A. E. Feiguin, G. Möller, and J. K. Slingerland. Competing topological orders in the $\nu = 12/5$ quantum Hall state. *Phys. Rev. Lett.*, 108:036806, Jan 2012.
- [10] R. Willett, J. P. Eisenstein, H. L. Stormer, D. C. Tsui, A. C. Gossard, and J. H. English. Observation of an even-denominator quantum number in the fractional quantum Hall effect. *Phys. Rev. Lett.*, 59:1776–1779, Oct 1987.
- [11] W. Pan, J.-S. Xia, V. Shvarts, D. E. Adams, H. L. Stormer, D. C. Tsui, L. N. Pfeiffer, K. W. Baldwin, and K. W. West. Exact quantization of the even-denominator fractional quantum Hall state at $\nu = 5/2$ Landau level filling factor. *Phys. Rev. Lett.*, 83:3530–3533, Oct 1999.
- [12] P. L. Gammel, D. J. Bishop, J. P. Eisenstein, J. H. English, A. C. Gossard, R. Ruel, and H. L. Stormer. Ultralow-temperature behavior of the $\nu = \frac{5}{2}$ fractional quantum Hall effect. *Phys. Rev. B*, 38:10128–10130, Nov 1988.
- [13] R. B. Laughlin. Anomalous quantum Hall effect: An incompressible quantum fluid with fractionally charged excitations. *Phys. Rev. Lett.*, 50:1395–1398, May 1983.
- [14] E. H. Hall. On a new action of the magnet on electric currents. *American Journal of Mathematics*, 2(3):pp. 287–292, 1879.
- [15] T. Chakraborty and P. Pietiläinen. *The quantum Hall effects: integral and fractional*. Springer series in solid-state sciences. Springer-Verlag, 1995.
- [16] A.H. MacDonald. *Quantum Hall effect: a perspective*. Perspectives in condensed matter physics. Kluwer Academic Publishers, 1989.
- [17] Z.F. Ezawa. *Quantum Hall Effects: Field Theoretical Approach and Related Topics*. World Scientific, 2008.

- [18] N.W. Ashcroft and N.D. Mermin. *Solid State Physics*. Cengage Learning, 2011.
- [19] L. D. Landau and E. M. Lifshitz. *Quantum mechanics: non-relativistic theory*. Oxford; Boston: Butterworth-Heinemann, 3rd ed., rev. and enl., repr. 1991 with corrections edition, 1991. Translation of: Kvantovaya mekhanika.
- [20] R. B. Laughlin. Quantized Hall conductivity in two dimensions. *Phys. Rev. B*, 23:5632–5633, May 1981.
- [21] B. I. Halperin. Quantized Hall conductance, current-carrying edge states, and the existence of extended states in a two-dimensional disordered potential. *Phys. Rev. B*, 25:2185–2190, Feb 1982.
- [22] Qian Niu and D. J. Thouless. Quantum Hall effect with realistic boundary conditions. *Phys. Rev. B*, 35:2188–2197, Feb 1987.
- [23] Richard E Prange and Steven M Girvin. *The Quantum Hall effect*. New York: Springer-Verlag, 2nd ed edition, 1990.
- [24] F. D. M. Haldane. Fractional quantization of the Hall effect: A hierarchy of incompressible quantum fluid states. *Phys. Rev. Lett.*, 51:605–608, Aug 1983.
- [25] J.M. Caillol, D. Levesque, J.J. Weis, and J.P. Hansen. A monte carlo study of the classical two-dimensional one-component plasma. *Journal of Statistical Physics*, 28(2):325–349, 1982.
- [26] W. J. He, T. Cui, Y. M. Ma, C. B. Chen, Z. M. Liu, and G. T. Zou. Phase boundary between the fractional quantum Hall liquid and the Wigner crystal at low filling factors and low temperatures: A path integral monte carlo study. *Phys. Rev. B*, 72:195306, Nov 2005.
- [27] Daniel Arovas, J. R. Schrieffer, and Frank Wilczek. Fractional statistics and the quantum Hall effect. *Phys. Rev. Lett.*, 53:722–723, Aug 1984.

- [28] F. E. Camino, Wei Zhou, and V. J. Goldman. Realization of a Laughlin quasiparticle interferometer: Observation of fractional statistics. *Phys. Rev. B*, 72:075342, Aug 2005.
- [29] F. E. Camino, Wei Zhou, and V. J. Goldman. $e/3$ Laughlin quasiparticle primary-filling $\nu=1/3$ interferometer. *Phys. Rev. Lett.*, 98:076805, Feb 2007.
- [30] M. Oshikawa, Y. B. Kim, K. Shtengel, C. Nayak, and S. Tewari. Topological degeneracy of non-Abelian states for dummies. *Annals of Physics*, 322(6):1477 – 1498, 2007.
- [31] C. Nayak, S. H. Simon, A. Stern, M. Freedman, and S. Das Sarma. Non-Abelian anyons and topological quantum computation. *Rev. Mod. Phys.*, 80:1083–1159, Sep 2008.
- [32] N. E. Bonesteel, L. Hormozi, G. Zikos, and S. H. Simon. Quantum computing with non-Abelian quasiparticles. *International Journal of Modern Physics B*, 21(08n09):1372–1378, 2007.
- [33] P. Bonderson, M. Freedman, and C. Nayak. Measurement-only topological quantum computation. *Phys. Rev. Lett.*, 101:010501, Jun 2008.
- [34] L. Hormozi, N. E. Bonesteel, and S. H. Simon. Topological quantum computing with Read-Rezayi states. *Phys. Rev. Lett.*, 103:160501, Oct 2009.
- [35] S. Das Sarma, M. Freedman, and C. Nayak. Topologically protected qubits from a possible non-Abelian fractional quantum Hall state. *Phys. Rev. Lett.*, 94:166802, Apr 2005.
- [36] G. Moore and N. Read. Nonabelions in the fractional quantum Hall effect. *Nuclear Physics B*, 360(23):362 – 396, 1991.
- [37] E. Fradkin, C. Nayak, A. Tsvelik, and F. Wilczek. A Chern-Simons effective field theory for the Pfaffian quantum Hall state. *Nuclear Physics B*, 516(3):704 – 718, 1998.

- [38] N. Read and E. Rezayi. Beyond paired quantum Hall states: Parafermions and incompressible states in the first excited Landau level. *Phys. Rev. B*, 59:8084–8092, Mar 1999.
- [39] N. Read and E. Rezayi. Quasiholes and fermionic zero modes of paired fractional quantum Hall states: The mechanism for non-Abelian statistics. *Phys. Rev. B*, 54:16864–16887, Dec 1996.
- [40] P. Bonderson, A. Kitaev, and K. Shtengel. Detecting non-Abelian statistics in the $\nu = 5/2$ fractional quantum Hall state. *Phys. Rev. Lett.*, 96:016803, Jan 2006.
- [41] R. L. Willett, L. N. Pfeiffer, and K. W. West. Alternation and interchange of $e/4$ and $e/2$ period interference oscillations consistent with filling factor $5/2$ non-Abelian quasiparticles. *Phys. Rev. B*, 82:205301, Nov 2010.
- [42] X. Lin, C. Dillard, M. A. Kastner, L. N. Pfeiffer, and K. W. West. Measurements of quasiparticle tunneling in the $\nu = \frac{5}{2}$ fractional quantum Hall state. *Phys. Rev. B*, 85:165321, Apr 2012.
- [43] Guang Yang and D. E. Feldman. Influence of device geometry on tunneling in the $\nu = \frac{5}{2}$ quantum Hall liquid. *Phys. Rev. B*, 88:085317, Aug 2013.
- [44] Guang Yang and D. E. Feldman. Experimental constraints and a possible quantum Hall state at $\nu = 5/2$. *Phys. Rev. B*, 90:161306, Oct 2014.
- [45] V. Cheianov S. J. Huntington. Zero mode tunnelling in a fractional quantum Hall device. *To be published*, 2015.
- [46] X. G. Wen. Chiral Luttinger liquid and the edge excitations in the fractional quantum Hall states. *Phys. Rev. B*, 41, 1990.
- [47] C. W. J. Beenakker. Edge channels for the fractional quantum Hall effect. *Phys. Rev. Lett.*, 64:216–219, Jan 1990.

- [48] C. L. Kane and Matthew P. A. Fisher. Transmission through barriers and resonant tunneling in an interacting one-dimensional electron gas. *Physical Review B*, 46(23):15233, 1992.
- [49] C. L. Kane and Matthew P. A. Fisher. Resonant tunneling in an interacting one-dimensional electron gas. *Phys. Rev. B*, 46:7268–7271, Sep 1992.
- [50] C. L. Kane and Matthew P. A. Fisher. Transport in a one-channel Luttinger liquid. *Phys. Rev. Lett.*, 68:1220–1223, Feb 1992.
- [51] A. Furusaki and N. Nagaosa. Single-barrier problem and Anderson localization in a one-dimensional interacting electron system. *Phys. Rev. B*, 47:4631–4643, Feb 1993.
- [52] K. Moon, H. Yi, C. L. Kane, S. M. Girvin, and Matthew P. A. Fisher. Resonant tunneling between quantum Hall edge states. *Phys. Rev. Lett.*, 71:4381–4384, Dec 1993.
- [53] A.O. Gogolin, A.A. Nersesyan, and A.M. Tsvelik. *Bosonization and Strongly Correlated Systems*. Cambridge University Press, 2004.
- [54] F.P. Milliken, C.P. Umbach, and R.A. Webb. Indications of a Luttinger liquid in the fractional quantum Hall regime. *Solid State Communications*, 97(4):309 – 313, 1996.
- [55] S. Roddaro, V. Pellegrini, F. Beltram, G. Biasiol, and L. Sorba. Interedge strong-to-weak scattering evolution at a constriction in the fractional quantum Hall regime. *Phys. Rev. Lett.*, 93:046801, Jul 2004.
- [56] A. M. Chang, L. N. Pfeiffer, and K. W. West. Observation of chiral Luttinger behavior in electron tunneling into fractional quantum Hall edges. *Phys. Rev. Lett.*, 77:2538–2541, Sep 1996.
- [57] C. L. Kane and Matthew P. A. Fisher. Nonequilibrium noise and fractional charge in the quantum Hall effect. *Phys. Rev. Lett.*, 72:724–727, Jan 1994.

- [58] L. Saminadayar, D. C. Glattli, Y. Jin, and B. Etienne. Observation of the $e/3$ fractionally charged Laughlin quasiparticle. *Phys. Rev. Lett.*, 79:2526–2529, Sep 1997.
- [59] R. dePicciotto, M. Reznikov, M. Heiblum, V. Umansky, G. Bunin, and D. Mahalu. Direct observation of a fractional charge. *Nature*, 389(6647):162–164, SEP 11 1997.
- [60] M. Dolev, Y. Gross, Y. C. Chung, M. Heiblum, V. Umansky, and D. Mahalu. Dependence of the tunneling quasiparticle charge determined via shot noise measurements on the tunneling barrier and energetics. *Phys. Rev. B*, 81:161303, Apr 2010.
- [61] S. Baer, C. Rössler, T. Ihn, K. Ensslin, C. Reichl, and W. Wegscheider. Experimental probe of topological orders and edge excitations in the second Landau level. *Phys. Rev. B*, 90:075403, Aug 2014.
- [62] P. Fendley, A. W. W. Ludwig, and H. Saleur. Exact conductance through point contacts in the $\nu = 1/3$ fractional quantum Hall effect. *Phys. Rev. Lett.*, 74:3005–3008, Apr 1995.
- [63] R. Guyon, P. Devillard, T. Martin, and I. Safi. Klein factors in multiple fractional quantum Hall edge tunneling. *Phys. Rev. B*, 65:153304, Mar 2002.
- [64] C. L. Kane. Telegraph noise and fractional statistics in the quantum Hall effect. *Phys. Rev. Lett.*, 90:226802, Jun 2003.
- [65] I. Safi, P. Devillard, and T. Martin. Partition noise and statistics in the fractional quantum Hall effect. *Phys. Rev. Lett.*, 86:4628–4631, May 2001.
- [66] K. T. Law, D. E. Feldman, and Yuval Gefen. Electronic mach-zehnder interferometer as a tool to probe fractional statistics. *Phys. Rev. B*, 74:045319, Jul 2006.

- [67] S. Vishveshwara. Revisiting the Hanbury Brown-Twiss setup for fractional statistics. *Phys. Rev. Lett.*, 91:196803, Nov 2003.
- [68] C. Nayak, Matthew P. A. Fisher, A. W. W. Ludwig, and H. H. Lin. Resonant multilead point-contact tunneling. *Phys. Rev. B*, 59:15694–15704, Jun 1999.
- [69] V. V. Ponomarenko and D. V. Averin. Strong-coupling branching between edges of fractional quantum Hall liquids. *Phys. Rev. B*, 70:195316, Nov 2004.
- [70] T. Jonckheere, P. Devillard, A. Crépieux, and T. Martin. Electronic mach-zehnder interferometer in the fractional quantum Hall effect. *Phys. Rev. B*, 72:201305, Nov 2005.
- [71] N. Datta, R. Morf, and R. Ferrari. Edge of the Laughlin droplet. *Phys. Rev. B*, 53:10906–10915, Apr 1996.
- [72] T. Can, P. J. Forrester, G. Téllez, and P. Wiegmann. Singular behavior at the edge of Laughlin states. *Phys. Rev. B*, 89:235137, Jun 2014.
- [73] R. C. Gann, Sudip Chakravarty, and G. V. Chester. Monte carlo simulation of the classical two-dimensional one-component plasma. *Phys. Rev. B*, 20:326–344, Jul 1979.
- [74] D. Ceperley. Ground state of the fermion one-component plasma: A monte carlo study in two and three dimensions. *Phys. Rev. B*, 18:3126–3138, Oct 1978.
- [75] J. P. Hansen. Statistical mechanics of dense ionized matter. i. equilibrium properties of the classical one-component plasma. *Phys. Rev. A*, 8:3096–3109, Dec 1973.
- [76] J.M. Caillol, D. Levesque, J.J. Weis, and J.P. Hansen. A monte carlo study of the classical two-dimensional one-component plasma. *Journal of Statistical Physics*, 28(2):325–349, 1982.

- [77] D. Levesque, J. J. Weis, and A. H. MacDonald. Crystallization of the incompressible quantum-fluid state of a two-dimensional electron gas in a strong magnetic field. *Phys. Rev. B*, 30:1056–1058, Jul 1984.
- [78] R. Morf and B. I. Halperin. Monte carlo evaluation of trial wave functions for the fractional quantized Hall effect: Disk geometry. *Phys. Rev. B*, 33:2221–2246, Feb 1986.
- [79] M. E. J. Newman and G. T. Barkema. *Monte Carlo Methods in Statistical Physics*. Oxford University Press, 1999.
- [80] W. L. McMillan. Ground state of liquid He⁴. *Phys. Rev.*, 138:A442–A451, Apr 1965.
- [81] N. Metropolis, A. W. Rosenbluth, M. N. Rosenbluth, A. H. Teller, and E. Teller. Equation of state calculations by fast computing machines. *The Journal of Chemical Physics*, 21(6):1087–1092, 1953.
- [82] H. Müller-Krumbhaar and K. Binder. Dynamic properties of the monte carlo method in statistical mechanics. *Journal of Statistical Physics*, 8(1):1–24, 1973.
- [83] K. Binder, K. Binder, D.M. Ceperley, J.P. Hansen, H. Kalos, D.P. Landau, D. Levesque, H. Müller-Krumbhaar, D. Stauffer, and J.J. Weis. *Monte Carlo Methods in Statistical Physics*. Topics in Current Physics. Springer Berlin Heidelberg, 1986.
- [84] FDM Haldane. Edge states and boundary fluctuations in the quantum Hall fluid. *Bull. Am. Phys. Soc*, 35:254, 1990.
- [85] S. A. Trugman and S. Kivelson. Exact results for the fractional quantum Hall effect with general interactions. *Phys. Rev. B*, 31:5280–5284, Apr 1985.
- [86] X.G. Wen. Theory of the edge states in fractional quantum Hall effects. *International Journal of Modern Physics B*, 06(10):1711–1762, 1992.

- [87] M. Stone. Schur functions, chiral bosons, and the quantum-Hall-effect edge states. *Phys. Rev. B*, 42:8399–8404, Nov 1990.
- [88] J. M. Luttinger. An exactly soluble model of a manyfermion system. *Journal of Mathematical Physics*, 4(9):1154–1162, 1963.
- [89] S. Tomonaga. Remarks on bloch’s method of sound waves applied to many-fermion problems. *Progress of Theoretical Physics*, 5(4):544–569, 1950.
- [90] D. C. Mattis and E. H. Lieb. Exact solution of a manyfermion system and its associated boson field. *Journal of Mathematical Physics*, 6(2):304–312, 1965.
- [91] A. Luther and I. Peschel. Single-particle states, kohn anomaly, and pairing fluctuations in one dimension. *Phys. Rev. B*, 9:2911–2919, Apr 1974.
- [92] F. D. M. Haldane. ‘Luttinger liquid theory’ of one-dimensional quantum fluids. i. properties of the Luttinger model and their extension to the general 1d interacting spinless fermi gas. *Journal of Physics C: Solid State Physics*, 14(19):2585, 1981.
- [93] A. M. Chang. Chiral Luttinger liquids at the fractional quantum Hall edge. *Rev. Mod. Phys.*, 75:1449–1505, Nov 2003.
- [94] A. Boyarsky, V. V. Cheianov, and O. Ruchayskiy. Microscopic construction of the chiral Luttinger liquid theory of the quantum Hall edge. *Phys. Rev. B*, 70:235309, Dec 2004.
- [95] E. V. Sukhorukov I. P. Levkivskyi, J. Froehlich. Topological screening and interference of fractionally charged quasi-particles. *arXiv:1005.5703v1 [cond-mat.mes-hall]*, 2010.
- [96] I. K. Kostov, I. Krichever, M. Mineev-Weinstein, P. Wiegmann, and A. Zabrodin. Tau-function for analytic curves. *Random matrices and their applications, MSRI (eprint arXiv:hep-th/0005259)*, 40:285, may 2000.

- [97] P. Wiegmann and A. Zabrodin. Large N expansion for normal and complex matrix ensembles. In *Frontiers in Number Theory, Physics, and Geometry I*, pages 213–229. Springer, 2006.
- [98] A. Boyarsky, V. V. Cheianov, and O. Ruchayskiy. Fermions in the harmonic potential and string theory. *Journal of High Energy Physics*, 2005(01):010, 2005.
- [99] P. Wiegmann and A. Zabrodin. Large scale correlations in normal non-Hermitian matrix ensembles. *Journal of Physics A: Mathematical and General*, 36(12):3411, 2003.
- [100] A. Zabrodin. New applications of non-Hermitian random matrices. *Annales Henri Poincaré*, 4(2):851–861, 2003.
- [101] A. Zabrodin and P. Wiegmann. Large-N expansion for the 2d dyson gas. *Journal of Physics A: Mathematical and General*, 39(28):8933, 2006.
- [102] P. Bonderson, V. Gurarie, and C. Nayak. Plasma analogy and non-Abelian statistics for Ising-type quantum Hall states. *Phys. Rev. B*, 83:075303, Feb 2011.
- [103] D.E. Littlewood. *A University Algebra*. Heinemann, 1958.
- [104] I. G. Macdonald. *Symmetric Functions and Hall Polynomials*. Oxford mathematical monographs. Clarendon Press, 1998.
- [105] M. Stone, H. W. Wyld, and R. L. Schult. Edge waves in the quantum Hall effect and quantum dots. *Phys. Rev. B*, 45:14156–14161, Jun 1992.
- [106] B. Konopelchenko and L. M. Alonso. The KP hierarchy in Miwa coordinates. *Physics Letters A*, 258(46):272 – 278, 1999.